Torben Wilhelm Kühnast

Comparative analyses of *Cutibacterium acnes* and *Staphylococcus epidermidis* biofilms and therapeutic intervention strategies

DISSERTATION

supervised by

Assoz.Prof. Dipl.-Biol. Dr.rer.nat. Stefan Schild

Graz, 2019

Acknowledgement

There have been many people involved either directly or indirectly in the development of this PhD thesis and I would like to thank all of them. A few people, however, deserve to be specifically mentioned.

I would like to thank my supervisor Prof. Stefan Schild for introducing me into this project, for supporting me through all the years and giving me the freedom to develop myself. I would like to thank Prof. Achim Reidl for always being friendly minded and helping me whenever needed.

I would like to also extend my gratitude to Dr. Sanja Selak, Dr. Manfred Schuster and Dr. Theresa Weinhäupl from Origimm for the financial support, excellent collaboration and my first peeks into industrial practices.

Of course all my colleagues deserve my gratefulness, especially Dr. Dina Lopes, Dr. Fatih Cakar, Dr. Katharina Pressler, Franz Zingl, Paul Kohl and Fabian Mitterer. It has been the unmatched community solidarity that helped me to also cope with the exhausting phases, and it has been a great time.

My deepest thankfulness, last but not least, goes to my whole family, for always and unconditionally standing by my side. To my mother, to Robin and Pia for walking this PhD path together with me, to Rosi and Benji, to Colin and Birgit with her family.

Table of Contents

Zusammenfassung

Cutibacterium acnes (vormals *Propionibacterium acnes*) ist ein anaerobes, grampositives Bakterium der menschlichen Haut. Während es meistens als Kommensale auf unserer Haut lebt, kann es als opportunistischer Krankheitserreger fungieren, der zur Pathophysiologie der Hautkrankheit Akne vulgaris und zu implantat-assoziierten Infektionen beiträgt. Im Zuge dieses Prozesses ist bekannt, dass *C. acnes* Biofilme bildet. Detaillierte Analysen über die Struktur sowie über den Beitrag zur Virulenz sind jedoch noch begrenzt. Diese Arbeit konzentrierte sich auf dem Studium von *C. acnes* Biofilmbildung in situ, sowie auf antikörpervermittelten therapeutischen Interventionsstrategien. Dazu wurden zwei Assays etabliert, die die Biofilm-Menge durch einen Hochdurchsatz-Assay auf Mikrotiterplatte-Basis zeigten, sowie einem fluoreszenzmikroskopischen Assay, der mikroskopische Zellen quantifizierte und mögliche Biofilmstrukturen beschrieb. Es konnte nachgewiesen werden, dass der Phylotyp IA1 deutlich mehr Biofilm produzierte als die anderen Phylotypen. Insbesondere die SLST-Subtypen A1, A2 und A37 (entspricht dem *clonal complex* 18, Aarhus-Schema) waren wichtige Vermittler der erhöhten Biofilmbildung. Die Strukturen von *C. acnes* in situ Biofilmen wurden charakterisiert und quantifiziert. Dabei wurde gezeigt, dass IA1, IA2 und IC-Isolate typische Biofilmstrukturen ausbildeten und eine erhöhte Bindung an abiotische Oberflächen aufwiesen. Die Phylotypen IB, II und III zeigten dies nicht. Bei der Sortierung der Isolate nach ihrem Isolationspunkt (Haut versus Implantat) konnten keine signifikant erhöhten Unterschiede in der Biofilmbildung festgestellt werden. Darüber hinaus konnte gezeigt werden, dass sowohl die Biofilmstabilität von *C. acnes*, als auch dessen Anheftungsfähigkeit durch die Behandlung mit Proteinase K und teilweise mit DNase I für alle Phylotypen beeinträchtigt wurde. Ein planktonischer und ein Biofilm- Zustand wurde definiert, untersucht und hinsichtlich Aggregation, Bindung und Proteinzusammensetzung verifiziert. Um die Übertragbarkeit der Assays auf andere Bakterien zu testen, wurde die Biofilmbildung eines anderen kutanen grampositiven Kommensalen, *S. epidermidis*, erfolgreich gemessen, was zu ähnlichen Ergebnissen für alle getesteten Stämme aus den beiden unabhängigen Methoden führte. Im Rahmen einer industriellen Zusammenarbeit zu therapeutischen Interventionsstrategien wurden Antikörper gegen *C. acnes* Oberflächenproteine anhand ihrer Zellposition und Sekundärstruktur charakterisiert und quantifiziert, indem Fraktionierungs- und

Immunoblotprotokolle erstellt wurden. Die Fähigkeit der Antikörper, sich in situ an *C. acnes*-Oberflächen zu binden, wurde durch die Immunzytochemie untersucht. Schließlich wurden die Assays auf ihre Fähigkeit getestet, antikörpervermittelte Effekte auf *C. acnes* oder *S. epidermidis* Biofilmen zu zeigen.

Abstract

Cutibacterium acnes (formerly *Propionibacterium acnes*) is an anaerobic, Gram-positive bacterium of the human sebaceous skin. Whereas it commonly resides as commensal on our skin, it can act as opportunistic pathogen contributing to the pathophysiology of the skin disease acne vulgaris and to implant-associated infections. In course of this process, *C. acnes* is known to form biofilms. However, detailed analyses on its structure, as well as analyses on its contribution to virulence are still limited. This work focused on studying *C. acnes* biofilm formation in situ, as well as on antibody mediated therapeutic intervention strategies. For this, two assays were established, showing biofilm quantity by a high-throughput, MTP based assay, as well as a fluorescence microscopy based assay, quantifying microscopic cells and describing possible biofilm structures. It could be demonstrated that phylotype IA1 produced significantly higher biofilm than the other phylotypes. Especially SLST subtypes A1, A2 and A37 (translating to the clonal complex 18, Aarhus scheme) were key mediators of the increased biofilm formation. The structures of *C. acnes* of in situ biofilms were characterized and quantified, revealing that IA1, IA2 and IC isolates showed typical biofilm structures and increased attachment to abiotic surfaces and phylotypes IB, II and III did not. When sorting isolates according to their point of isolation (skin versus implant) no significantly increased biofilm formation differences could be identified. Furthermore, it could be shown that *C. acnes* biofilm stability, as well as attachment capacity was impaired by treatment with proteinase K and partially with DNase I for all phylotypes. A planktonic and biofilm state was defined, investigated and verified in terms of aggregation, attachment and protein composition. In an attempt to test the assays' translatability to other bacteria, biofilm formation of a different cutaneous Gram-positive commensal, *S. epidermidis*, was successfully measured, yielding in similar results for all tested strains from the two independent methods. Within an industrial collaboration on therapeutic intervention strategies, antibodies against *C. acnes* surface proteins were characterized and quantified on its cellular location and secondary structure, by establishing fractionation and immunoblot protocols. The antibodies' ability to bind to *C. acnes* surfaces in situ was investigated by immunocytochemistry. Finally, the assays were tested on their ability to show antibody-mediated effects on *C. acnes* or *S. epidermidis* biofilms.

I. Introduction

Prelog. From a macroscopic perspective the human skin is what we see from each other, what defines us superficially, what makes us unique, covering our physiology, seemingly being our physiology. With the skin as the representative of ourselves, it is constantly judged by our surrounding demanding no less than perfection. Woe betide anyone who strays from this cultural demand. It is blind chance that assigns whether or not superficial perfection is given to the one and not to the other. The biological lottery strikes hard on the unlucky loser, especially those of young age and mind. Even though completely healthy, the stigma is engraved into the face by red stains, scars forming crater landscapes, yellow-reddish liquids erupting like volcanoes and the odor of decay, possibly lasting a lifetime. Within this anarchy of injustice, there is a chance. A chance for equality. A chance for fairness. A chance for a cure. Maybe, maybe history will say at one point that this work contributed a tiny fraction to this chance.

Introduction. On a microscopic level, the skin does not merely resemble a simple barrier to the outside, but one of the most important organs of the human, comprising a microbiome of epithelial cells and bacteria in tight equilibrium (Byrd et al., 2018). The skin can be differentiated into three ecological systems: moist skin, dry skin and sebaceous skin. The latter contains areas where sebaceous glands are present mostly (face, back and chest). These glands can be found deeper within the epidermidis in follicles or hair follicles and change the environment by producing lipid-rich sebum (Byrd et al., 2018; Christensen and Brüggemann, 2014). Whereas *Cutibacteria* (formerly *Propionibacteria)* dominate the sebaceous skin (and with less abundance in the other skin areas), *Staphylococci* can be found in both, sebaceous and moist surface skin areas (Byrd et al., 2018; Grice et al., 2009). This work focused on *Cutibacterium acnes* (formerly *Propionibacterium acnes*) from the *Cutibacteria*, and tried to apply core assays on *Staphylococcus epidermidis* from *Staphylococci*.

Cutibacterium acnes is an anaerobic, rod-shaped Gram-positive bacterium from the phylum of Actinobacteria. As human skin commensal, it is adapted to the ecological niche by various adaptions. Its specialized peptidoglycan structure makes it immune to human lysozyme, a bactericidal enzyme ubiquitous in human secretions and serum (Kamisango et al., 1982). It is able to adhere to lipid species secreted by the sebaceous gland (Gribbon et al., 1993). Lipases (like GehA) are secreted to degrade and

metabolize lipids (Falcocchio et al., 2006). As iron surrounding the human host is limited by iron-binding proteins like lactotransferrin, *C. acnes* evolved for genes of iron acquisition (Bek-Thomsen et al., 2014; Scholz and Kilian, 2016). The adaption to the human skin was also reflected by the recent reclassification of *Cutibacterium acnes* from *Propionibacterium*. It was suggested to create a novel cutaneous based genus (*Cutibacterium* gen. nov.), including the former species *Propionibacterium avidum*, *Propionibacterium granulosum* and '*Propionibacterium humerusii*' and *Propionibacterium acnes* (Scholz and Kilian, 2016). This work followed the suggestion.

For most healthy people *C. acnes* acts as commensal and occupies the sebaceous niche. For example, fermentative products like propionic acid and other short-chain fatty acids (SCFAs) can lower the pH and make it less attractive for possible pathogenic bacteria, in particular *S. aureus* (Christensen and Brüggemann, 2014; Shu et al., 2013). However, under certain conditions *C. acnes* exhibits opportunistic pathogenic character associated with invasive infections of the skin, soft tissue, cardiovascular system, sarcoidosis, deep-organ tissues, prostate cancer and implant-associated infections (Achermann et al., 2014; Davidsson et al., 2016; McGinley et al., 1980; Schupp et al., 2015). The skin inflammatory disorder which also contributed to the bacteria's name - acne vulgaris - can manifest ranging from mild or transient acne in teenage years to more severe, chronic acne that continues well into adulthood primarily covering the face, shoulders and the back (Achermann et al., 2014). Acne affects not only more than 80% of teenagers, but also a significant percentage of adults who continue to be affected even into their 40s and beyond. *C. acnes* is also a relevant causative agent of implant-associated infections with constantly increasing incidence rates, likely due to improved diagnostic techniques (Aubin et al., 2014).

The molecular basis for the sudden immunogenic human host reaction to surface-associated *C. acnes* is still under debate. As a prerequisite, the human host has to undergo changes in its physiology. These involve hormonal changes like increased androgen levels, especially in the teenage years (Makrantonaki et al., 2011). Androgen among others increases sebum secretion and as *C. acnes* feeds on sebum lipids, more sebum means higher nutriment availability. At the same time excessive sebum production can cause clogging of the follicles and the formation of microcomedones. The resulting microaerobic to anaerobic environments are necessary for *C. acnes* proliferation. Still, these conditions alone are not sufficient to automatically induce

inflammation, as there are microcomedones without inflammation. Actually, it has been shown that an elevated inflammatory status can be reported in acne patients before formation of microcomedones (Jeremy et al., 2003). Summarizing this data, the chain of incidents for the establishment of acne seemingly requires an inflammatory dysfunction first (whereas the actual pathway is still unknown), followed by the formation of microcomedones and the presence of *C. acnes* (Metiko et al., 2015).

Within the *C. acnes* species, several phylotypes and subgroups exist, which seem to be differentially capable of causing and maintaining human infections. Initially, *C. acnes* isolates were classified into different phylogenetic divisions based on serological differentiation and phage typing, later confirmed by sequence analysis of *recA*, *tly* and the CAMP genes (McDowell et al., 2005; McDowell et al., 2008; McDowell et al., 2011). A comprehensive classification system by multilocus sequence typing (MLST) or multiplex touchdown PCR categorized *C. acnes* isolates into the six phylotypes IA1, IA2, IB, IC, II and III (Barnard et al., 2015; Lomholt and Kilian, 2010; McDowell et al., 2012). An alternative single locus sequence typing (SLST) technique allowed for quick differentiation of phylotypes into subtypes, correlating with MLST results (Scholz et al., 2014). Herein, all *C. acnes* strains were categorized by multiplex touchdown PCR and all IA1 strains were additionally sorted by SLST. See table 1 for an overview of all main phylotypes and clonal complexes and table 2 for a list of all *C. acnes* strains and phylotypes used in this work.

Several recent studies could show statistically significant associations of *C. acnes* IA1 phylotype to acne (Fitz-Gibbon et al., 2013; Lomholt et al., 2017; Lomholt and Kilian, 2010; McDowell et al., 2011; McDowell et al., 2012; McDowell et al., 2013). In a proteome analysis, bacterial proteins extracted from sebaceous follicles of 20 acne patients could be annotated to *C. acnes* (Bek-Thomsen et al., 2014). Moreover, *C. acnes* isolated from follicles or cotton swap of mild or severe acne patients belonged exclusively to the IA1 phylotype (Lomholt et al., 2017). The healthy individuals used as control in all studies showed a heterologous distribution of all phylotypes (McDowell et al., 2013).

Table 1: Sequence typing of *C. acnes*. Summary of the main phylotypes and clonal complexes according to Belfast scheme (expanded multilocus sequence typing), Aarhus scheme (multilocus sequence typing) or single locus sequence typing (SLST) (Dréno, 2017; Fitz-Gibbon et al., 2013; Lomholt and Kilian, 2010; McDowell et al., 2012; McDowell, 2017; Scholz et al., 2014; Yu et al., 2015). For general discussion this work refers to the eMLST8 phylotype nomenclature and SLST for detailed differentiations.

Belfast scheme		Aarhus scheme		
eMLST8		MLST9		SLST
Phylotype	Clonal complex	Phylotype	Clonal complex	
IA1	CC-1	I-1a	CC18	A1 - A34
IA1	CC-3	I-1a	CC3	C1 - C5
IA1		I-1a	CC28	D1- D5
IA1	CC-4	I-1a	CC31	E1 - E5
IA2	CC-2	I-1b	CC28	F1 - F14
IB	CC-5	I-2	CC36	H1 - H8
IC	CC-107	NA	CC53	G1
II	CC-72	II	CC60	K1 - K25
III	CC-77	NA	CC43	L1 - L10

Surprisingly, according to metagenomic studies the overall abundance of *C. acnes* did not change, pointing out that inflammation does not correlate with an increase in proliferation of bacteria (Barnard et al., 2016; Fitz-Gibbon et al., 2013). However, not all studies were able to show clear significances, emphasizing the importance of choosing the correct sampling technique (Alexeyev and Jahns, 2012; Omer et al., 2017; Sadhasivam et al., 2016)

Implant-associated phylotypes seemed more heterologous. A study analyzing 61 orthopedic implants colonized by *C. acnes* found most frequently phylotype I, followed by type II, while type III could not be detected on any implant (Sampedro et al., 2009). However, a clear association between a specific phylotype and infection of failed orthopedic implants could not be observed (McDowell et al., 2013; Sampedro et al., 2009). Importantly, a recent report suggests that samples collected from deep tissue infections can be also contaminated by the medical personnel in the progress of surgery due to the great abundance of *C. acnes* on everyone's skin (Mollerup et al., 2016). Thus, false positive detection of *C. acnes* cannot be excluded. The quality of tissue sampling is crucial to avoid false positive detection of *C. acnes* in the future and retrieve better insights in the epidemiology of *C. acnes*.

As pathogenicity of *C. acnes* does not strictly follow Koch's postulates (i.e. cells isolated from acne patients do not necessarily cause new acne in previously healthy individuals), virulence factors are harder to pinpoint. Genomic, transcriptomic and proteomic analyses have tried to pinpoint opportunistic pathogenicity to certain genes or proteins (Bek-Thomsen et al., 2014; Brüggemann et al., 2004; Brzuszkiewicz et al., 2011; Holland et al., 2010; Lomholt and Kilian, 2010). For example, secreted CAMP factors could be found ubiquitously surrounding *C. acnes* tissue. In combination with *S. aureus*' sphingomyelinase CAMP factors lead to hemolysis of erythrocytes and potentially lyse keratinocytes and macrophages (Bek-Thomsen et al., 2014; Beylot et al., 2014; Nakatsuji et al., 2011; Sörensen et al., 2010). Surprisingly, CAMP1 and 2 appearance in acne patients' follicles was reduced compared to healthy individuals (CAMP1 reduced from 72% of all individuals to 10% of acne patients, CAMP2 reduced from 14% in healthy samples to no detection in acne patients) (Bek-Thomsen et al., 2014). Although other factors might be involved in these results (like host defensive mechanism), it demonstrates the difficulty in identifying virulence factors for *C. acnes*.

A particular defensive virulence factor, however, could be of greater importance: the biofilm. Generally, to form a common biofilm non-sessile cells usually find a random new niche, an unpopulated surface for example, and bind to it with adhesion factors (like sticky proteins or extracellular DNA). Subsequently, cells change metabolism to surround itself by an extracellular matrix consisting of polysaccharides, proteins, DNA and/or lipids to protect from mechanical stress and dehydration (Abee et al., 2011). Intercellular communication is mediated by quorum sensing while modulating the surrounding matrix with proteinases and DNases. All layers of bacteria have to be similarly supplied with nutrients and metabolic end-products have to be disposed of. For this, growth direction and matrix structure are modulated to alternate aggregates of cells by corridors of water. Finally, metabolism is slowed down, increasing its resistance to antimicrobial substances such as antibiotics (Abee et al., 2011).

Studies confirmed the potential of *C. acnes* to form biofilms on a variety of surfaces, such as plastic, glass, silicone, titanium and steel (Bayston et al., 2007; Furustrand Tafin et al., 2012; Holmberg et al., 2009). In parallel, biofilm aggregates could be visualized in the stratum corneum and the hair follicles of acne patients, as well as on implant devices (Bayston et al., 2007; Jahns et al., 2012; Tunney et al., 2007). *C. acnes* biofilm-like aggregates could be more frequently observed in skin biopsies of acne

vulgaris patients compared to healthy control groups. Furthermore, *C. acnes* isolates derived from invasive infections have been associated with better biofilm production compared to skin isolates (Holmberg et al., 2009; Jahns et al., 2012). Most importantly and consistent with the general physiology of biofilm, *C. acnes* within a biofilm have been shown to be more resistant to antimicrobial killing compared to planktonic bacteria (Coenye et al., 2007; Ramage et al., 2003). Overall these findings point to an important role of biofilm formation in the pathogenesis of *C. acnes*. Taken together, the emergence of acne seems to be dependent on a dysfunction of the immune system, the establishment of microcomedones and the presence of *C. acnes*, particularly the phylotype IA1 and the establishment of biofilm (Metiko et al., 2015).

Following the hypothesis of biofilm being a major player in pathogenicity, the goal of this work was to characterize *C. acnes* biofilms of the different phylotypes in situ from a quantitative point of view, as well as from a structural by using fluorescence microscopy. The quantification was done by establishing two assays: a) an MTP based quantification assay and b) a microscopical chamber system with fluorescence signal quantification. Characterization and visualization of the three dimensional biofilm structures was done by fluorescence microscopy. These investigations were described in detail in section 1 and 2, with parts of it already published in 2018 (Kuehnast et al., 2018). Additionally, the *C. acnes* surface was to be investigated, looking for possible factors involved in biofilm formation. To do so, a growth condition had to be found as comparison which is not biofilm. Thus, a biofilm and planktonic condition was established and tested for biofilm typical phenotypes. Afterwards, surface-associated proteins from both conditions were analyzed using mass spectrometry.

Currently, therapeutic strategies for curing acne involve (among others) the usage of antibiotics, retinoids, isotretinoids or androgen blocker. Therapies take between 6 to 12 weeks (antibiotics) or up to 8 month (retinoids) while causing adverse side effects. These include interfering into the hormonal balance and counteracting testosterone, alteration of the microbiome over a long period including possibly developing antibiotic resistances, dry and fragile skin and in further consequence cheilitis or dermatitis. Regularly therapies fail or reoccur after discontinuing treatment.

To find a mild and permanent alternative to these heavy medications, our industrial collaboration partner Origimm Biotechnology (Vienna, Austria) started as startup to develop a different treatment relying on host defense mechanism. With *C. acnes*

resistant to many innate immune responses like complement system and lysozyme, the focus laid on the adaptive immune response: vaccination. In particular, Origimm screened specifically for proteins (antigens) on the surface of *C. acnes* increasing the adaptive immune system's efficacy. The resulting antibodies should be highly functional and protective by initiating or increasing opsonization of *C. acnes* and consecutively enhancing phagocytosis. The strategy to this point included in silico identification of *C. acnes* surface proteins, heterologous expression, purification and immunization of rabbits and mice using these proteins as antigens. The resulting antisera, containing polyclonal antibodies against the protein antigens, were used to characterize the proteins' ability to enhance the immune system protective functions against *C. acnes*. These characterizations consisted of multiple, company-internal assays from Origimm's side. It should be noted that due to intellectual property rights and ongoing patent applications, the exact function of the protein candidates could not be disclosed. Within this work, additional assays were established to support Origimm characterize the antibodies from a biofilm perspective. Antibodies in general, when bound to sticky biofilm matrix proteins, could significantly reduce the attachment capacities of the respective strain and with it inhibit initial biofilm colonization (Lam et al., 2014). In surgery, a high titer of these antibodies could decrease *C. acnes* or *S. epidermidis* attachment to the implant. In further consequence this could lead to reduced implant-associated infections.

Based on the research on biofilm vs planktonic state (section 3), a fractionation protocol was established, separating whole cell lysates into a cytosolic, membrane-associated and secreted fraction (section 6). The antisera were incorporated into a Western blot protocol, testing the different fractions from planktonic and biofilm mode on the binding characteristic (kDa size and binding pattern) and quantity. In parallel, the antibodies were tested on in situ accessibility on viable planktonic and biofilm derived *C. acnes* cells by immunocytochemistry (section 4). Finally, to elucidate antibody mediated efficacy, the HL60 cell line was differentiated into phagocytic cells, co-incubated with antibody opsonized *C. acnes* and observed under the microscope.

An important aspect of the biofilm quantification assays, as well as the whole antibody based therapeutic intervention strategy, was the translatability from *C. acnes* to different biofilm producing strains. *S. epidermidis* is a skin commensal similar to *C. acnes* and even though it is not associated to acne, it can cause implant associated

infections and carry antibiotic resistance with similar implications as with *C. acnes*. The goal of the *S. epidermidis* project was to adapt the biofilm assays to *S. epidermidis* and quantify biofilm production from an MTP and a fluorescence microscopy perspective (sections 1 and 2). The MTP assay was additionally used to test antibodies derived from *S. epidermidis* whole cell lysate immunization on biofilm formation.

II. Materials and Methods

1. Materials

1.1. Media

BHI broth – Bacto™ brain heart infusion (Becton Dickinson)	
BHI powder	37 g / l
H_2O_{dd}	Double-distilled tap water

BHI powder ingredients	
Calf brain	7.7 g / l
Beef heart	9.8 g / l
Proteose peptone	10 g / l
Dextrose	2 g / l
Sodium chloride	5 g / l
Disodium phosphate	2.5 g / l

BHI agar	
BHI powder	37 g / l
Agar	16 g / l
H_2O_{dd}	Double-distilled tap water

TSB – trypic soy broth (Sigma Aldrich)	
TSB powder	30 g / l
H_2O_{dd}	Double-distilled tap water

TSB powder ingredients	
Casein peptone	17 g / l
Soya peptone	3 g / l
Sodium chloride	5 g / l
Dipotassium hydrogen phosphate	2.5 g / l
Glucose	2.5 g / l

TSB agar	
TSB powder	30 g / l
Agar	16 g / l
H_2O_{dd}	Double-distilled tap water

RPMI medium	
RPMI 1640 Medium	
Glutamine	2 mM
Glucose	20 mM

1.2. Chemicals and buffers

H_2O variations	
H_2O_{ve}	De-ionized tap water
H_2O_{dd}	Double-distilled tap water
H_2O_f	Aqua bidest. “Fresenius”

Chemicals	
Acetone	Liquid (≥99.8%, Roth)
APS (ammonium persulfate)	Powder (≥98%, Roth)
Albumin fraction V	Powder (≥98%, Roth)
Aluminium sulfate hexadecahydrate	Powder (≥98%, Roth)
Bromophenol blue	Powder (Roth)
CAPS (N-cyclohexyl-3-aminopropanesulfonic acid)	Powder (≥99%, Roth)
Coomassie G250	Powder (Roth)
Crystal violet	Powder (Roth)
DMSO – dimethyl sulfoxide	Liquid (≥99,8%, Roth)
EDTA (ethylenediaminetetraacetic acid)	Powder (≥95%, Roth)
Ethanol (absolute)	Liquid (100%, Chem-Lab)
Gel 30	Rothiphorese ®, 30% acrylamide
Glycerol	Liquid (87%, AppliChem)
2-Mercaptoethanol	Powder (99%, Roth)

$Na_2HPO_4 * 2H_2O$	Powder (≥99,5%, Roth)
Phosphoric acid	Liquid (≥85%, Roth)
SDS (sodium dodecyl sulfate)	Pellets (Serva)
TCA (trichloroacetic acid)	Liquid (≥99%, Roth)
TEMED (tetramethylethylenediamine)	Liquid (≥99%, Roth)
TRIS	Powder (99,9%, Roth)
Tween® 20	Liquid (Roth)

Saline 10x	
NaCl	1,37 M (80 g / l) in H_2O_{dd}

PBS 10x – phosphate buffered saline	
NaCl	1,37 M (80 g / l)
KCl	27 mM (2 g / l)
$Na_2HPO_4 * 2H_2O$	100 mM (17,8 g / l)
KH_2PO_4	18 mM (2,4 g / l)
+ 900 ml H_2O_{dd}	
Adjust to pH 7,4 with NaOH	
Fill to 1 l	

BSA 0.5% or 2%	
Albumin fraction V	0.5% or 2% (w/v) in PBS

Lämmli buffer (6x)	
SDS	1.1 g
EDTA	0.41 g
$Na_2HPO_4 * 2H_2O$	0.17 g
Resolve in 10 ml H_2O_{dd}	
Adjust to pH 7,2 with NaOH	
+10 ml glycerol (50%)	
+ Bromophenol blue	40 mg

+ Mercaptoethanol	1.1 ml

Running buffer 5x (SDS-PAGE)	
Tris	15.2 g
Glycerol (87%)	94 g
Resolve in 950 ml H_2O_{dd}	
+ SDS (10%)	50 ml

CAPS buffer	
CAPS	4.43 g
Resolve in 1.5 l H_2O_{dd}	
Adjust to pH 11 with NaOH	
Fill to 1.8 l with H_2O_{dd}	
+ Methanol	200 ml

TBS – Tris-buffered saline	
1 M Tris/HCl, pH 7.5	20 ml
5 M NaCl	50 ml
Fill to 1 l with H_2O_{ve}	

TBS-T – Tris-buffered saline with Tween20	
1 M Tris/HCl, pH 7.5	20 ml
5 M NaCl	50 ml
Tween 20	2 ml
Fill to 1 l with H_2O_{ve}	

1 M Tris/HCl, pH 7.5	
Tris	121.14 g
H_2O_{dd}	800 ml
Adjust pH to 7.5 with HCl	

Fill to 1 l with H_2O_{dd}	

1 M Tris/HCl, pH 6.8	
Tris	121.14 g
H_2O_{dd}	800 ml
Adjust pH to 6.8 with HCl	
Fill to 1 l with H_2O_{dd}	

2 M Tris/HCl, pH 8.8	
Tris	242.28 g
H_2O_{dd}	800 ml
Adjust pH to 8.8 with HCl	
Fill to 1 l with H_2O_{dd}	

TBS+10%MP	
TBS	
Milk powder	10% (w/v)

APS solution	
APS powder	10% (w/v) in H_2O_f

Stacking solution stock (self-made gel)	
1 M Tris/HCl, pH 6.8	100 ml
SDS (10%)	8 ml
H_2O_{dd}	92 ml

Stacking solution (for 4 self-made gels)	
Stacking solution stock	2.5 ml
H_2O_{dd}	6.14 ml

Gel 30 (Rothiphorese ®)	1.3 ml
TEMED	30 µl
APS (10%)	50 µl

Separation solution stock (self-made gel)	
2 M Tris/HCl, pH 8.8	300 ml
SDS (10%)	10 ml
H_2O_{dd}	84 ml

Separation solution (for 4 self-made gels, 12%)	
Separation solution stock	5 ml
H_2O_{dd}	6.9 ml
Gel 30 (Rothiphorese ®)	8 ml
TEMED	30 µl
APS (10%)	50 µl

Bipyridyl stock (2,2'-bipyridyl, Sigma-Aldrich)	
Bipyridyl	33 mM in H_2O_{dd}, sterile filtrated

1.3. Dyes, antibodies and enzymes

Crystal violet	
Crystal violet powder	0.1 g / l in H_2O_{dd}

Kang / Coomassie solution	
Aluminium sulfate hexadecahydrate	50 g
Resolve in 300 ml H_2O_{dd}	
+ Ethanol (absolute)	100 ml
Mix until becoming transparent	
+ Coomassie G250	0.2 g
+ Phosphoric acid (84%)	23.4 ml

Fill to 1 l with H_2O_{dd}	

Antibodies and fluorescence dye stocks	
Cy3-GoatAntiRabbit (Jackson ImmunoResearch)	0.75 mg / ml in glycerol (44%)
Cy3-GoatAntiMouse (Jackson ImmunoResearch)	0.75 mg / ml in glycerol (44%)
DyLight 350-GoatAntiRabbit (Invitrogen)	1 mg / ml in PBS
DAPI (4′,6-Diamidino-2-phenylindole dihydrochloride, Roche)	5 mg / ml in H_2O_f
DHR (dihydrorhodamine 1213, Sigma-Aldrich)	2 mg / ml in DMSO
SYTO9 (single usage, Invitrogen)	5 mM in DMSO
SYTO9 (live/dead™ BacLight™ kit, Invitrogen)	3.34 mM in DMSO
PI (propidium iodide, BacLight kit, Invitrogen)	20 mM in DMSO

Proteinase K stock (Roth, 30 mAnson U / mg)	
Proteinase K powder	10 mg / ml in BHI, sterile filtrated

DNase I stock (AppliChem, 5,000 U / mg)	
DNase I powder	10 mg / ml in BHI, sterile filtrated

1.4. Strain list

Table 2: *Cutibacterium acnes* strains used in this study. Ref. stands for reference, St.Co. for strain collection number at the institute of molecular biosciences, university of Graz. 1: (Douglas and Gunter, 1946), 2: (Barnard et al., 2015), 3: (Horváth et al., 2012), 4: (Kuehnast et al., 2018), 5: Queen's University, Belfast, 6: Origimm Biotechnology, 7: Pro-Implant Foundation, 8: Biological Research Centre of the Hungarian Academy of Sciences, 9: DSMZ, 10: (Brüggemann et al., 2004).

Species	Strain	Alternative nomenclature	Phylogroup, SLST type	Isolated from	Source	Ref.	St.Co.
C. acnes	**IA1-s1**	NCTC 737, ATCC 6919	IA1, A1	acne	9	1	1560
C. acnes	**IA1-s2**		IA1, A1	healthy skin	6		1586
C. acnes	**IA1-s3**	P. acn 25	IA1, D1	corneal scrape	5		1561
C. acnes	**IA1-s4**	PV10	IA1, D1	acne	5		1562
C. acnes	**IA1-s5**		IA1, A37	acne	6	4	1573
C. acnes	**IA1-s6**		IA1, A37	acne	6	4	1574
C. acnes	**IA1-s7**		IA1, C1	acne	6	4	1575
C. acnes	**IA1-s8**		IA1, C1	acne	6	4	1576
C. acnes	**IA1-s9**		IA1, A1	acne	6	4	1577
C. acnes	**IA1-s10**		IA1, A1	acne	6	4	1578
C. acnes	**IA1-s11**		IA1, A1	acne	6	4	1579
C. acnes	**IA1-s12**		IA1, A1	acne	6	4	1580
C. acnes	**IA1-s13**		IA1, C2	healthy skin	6	4	1581
C. acnes	**IA1-s14**		IA1, A1	acne	6	4	1582
C. acnes	**IA1-s15**		IA1, D1	acne	6	4	1583
C. acnes	**IA1-s16**		IA1, A1	acne	6	4	1584
C. acnes	**IA1-s17**		IA1, A1	healthy skin	6	4	1585
C. acnes	**IA1-s18**		IA1, A1	healthy skin	6	4	1589
C. acnes	**IA1-s19**		IA1, A1	healthy skin	6	4	1590
C. acnes	**IA1-s20**		IA1, A1	healthy skin	6	4	1591
C. acnes	**IA1-i1**		IA1, A1	implant	7	4	1814
C. acnes	**IA1-i2**		IA1, A1	implant	7	4	1812
C. acnes	**IA1-i3**		IA1, A1	implant	7	4	1815
C. acnes	**IA1-i4**		IA1, A1	implant	7	4	1819
C. acnes	**IA1-i5**		IA1, A1	implant	7	4	1821
C. acnes	**IA1-i6**		IA1, H1	implant	7	4	1823
C. acnes	**IA1-i7**		IA1, D1	implant	7	4	1824
C. acnes	**IA1-i8**		IA1, A1	implant	7	4	1828
C. acnes	**IA1-i11**		IA1, A1	implant	7	4	1934
C. acnes	**IA1-i12**		IA1, A2	implant	7	4	1936
C. acnes	**IA1-i13**		IA1, A1	implant	7	4	1940
C. acnes	**IA1-i14**		IA1, A1	implant	7	4	1941
C. acnes	**IA1-i16**		IA1, A1	implant	7	4	1947
C. acnes	**IA1-i17**		IA1, C1	implant	7	4	1948
C. acnes	**IA1-i18**		IA1, D1	implant	7	4	1950

Species	Strain	Alternative nomenclature	Phylogroup, SLST type	Isolated from	Source	Ref.	St.Co.
C. acnes	**IA2-s1**	P. acn 10	IA2	corneal scrape	5		1563
C. acnes	**IA2-s2**	P. acn 31	IA2	aqueous humor	5	2	1564
C. acnes	**IA2-i1**		IA2	implant	7	4	1826
C. acnes	**IB-s1**	P. acn 87	IB		5		1565
C. acnes	**IB-s2**	W1392	IB	dental	5		1566
C. acnes	**IB-i1**		IB	implant	7	4	1811
C. acnes	**IB-i2**		IB	implant	7	4	1813
C. acnes	**IB-i3**		IB	implant	7	4	1817
C. acnes	**IB-i4**		IB	implant	7	4	1822
C. acnes	**IB-i5**		IB	implant	7	4	1825
C. acnes	**IB-i6**		IB	implant	7	4	1827
C. acnes	**IC-s1**	PV66	IC	acne	5	2	1567
C. acnes	**IC-i1**		IC	implant	7	4	1816
C. acnes	**IC-i2**		IC	implant	8		1930
C. acnes	**II-s1**		II	healthy	6	4	1587
C. acnes	**II-s2**	ATCC11828	II	subcutaneous abscess	9	3	1568
C. acnes	**II-s4**		II	healthy skin	6	4	1588
C. acnes	**II-i1**		II	implant	7	4	1820
C. acnes	**II-i2**		II	implant	7	4	1945
C. acnes	**II-i3**		II	spinal disk material	5		1571
C. acnes	**III-s1**	20C	III	skin	5		1570
C. acnes	**III-i1**		III	implant	7	4	1818
C. acnes	**III-i2**	Asn12	III	spinal disk material	5	2	1572
C. acnes	**IB-x1**	KPA171202, DSMZ 16379	IB	anaerobic culture contamination	9	10	1929
C. acnes		HL053PA2	IA1		6		2213
C. acnes		HL067PA1	IA2		6		2214
C. acnes		HL001PA1	II		6		2249
C. acnes		HL050PA2	II		6		2250
C. acnes		ATCC 11827	IA1		6		2480
C. acnes		HL030-PA1	IB		6		2481
C. acnes		HL043PA1	IA1		6		2482
C. acnes		HL110PA4	II		6		2483
C. acnes		HL050PA3	IA2		6		2484

Table 3: *Staphylococcus epidermidis* strains used in this study. St.Co. stands for strain collection number at the institute of molecular biosciences, university of Graz. 6: Origimm Biotechnology, 9: DSMZ.

Species	Strain	Alternative nomenclature	Serotype	Source	St.Co.
S. epidermidis	#51	S. epi PIA7	ST2	6	2251
S. epidermidis	#52	S. epi PIA 73	ST5	6	2252
S. epidermidis	#53	S. epi PIA 78	ST5	6	2253
S. epidermidis	#54	S. epi PIA12	ST12	6	2254
S. epidermidis	#55	S. epi PIA83	ST59	6	2255
S. epidermidis	#56	S. epi PIA 101	ST59	6	2256
S. epidermidis	#57	S. epi 1457,		6	2257
S. epidermidis	#58	S. epi LZ 4709		6	2258
S. epidermidis	#59	S. epi LZ 5128		6	2259
S. epidermidis	#150	DSMZ 1798; ATCC12228	ST8	9	2477
S. epidermidis	#151	DSMZ 20044; ATCC14990		9	2478
S. epidermidis	#152	DSMZ 28319; RP62A	ST10	9	2479

2. Methods

2.1. Strain handling and growth conditions

C. acnes and *S. epidermidis* strains obtained from commercial and academic sources [e.g. Leibniz Institute - German Collection of Microorganisms and Cell Cultures (DSMZ, Braunschweig, Germany), Sheila Patrick at Queen's University Belfast (Northern Ireland, UK), Andrej Trampuz at Pro-Implant Foundation, (Berlin, Germany), István Nagy at Biological Research Centre of the Hungarian Academy of Science (Budapest, Hungary), Origimm Biotechnology (Vienna, Graz)] were comparatively analyzed in this study (Tables 2 and 3). The *C. acnes* strain collection comprised 29 strains from human skin (healthy individual or acne patients) and 29 from deep tissue or implant-associated infections. All *C. acnes* strains were categorized into six phylotypes IA1, IA2, IB, IC, II and III by multiplex touchdown PCR for rapid typing (Barnard et al., 2015; McDowell et al., 2012). IA1 isolates were further sub-classified into SLST types according to Scholz et al. (Scholz et al., 2014). Incubation under anaerobic conditions took place by using (one or two) AnaeroGen™ 2.5 l (Thermo Scientific) sachets in combination with anaerobic containers (Thermo Scientific™ AnaeroPack™ Rectangular Jar or BD GasPak EZ incubation container). *C. acnes* was incubated using BHI as medium and *S. epidermidis* was incubated in TSB. As both species didn't harbor any antibiotic resistances, all laboratory work with opened bacteria cultures took place in the sterile work bench, with regularly ethanol sterilized surfaces, gloves and equipment.

2.2. Single locus sequence typing (SLST)

IA1 strains were further sub-typed using SLST technique previously published (Scholz et al., 2014). In short, cells were grown for 4 days on BHI agar plates and a large pellet was transferred into a screwable cryotube together with 200 µl of 0.1 mm glass beads and 500 µl of H_2O_f. After opening up the cells (by 6 alteration of shaking at 3000 rpm in the PowerLyzer for 30'' and 30'' cooling on ice) the glass beads were spun down for 1' (2000 x g) and the supernatant served as template for a PCR. The PCR was done according to New England Biolabs (NEB) protocol for Q5® High-Fidelity DNA Polymerase with following new primers according to Scholz et al.: forward 5'-CGCCATCAAGGCACCAACAA-3' and reverse 5'-ATATCGGCCCGTATTTGGGC-3'. DNA from PCR was purified by QIAquick PCR

purification kit according to the manufacturer protocol and eluted in H_2O_f. DNA eluate was combined with the forward primer according to protocol and sent in for sequencing by LGC Genomics.

2.3. MTP Biofilm Assay

Basic MTP biofilm quantification protocol. The initial assay based on published protocols for *C. acnes* biofilm, as well as expertise from the laboratory about *Vibro cholerae* biofilm (Coenye et al., 2007; Holmberg et al., 2009; Seper et al., 2014). The *C. acnes* strain was streaked onto a BHI agar plate from -80°C stock, incubated for 4 - 5 days anaerobically at 37°C and resolved in fresh BHI to an OD_{600} of 0.1. 150 µl of suspension were pipetted into the respective wells in a 96-well plate (U-bottom, polystyrene, Thermo Scientific) and incubated anaerobically at 37°C for 3, 5 or 7 days to assess biofilm dynamics. Afterwards, two wells per strain were resuspended by pipette and OD_{600} was measured in a platereader (SPECTOstarNano, BGM Labtech) to determine growth. The remaining wells (at least 6 per strain per plate) were used for biofilm quantification. After removing the supernatant containing non-sessile cells by pipette the biofilm was dried for approx. 50’ at 100°C on a heating block. To further dehydrate the biomass and increase fixation to the surface, 100 µl methanol was added for 10’ and removed again by pipetting. The plates were dried again for 30’ at 100°C and the remaining biofilm was stained with 0.1% crystal violet for 2’. Two washing steps followed by submerging the plates into basins of H_2O_{ve}. After gently tapping the plates onto a paper surface (to remove water residues) 150 µl of ethanol (96%) were added. The plates were incubated overnight at 4°C, followed by resuspension of the biofilm by pipette and a glass rod and measurement of the crystal violet concentration in ethanol by a platereader at 595 nm. At least 8 wells filled with sterile BHI served as sterile control and blank for quantification. The mean of all BHI control values was taken as blank and subtracted from each individual raw biofilm well value and served as biofilm quantification. All values from the same strain/condition were taken together and summed up in columns and displayed as median with interquartile range. For each strain at least 12 independent values from at least three different microtiter plates were used for the analysis.

Optimized MTP biofilm quantification assay. After investigating sources of variations in the biofilm processing, the assay was adjusted as follows. The *C. acnes*

strain was streaked onto a BHI agar plate from -80°C stock, incubated for 4 - 5 days anaerobically at 37°C and resolved in fresh BHI by vortexing to an OD_{600} of 0.01. The total volume of required bacterial suspension was mixed with the antiserum, affinity purified antibodies or saline / PBS and incubated for 1 h in rotation (1 spin per 2 seconds) at RT, aerobically, to reach full opsonization of the cells. A sample / condition combination was pipetted into a single row of 8 wells, into at least 4, optimally 8 replicates of plates. The plates were incubated for 16 – 17 h at 37°C, anaerobically. One well per sample/condition combination was resuspended by pipette and OD_{600} was measured in a platereader (SPECTOstarNano, BGM Labtech) to determine growth. The remaining six wells were used for biofilm quantification. After removing the supernatant by a 96-well platewasher the biofilm was dried for 1h 15' at 50°C in an incubator. To further dehydrate the biomass and increase fixation to the surface, 100 µl methanol was added for 10' and removed again by the platewasher. The plates were dried again for 10' at 50°C in the incubator and the remaining biofilm was stained with 0.1% crystal violet for 2'. Crystal violet was removed by multichannel-pipette. Two washing steps followed by adding 180 µl H_2O_{ve} to each well by multichannel-pipette and removing the supernatant again. After gently tapping the plates onto a paper surface (to remove water residues), 150 µl of ethanol (96%) were added. To minimize ethanol evaporation in the wells, a box (usually used for anaerobic incubation) was prepared by covering its ground with a thin layer of ethanol (96%). The plates were sealed with Parafilm, placed in the box and after closing incubated at RT for at least 3 h. 50 µl of ethanol/crystal violet suspension were pipetted to 100 µl fresh ethanol (96%) (1:3 dilution) into a new 96-well plate and measured at 595 nm. After subtracting blank (wells filled only with sterile BHI and processed equally) from each well, the dilution was back-calculated and biofilm formation shown by median and interquartile range.

***S. epidermidis* MTP biofilm quantification assay.** *S. epidermidis* strain was streaked onto a TSB agar plate from -80°C stock, incubated ON aerobically at 37°C and resolved in fresh TSB by vortexing to an OD_{600} of 0.1. Strain #51, #53, #54, #56, #57, #58 and #152 were further diluted to 0.001, strain #52, #55, #59, #150 and #151 to 0.01 in TSB. If the experiment contained antibodies, then the total volume of required bacterial suspension was mixed with the affinity purified antibodies and incubated for 1 h in rotation (1 spin per 2 seconds) at RT, aerobically,

to reach full opsonization of the cells. For an initial test, flat-bottomed (Greiner bio-one) 96-well plates were tested. All other experiments were performed in U-formed 96- MTPs (Thermo scientific). A sample / condition combination was pipetted into a single row of 7 wells, into at least 5 (condition testing) or 6 (antibody testing) replicates of plates. The plates were incubated for 20 – 22 h either at 37°C aerobically (antibody testing), or under variations of temperature (37°C and RT) and oxygen condition (aerobically or anaerobically). One well per sample / condition combination was resuspended by pipette, diluted 1:2 and OD_{600} was measured in a platereader (SPECTOstarNano, BGM Labtech) to determine growth. The remaining six wells were used for biofilm quantification. Two replicates (of the six antibody test plates) were washed in 200 µl H_2O_{ve} three times by multichannel pipette. After removing the supernatant by a 96-well platewasher, the biofilm was dried for 1h 15' at 50°C in an incubator. To further dehydrate the biomass and increase fixation to the surface, 100 µl methanol was added for 10' and removed again by the platewasher. The plates were dried again for 10' at 50°C in the incubator and the remaining biofilm was stained with 0.1% crystal violet for 2'. Crystal violet was removed by multichannel-pipette. Two washing steps followed by adding 180 µl H_2O_{ve} to each well by multichannel pipette and removing the supernatant again. After gently tapping the plates onto a paper surface (to remove water residues), 150 µl of ethanol (96%) were added. To minimize ethanol evaporation in the wells, a box (usually used for anaerobic incubation) was prepared by covering its ground with a thin layer of ethanol (96%). The plates were sealed with Parafilm, placed in the box and after closing incubated at RT ON. 50 µl of ethanol / crystal violet suspension were pipetted to 100 µl fresh ethanol (96%) (1:3 dilution) into a new 96-well plate and measured at 595 nm. After subtracting blank (wells filled only with sterile TSB and processed equally) from each well the dilution was back-calculated and biofilm formation shown by median and interquartile range.

2.4. Microscopical evaluation of biofilms

Attachment, biofilm fluorescence microscopy and Comstat quantification. The "flowcell" comprised a three-channel flow-cell chamber (DTU Systems Biology, Technical University of Denmark) with a cover slip (24 x 50 mm, Menzel-Glaeser) glued on top with AquaSil® glue. Each channel contained two holes at the end (~ 1 mm in diameter) and ~ 200 µl of volume. To grow a mature biofilm on the surface of

the cover slip, 200 µl of the inoculum (*C. acnes* resolved in BHI broth with starting OD_{600} of 0.1) was injected into a chamber of the flowcell and incubated for 5 days anaerobically at 37°C. Afterwards, non-attached cells were removed by washing the biofilm with 3 ml of BHI broth (33 µl / second flow rate) and staining with 200 µl BHI broth supplemented with SYTO 9 (5 µM final concentration) to visualize biofilm structures or SYTO9 (5 µM final concentration) in combination with propidium iodide (30 µM final concentration) to evaluate viability. To measure attachment capacities of *C. acnes*, 200 µl of the inoculum (*C. acnes* resolved in BHI broth with a starting OD_{600} of 1) was injected into a chamber of the flowcell and incubated for 1 h aerobically at RT to allow sedimentation and attachment to the cover slip. Afterwards, non-attached cells were removed by washing the attached cells with 3 ml of BHI broth (33 µl / second flow rate) and staining with 200 µl BHI broth supplemented with SYTO 9 (5 µM). Z-stack images of biofilms or attached cells were recorded with an Inverted Microscope Eclipse Ti-E (Nikon™) using either an FITC-3540C (SYTO9) or TXRED-4040C filter (PI). Optical sectioning was performed in 0.3 µm steps. For visualization and processing of image data, the Leica LAS AF Lite and ImageJ 1.46 software was used. Quantification and morphological analysis of image stacks was performed using the computer program COMSTAT 2 (Heydorn et al., 2000; Vorregaard, 2008). Attachment was determined by surface coverage evaluation of at least ten images from at least four independent experiments. In case of the three-dimensional analysis of biofilms at least twelve image stacks from four independent experiments with each of the *C. acnes* isolates were used.

***S. epidermidis* biofilm fluorescence microscopy and Comstat quantification.** To grow a mature biofilm on the surface of the cover slip, 200 µl of the inoculum (*S. epidermidis* resolved in TSB broth with starting OD_{600} of 0.01) was injected into a flowcell chamber and incubated for 20 – 22 h aerobically or anaerobically at 37°C. Afterwards, non-attached cells were removed by washing the biofilm with 2 ml of TSB saline (66 µl / second flow rate) and staining with 200 µl saline supplemented with SYTO 9 (5 µM final concentration) to visualize biofilm structures. Z-stack images of biofilms or attached cells were recorded with an Inverted Microscope Eclipse Ti-E (Nikon™) using an FITC-3540C (SYTO9) filter. Each sample combination was performed in three flowcell chambers, imaging two z-stacks in each. Optical sectioning was performed in 0.5 µm steps. Laser was set to 1 / 32th (weakest) intensity for 300 ms to reduce bleaching effects. For visualization and

processing of image data, the Leica LAS AF Lite and ImageJ 1.46 software was used. Quantification and morphological analysis of image stacks was performed using the computer program COMSTAT 2 (Heydorn et al., 2000; Vorregaard, 2008).

2.5. Proteinase K / DNase I sensitivity and efficacy assays

Impact of proteinase K or DNase I treatment on *C. acnes* viability. *C. acnes* (final OD_{600} = 1) and proteinase K or DNase I (final concentration = 1 mg / ml) were mixed in BHI broth and incubated for 4 h at 37°C. BHI broth only served as mock-treated control. Subsequently, 10 fold dilutions in BHI were plated onto BHI agar plates and incubated for 4 days anaerobically at 37°C. Only plates with CFU count between 20 and 400 were evaluated. The assay was performed in triplicate.

Proteinase K- and DNase I-treated basic biofilm quantification protocol in MTP assay. To quantify proteinase K and DNase I effects on biofilm formation, the basic MTP biofilm assay was slightly modified. Sterile filtrated stock solutions (both 10 mg / ml) of proteinase K (Roth, 30 mAnson U / mg) and DNase I (AppliChem, 5,000 U / mg) were freshly prepared in BHI broth for each experiment. Strains IA1-s1 and IA1-i1 were prepared for these experiments according to the optimized protocol and incubated for 5 days to form a mature biofilm (in BHI, 37°C, anaerobically). 50 µl of DNase I or proteinase K stock solution dilutions were added to each well to reach the respective 125 mg / ml to 0.12 ng / ml. Addition of 50 µl sterile BHI broth served as mock-treated control. After incubation (37°C, 4 h, aerobically) the biofilms were washed and finally quantified according to the optimized MTP protocol.

Proteinase K and DNase I treatment of *C. acnes* attachment and biofilms in flowcell chambers. To test the effects of proteinase K or DNase I on biofilm formation and surface attachment, the flow-cell chamber assays were performed (as described above) with following modifications: Filter-sterilized stock solutions (10 mg / ml) of proteinase K (Roth, 30 mAnson-U / mg) and DNase I (AppliChem, 5.000 U / mg) were prepared freshly in BHI broth prior to each experiment. For the attachment assay, before injecting the inoculum of 1 OD_{600} into the flowcell, it was mixed with proteinase K or DNase I (final concentration 1 mg / ml) and incubated for 4 h at 37°C, aerobically. An inoculum treated with BHI only served as mock control. For the biofilm assay, after the cells grew into 5-day old biofilm in a flowcell chamber, 200 µl of BHI broth supplemented with proteinase K or DNase I (final

concentration 1 mg / ml) was injected into the chamber and incubated at 37°C for 4h aerobically. Injection of 200 µl BHI broth served as mock-treated control. Afterwards, the standard protocol was continued with the 3 ml BHI washing step.

2.6. Planktonic and biofilm stage characterization

Microscopy of planktonic and biofilm cells. The strain was streaked from -80°C stock onto a BHI agar plate and incubated for 3 to 5 days anaerobically at 37°C. The grown colonies were used to set BHI broth to an OD_{600} of 0.1. An aliquot was diluted 1 to 5 in fresh BHI broth to an OD_{600} of 0.02 and incubated for 75 hours at 160 rpm (37°C, anaerobically) for biofilm derived cells. The rest was pelletized by centrifugation (10', RT, 3000 x g), plated onto a fresh BHI agar plate and incubated for 58 h as passage (37°C, anaerobically). After time passed, the passage cells were used to set BHI broth to an OD_{600} of 0.1 and incubated for 16 hours for planktonic derived cells (37°C, anaerobically). Aliquots of both physiological states were mixed with SYTO9 fluorescence dye (to 5 µM final concentration), injected into a flowcell and microscoped.

Coomassie staining of planktonic and biofilm derived proteins. Planktonic and biofilm derived cells were grown as described above. Cells were centrifuged (17,000 x g, 4°C, 20') and the pellet was transferred to a screwable cryotube together with 200 µl volume of 0.1 mm glass beads and 1.5 ml of PBS. After opening up the cells (by 6 alteration of shaking at 3000 rpm in the PowerLyzer for 30'' and 30'' cooling on ice), the glass beads were spun down for 1' (2000 x g, 4°C) and the supernatant (carefully without glass beads and non-lysed cells) was transferred to a fresh Eppendorf tube and termed whole cell lysate (WCL). This was centrifuged (1', 10,000 x g, 4°C) and the supernatant brought to a new tube, followed by centrifugation (30', 16,000 x g, 4°C). The pellet was resolved in 20 – 75 µl PBS and termed membrane-associated fraction (MF). WCL and MF of planktonic and biofilm mode and all phylotype reference strains were applied to self-made 12% gel, separated by SDS-PAGE and stained by Coomassie. See immunoblot section (chapter II, section 2.9) for self-made gel SDS-PAGE protocol. Prestained Protein Marker Broad Range (New England Biolabs) was used as molecular mass standard (7 – 175 kDa).

Large scale protein separation for Mass Spectrometry. Approx. 500 µg protein of WCL or MF were mixed with Lämmli, boiled for 20’ at 100°C and loaded onto each slot. Prestained Protein Marker Broad Range (New England Biolabs) was used as molecular mass standard (7 – 175 kDa). SDS-PAGE was performed for at least 6 h at 300 V at 4°C. Kang solution staining took place overnight at RT. Bands of interest were cut out and sent for mass spectrometry.

Mass Spectrometry. Mass spectrometry-based protein identification was performed at the IZKF Core Unit Proteomics of the Medical Faculty of the University of Münster. The LC-MS/MS data were analyzed by searching the non-redundant Uniprot database.

2.7. Immunocytochemistry

Cy3-visualization of antisera in situ. The strain was streaked from -80°C stock onto a BHI agar plate and incubated for 3 to 5 days anaerobically at 37°C. The grown colonies were used to set BHI broth to an OD_{600} of 0.1. An aliquot was diluted 1 to 5 in fresh BHI broth to an OD_{600} of 0.02 and incubated for 75 hours at 160 rpm (37°C, anaerobically) for biofilm derived cells. Another aliquot at 0.1 OD_{600} was directly incubated for 16 hours for planktonic derived cells (37°C, anaerobically). When finished, the cells were brought an OD_{600} of 0.3 and 1 ml was centrifuged for 15’ (10,000 x g, RT). The pellet was resolved in 1 ml PBS + 2% BSA by vortexing (for all pellets in this protocol, until all macroscopically visible aggregates disappeared) and incubated for 15’ in rotation (1 spin per 2’’). Antiserum was added to the solution in a dilution of 1:5000 and incubated for 1 h in rotation. The cells were centrifuged (15’, 10,000 x g, RT) and the pellet was washed two times by resolving in PBS + 0.5% BSA and centrifuged for 15’ at 10,000 x g and RT. The pellet was resolved in 1 ml PBS + 2% BSA and the secondary antibody Cy3 (1:2000) and incubated for 1 h in rotation. Finally, three washing steps followed (see above). The pellet was resolved in 1 ml PBS + DAPI (5 µg / ml), injected into a flowcell chamber and microscoped after 20’ of incubation. Cell DNA was visualized by DAPI staining in DAPI filters (DAPI-1160B Filter) and serum antibody binding location was shown by Cy3 fluorescence in TRITC filters (TRITC-B Filter).

Iron starvation conditions by bipyridyl. Bipyridyl powder was stirred in H_2O_{dd} for approximately 1 – 2 h at RT to a final stock concentration of 33 mM. The liquid was

sterile filtrated (0.2 µm) and stored at 4°C. To create iron starvation conditions, bipyridyl was added to planktonic cells in exponential growth phase and to biofilm cells in late exponential / early stationary phase cells, both 16 h before harvest and microscopy. 100 µM bipyridyl was chosen as final concentration for phylotype III strains, 250 µM for IA2, IC and IB and 500 µM for type IA1 and II. Addition of sterile H_2O_{dd} instead served as mock-treated control.

2.8. Opsonophagocytosis

HL60 cells were differentiated into phagocytic cells (dHL60) according to previously published protocol (Manda-Handzlik et al., 2018). In parallel, *C. acnes* was taken from the BHI agar plate, resuspended in saline, prepared to an OD_{600} of 0.5 and incubated with antiserum (1:1000 dilution) for 1 hour in rotation (1 spin / 2 seconds) at RT. After two washing steps in saline (centrifugation 10.000 x g, RT, 8' and resolving the pellet in fresh saline), Cy3 secondary antibodies were added (1:1000 dilution) and again incubated the same way. Excessive antibodies were washed away thrice in saline and the remaining pellet was resolved in fresh saline in a final OD_{600} of 0.1. 450 µl of dHL60 in RPMI medium were gently mixed with 50 µl of *C. acnes* suspension with 0.1 OD_{600}, leading to a final OD_{600} of ~ 0.01, 90% CCM, 10% saline solution and ~ 5 *10^5 cells / ml. DAPI (1 µl stock per 1 ml) and optionally DHR (to 500 mM final concentration) were added, gently mixed and ~ 200 µl were injected into a flowcell and incubated in a cell-culture incubator (37°C, aerobically, 5% CO_2, 90% humidity). While performing microscopy, environment changed to normal room conditions.

PI-protocol. Cells were treated as above, with following adaptions: in the first antibody opsonization step SYTO9 and DAPI were added additionally. Cy3 secondary antibodies were left out and in the co-incubation mixture DAPI was replaced by PI.

DL-350-protocol. Cells were treated as in the Cy3-protocol, with following adaptions: DyLight 350 secondary antibodies (1:500) replaced Cy3 antibodies, DAPI was left out and DHR added.

2.9. Immunoblot Assays

Creating planktonic and biofilm cells. The strain was streaked from -80°C stock onto a BHI agar plate and incubated for 3 to 5 days anaerobically at 37°C. The

grown colonies were used to set BHI broth to an OD_{600} of 0.1. An aliquot was diluted 1 to 5 in fresh BHI broth to an OD_{600} of 0.02 and incubated for 75 hours at 160 rpm (37°C, anaerobically) for biofilm derived cells. Another aliquot at 0.1 OD_{600} was directly incubated for 16 h for planktonic derived cells (37°C, anaerobically). To create iron starvation conditions, bipyridyl was added to planktonic cells in exponential growth phase and to biofilm cells in late exponential / early stationary phase cells (final concentrations: 100 µM for phylotype III, 250 µM for IA2, IC and IB, and 500 µM for type IA1 and II), both 16 h before harvest. Addition of sterile H_2O_{dd} instead served as mock-treated control.

Fractionation protocol. Cells were centrifuged (17,000 x g, 4°C, 20') and the pellet was transferred to a screwable cryotube together with 200 µl volume of 0.1 mm glass beads and 1.5 ml of PBS. The supernatant was sterile filtrated, stored at -20°C and processed by TCA treatment later. After opening up the pellet cells (by 6 alteration of shaking at 3000 rpm in the PowerLyzer™ for 30'' and 30'' cooling on ice), the glass beads were spun down for 1' (2000 x g, 4°C) and the supernatant (carefully without glass beads and non-lysed cells) was transferred to a fresh Eppendorf tube and termed whole cell lysate (WCL). This was centrifuged (1', 10,000 x g, 4°C) and the supernatant brought to a new tube, followed by centrifugation (30', 16,000 x g, 4°C). The pellet was resolved in 20 – 75 µl PBS and termed membrane-associated fraction (MF). The supernatant was brought to a new tube and resembled the cytosolic fraction (CY). The initial supernatant (containing secreted proteins, stored at -20°C) was thawed, mixed with TCA to a final concentration of 10%, stored at 4°C for 1 h and frozen overnight at -20°C. The precipitated supernatant was thawed and centrifuged (30,000 x g, 4°C, 1 h). The pellet was washed thrice in acetone by resolving the pellet by ultrasonic bath and centrifugation (50,000 x g, 4°C, 1 h). The final pellet was air-dried and resolved in Lämmli buffer (200 µl Lämmli per 120 ml initial BHI volume) and named secreted fraction (SE).

SDS-PAGE, Coomassie staining and immunoblot. Self-made polyacryamide gels (consisting of a stacking gel and 10% polyacrylamide separation gel) were used for concentration determination of fractionated lysate (chapter III, section 6, immunoblot) or visualization of planktonic and biofilm derived whole cell lysate proteins or membrane-associated proteins of the different phylotypes (chapter III,

section 3, planktonic and biofilm stage determination). All immunoblots were performed using BioRad's 10% Stain-Free™ precast gels and PageRuler™ Prestained Protein Ladder (Thermo Scientific™) as molecular mass standard (10 – 180 kDa). Protein samples were mixed with Lämmli buffer, boiled for 20' and separated using the respective gel system (self-made or Stain-Free™) by sodium dodecyl sulfate-polyacrylamide gel electrophoresis (SDS-PAGE) in running buffer for approximately 1 h at 100 V or at least 18 mA per gel. For protein visualization, the self-made gel was washed twice in H_2O_{ve} (for 10') and incubated in Kang solution overnight until proteins were stained by Coomassie (Kang et al., 2002).

For continuing the immunoblot, the Stain-Free™ gel was transferred to a PBS filled tray and UV-activated for 1' in the ChemiDoc™. An image of protein bands was taken. The LF PVDF membrane (low fluorescence polyvinylidene difluoride, BioRad) was activated for a few minutes in methanol and proteins within the Stain-Free™ gel were blotted onto it in 4°C cooled CAPS buffer for 90' and 220mA. The membrane was again transferred to a PBS filled tray and an image taken in the ChemiDoc™ to evaluate blotting quality. Blots with altered or bad blotting quality were discarded. Now, the membrane was blocked by TBS+10%MP for 2 h at RT. TBS+10%MP was discarded and antiserum was added to fresh TBS+10%MP (1:7500) and incubated together with the membrane overnight at 4°C. Three washing steps followed using TBS-T for 10' and once TBS for 10'. Secondary antibody (GAM-HRP or GAR-HRP) was mixed in TBS+10%MP (1:7500) and incubated for 2 h at RT. Again, membrane was washed 3x in TBS-T for 15' and 1x in TBS for 10'. TBS was removed and 2 ml of Clarity™ ECL (BioRad) were added for 1' and antibody mediated protein signals were immuno-detected in the ChemiDoc™. The immunoblot's signal intensity was quantified using BioRad's ImageLab™ software. The last recorded image before the recombinant protein's signal reached saturation was chosen for evaluation. Each complete lane was quantified and divided by the recombinant protein's signal of the respective western blot. This way quantitative values were normalized to the recombinant protein's signal with defined protein amounts (40 ng).

III. Results and Discussion

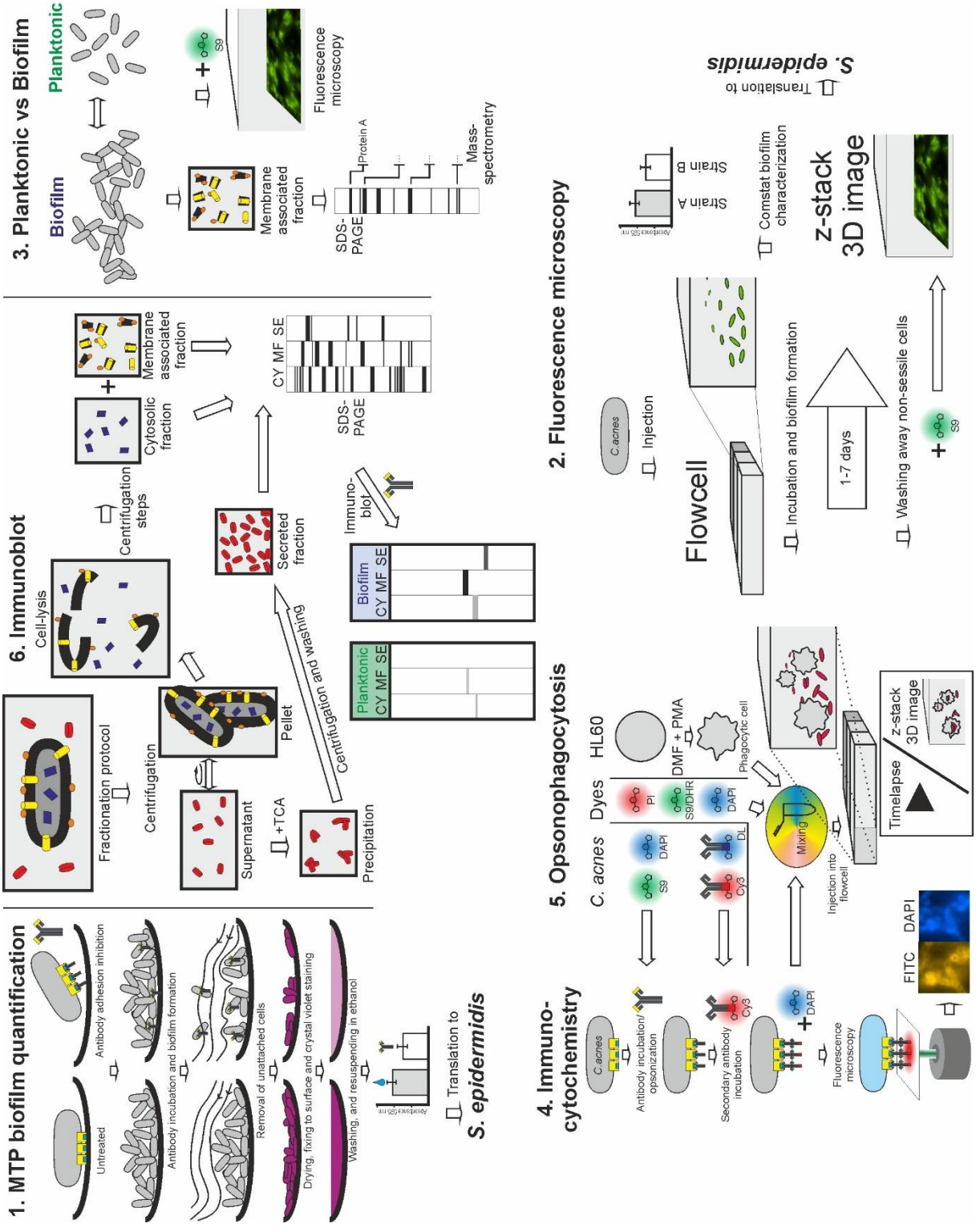

Figure 1: Overview of the thesis projects.

1. MTP Biofilm Assay

This section describes the establishment of an MTP assay, as well as the biofilm quantification of *C. acnes* and *S. epidermidis* strains. Furthermore, effects of DNase, proteinase K and antibodies were tested.

Sub-sections 1, 2 and 3 were previously published in the International Journal of Medical Microbiology (Kuehnast et al., 2018) and either taken as a whole or modified for this thesis.

1.1. Biofilm formation capacity correlated with phylotype

58 *C. acnes* isolates comprising 29 strains from human skin (healthy individuals or acne patients) and 29 from deep tissue or implant-associated infections were used for comparative analyses of biofilm formation (Table 2). All strains were categorized into the six phylotypes (IA1, IA2, IB, IC, II and III) by multiplex touchdown PCR for rapid typing (Barnard et al., 2015; McDowell et al., 2012). To determine the biofilm formation capacity of diverse *C. acnes* isolates on abiotic surfaces, a basic microtiter plate (MTP) biofilm assay was previously established (Fig. 1, part 1, MTP biofilm quantification). In short, *C. acnes* was incubated in 96-well plates forming biofilm on its surface, then non-sessile cells were removed by aspiration and the plate was dried, fixed by methanol, dried again and the remaining biomass was stained by crystal violet. After washing away excessive dye, the remaining crystal violet (bound to biomass) was resolved again by ethanol. Finally, the crystal violet concentration in ethanol was quantified by a platereader at 595 nm. The assay thus translated attached biomass after aspiration to a quantitative value. These preliminary studies also showed that Brain Heart Infusion medium (BHI) delivered the most pronounced and stable biofilm formation results (see master thesis, Torben Kühnast, 2016). This research was further pursued by determining individual biofilm formation of all available isolates (Fig. 2). As the diverse *C. acnes* isolates featured variations in growth speed (Fig. 2A, B and C), the amount of biofilm detected at a given time was normalized to the respective growth (OD_{600}) and termed ratio. Biofilm formation was quantified at 72 h, 120 h and 168 h to monitor the biofilm formation dynamics of the different *C. acnes* isolates (Fig. 2).

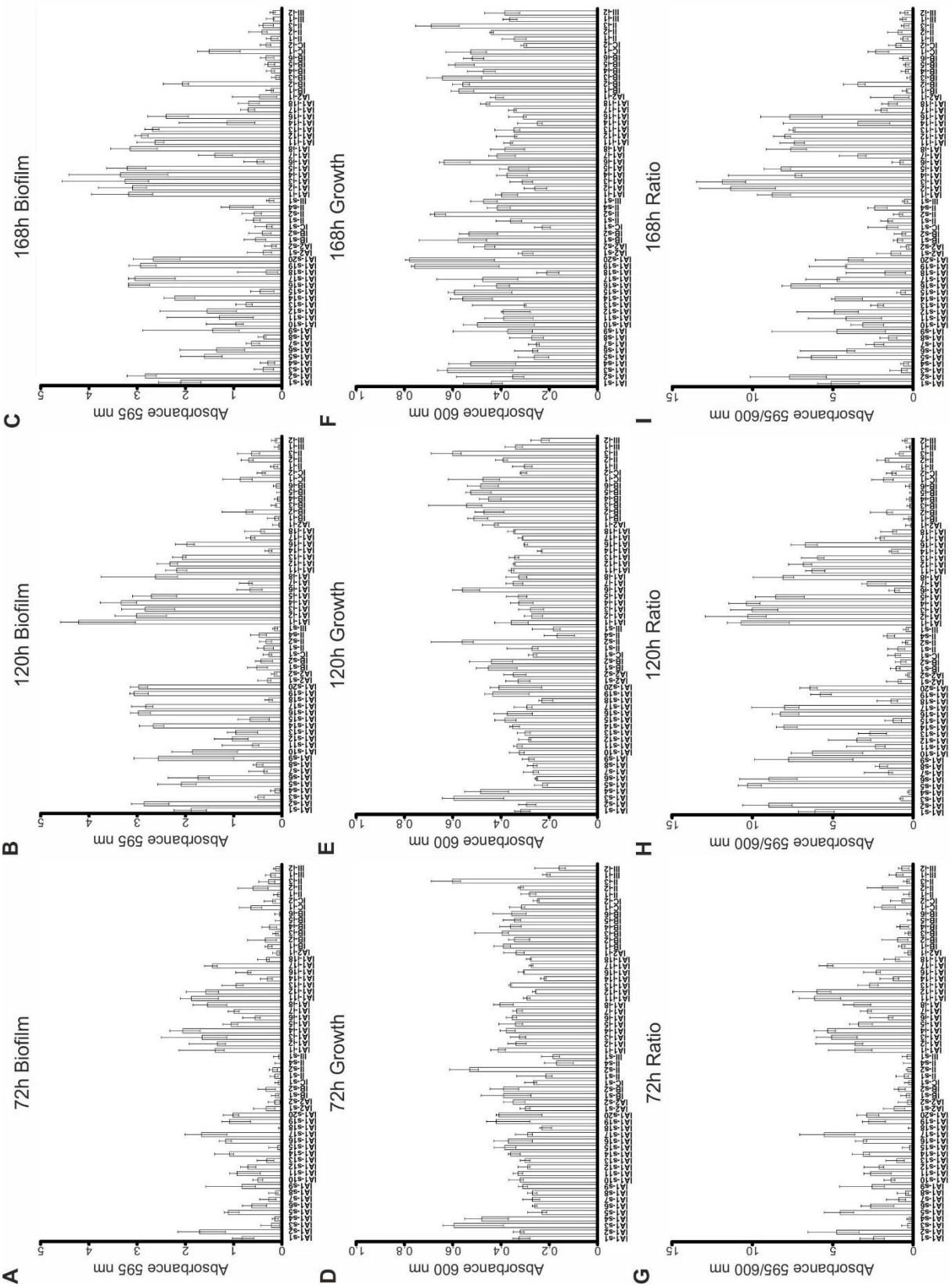

Figure 2: MTP biofilm quantification of single *C. acnes* isolates Biofilm formation of *C. acnes* isolates was quantified after 72 h (A, D, G), 120 h (B, E, H) and 168 h (C, F, I). The biofilm formation capacity is shown as OD_{595} obtained after crystal violet staining (A, B, C), growth by OD_{600} measurement (D, E, F) or as ratio of biofilm formation divided by growth (G, H, I). The amount of individual isolates incorporated in each data set is given in parenthesis.

12 independent values from each individual isolate are included in each data set and visualized by median and interquartile range. Figure was taken from Kuehnast et al., 2018.

In case of *C. acnes* isolates with low biofilm formation, maximum levels were already reached at 72 h. In contrast, isolates with robust biofilm formation generally showed an increase in biofilm production from 72 h to 120 h, but then leveled off and showed no further increase from 120 h to 168 h. As for most isolates biofilm formation did not significantly increase between 120 h to 168 h, the investigated period likely covered biofilm formation up to mature biofilms. Both, biofilm and growth varied greatly between the isolates. This paragraph was modified from Kuehnast et al., 2018.

After 120 h of incubation, strains IA1-s6 to IA1-s9 grew to a similar OD_{600} of ~ 0.3 (Fig. 2E). On the other hand, the same isolates on the same plates with same growth speed led to distinct biofilm formations of 2-3 relative absorbance units (RAU) for strain IA1-s6 and IA1-s9 and 0.5 RAU for IA1-s7 and IA1-s8. These results generally verified the assay's functionality and shed light onto *C. acnes* biofilm heterogeneity even between skin derived isolates from the same IA1 phylotype. To analyze whether the capacity for biofilm formation depends on the phylotype or the anatomical site of isolation (skin or implant), all 58 strains were sorted into the respective groups (Fig. 3). Although, as described above, isolates of a particular phylotype exhibited a distinct heterogeneity in biofilm formation, there were obvious differences between the phylotype groups. IA1 isolates from skin and implants formed significantly more biofilm, 2–8 fold more than other phylotypes in almost all cases (Fig. 3A and B, black asterisks comparing IA1 skin isolates to the other phylotypes, blue asterisk comparing implant-associated IA1 isolates to the other phylotypes). Similar patterns of biofilm formation with and without normalization to growth were observed, suggesting that growth differences of the same phylotypes have only minor impact on the overall biofilm production (Fig. 3A and B). Based on median biofilm levels, IA1 strains were followed by IC, IA2 and II isolates, whereas isolates of the IB and III phylotype showed lowest biofilm formation in these assays. However, it should be noted that the differences in biofilm formation among non-IA1 phylotypes under the chosen conditions of the MTP assay were rather small. From the perspective of all IB grouped isolates, which represented poor biofilm producers, significantly higher biofilm formation was detectable only for phylotype IA1 at all time points (Fig. 3A and B, orange asterisk). Phylotype IC showed significantly increased biofilm formation as well, though not under all conditions. In general, the site of isolation had no significant impact on the biofilm formation capacity. Notably,

implant-derived IA1 strains (IA1-i) showed slightly, but not significantly increased biofilm amounts compared to the skin-derived IA-1 strains (IA1-s), especially at 168 h. In summary, biofilm formation predominantly depended on the phylotype and not on the anatomical site of isolation. This paragraph was adapted from Kuehnast et al., 2018.

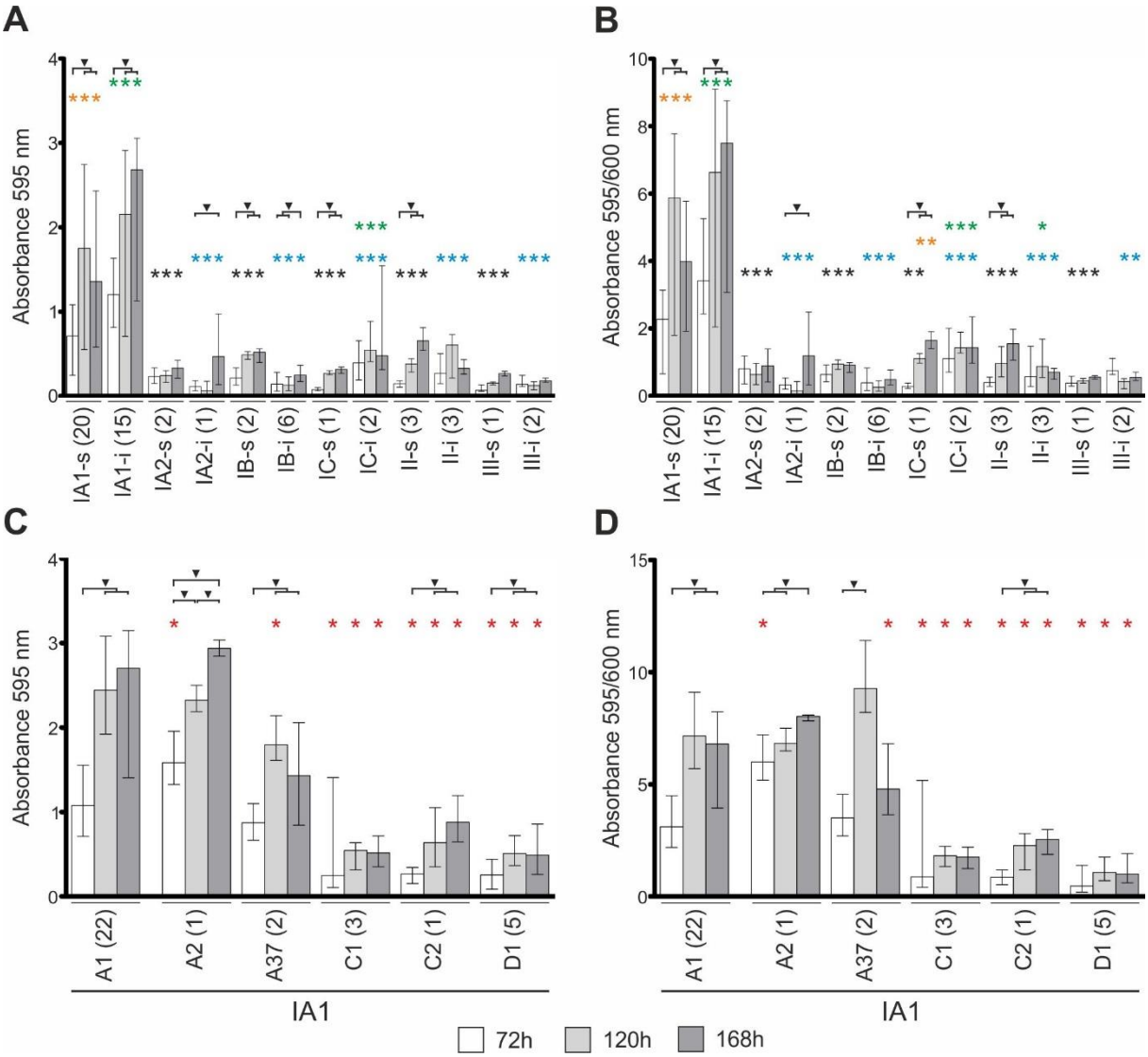

Figure 3: MTP biofilm quantification sorted by phylotype and SLST. (A and B) The biofilm formation of *C. acnes* isolates was categorized into the six phylotypes IA1, IA2, IB, IC, II and III and anatomical isolation sites (-s = skin and –i = implant) and quantified after 72 h (open bars), 120 h (light gray) and 168 h (dark gray). (C and D) Biofilm formation of *C. acnes* IA1-s and IA1-i isolates was further discriminated by SLST into the sub-types A1, A2, A37, C1, C2 and D1. The biofilm formation capacity is shown as OD_{595} (A, C) obtained after crystal violet staining or as ratio (B, D) of OD_{595} obtained after crystal violet staining divided by growth determined by OD_{600} measurement. (A–D) The amount of individual isolates incorporated in each data set is given in parenthesis. 12 independent values from each individual isolate are included in each data set (isolate-specific data sets are provided in Fig. 2). Shown are the medians with interquartile range. Significant differences are indicated as follows ($P < 0.05$, Kruskal-Wallis test followed by post hoc Dunn's multiple comparisons): Significant differences

in the biofilm amount of a respective isolates at 72 h, 120 h or 168 h are indicated by black triangles, significant differences of IA1-s to other skin-derived isolates at a given time point are indicated by black asterisks, significant differences of IA1-i to other implant-derived isolates at a given time point are indicated by blue asterisks, significant differences of IB-s or IB-i to other skin- or implant-derived isolates at a given time point are indicated by orange or green asterisks respectively. Significant differences of A1 to other clusters at a given time point are indicated by red asterisks. Figure and legend were taken and modified from Kuehnast et al., 2018.

1.2. SLST sub-types A1 and A2 of phylotype IA1 constituted high biofilm formation

As the variation in biofilm formation of IA1 isolates was high, all available IA1 strains were further sub-classified by single locus sequence typing (SLST) (Fig. 3C and D). By that the grouped variation was reduced, with highest biofilm amounts produced by sub-type A1 (22 isolates) and A2 (1 isolate), both corresponding to MLST clade CC18 of the Aarhus scheme or CC-1 of the Belfast scheme, respectively (Lomholt and Kilian, 2010; McDowell et al., 2012; Scholz et al., 2014). Sub-types C1, C2 (corresponding to CC-3 in the Aarhus and Belfast scheme) and D1 (corresponding to CC28 of the Aarhus scheme or CC-4 of the Belfast scheme, respectively) showed significantly lower biofilm formation compared to A1. Thus, the higher biofilm formation capacity of the grouped IA1 strains mainly relied on sub-types A1, A2 and the newly identified sub-type A37. It was reported that the clonal complexes CC3, CC18 and CC28, as well as sequence type 18 (ST) within CC18, were strongly associated with moderate to severe acne (Kilian et al., 2012; Lomholt and Kilian, 2010). Another study targeting the population of Southern California found a strong association of ribotype RT4 and RT5 to acne, and RT6 (phylotype II) to healthy skin (Fitz-Gibbon et al., 2013). RT4 corresponds to CC3 (Belfast/Aarhus) and C1-5 (SLST). RT5 corresponds to CC18 and CC28 (Aarhus), CC-1 and CC-107 (Belfast) and A1 – A37, D1 – D5 and G1 (SLST). These resembled mostly IA1 phylotype and IC (based on classic *tly* and *recA* gene typing). In a more recent study, Lomholt et al. pinpointed follicular isolates from Danish acne patients to IA1 phylotype, in particular to mostly CC18 of phylotype IA1 or ST3 in one case (Lomholt et al., 2017). Follicular isolates of healthy individuals contained a more heterogeneous population (IA1, IA2, IB and II). Taken together, mostly IA1 subtypes could be isolated from mild to severe acne. In particular, clonal complex 18 seemed to play key roles in all of the studies, peaking in the most recent one where it was found almost exclusively in acne follicles. This paragraph was adapted from Kuehnast et al., 2018.

However, it must be mentioned that CC18 was not a necessity for acne to occur, admitting virulent features also to the other phylotypes. Interpreting former studies and our results, it seems the *C. acnes* species possesses a wide arsenal of very soft (and hard to pinpoint) virulence factors, gradually increasing from phylotype IA2 and IC over IA1 to specific subpopulations like ST3 and CC18 (Aarhus scheme). All are able to cause acne, but the latter ones may have a slight advantage the harder the selection pressure becomes. One of these advantages might be connected to biofilm and the factors which mediate the increased results under the MTP conditions. These factors might include the formation of significantly more robust biofilm. In particular, it was able to adhere to the steep abiotic polystyrene surface while others partially sedimented to the bottom of the well. While being attached, it also reinforced attachment and built up a biofilm structure compact enough to resist the applied aspiration forces. Taking into account that such features as compact biofilm could be beneficial as defense strategy against host immune cells, this correlation could have causative connections and should be investigated further.

1.3. Proteinase K and DNase I treatment significantly reduced biofilm formation

The biofilm matrix of *C. acnes* strain KPA171202 (type IB) is composed of (among others) carbohydrates, proteins and extracellular DNA (Jahns et al., 2016). If proteins and eDNA mediated key factors of biofilm integrity, treatment with proteinase K or DNase I would affect biofilm quantification. Simultaneously, detecting effects would verify validity of the MTP assay in general. Therefore, phylotype IA1 reference strains (from skin and implant) were grown to form a mature biofilm, exposed to several different enzyme concentrations and processed according to biofilm quantification assay protocol. IA1 biofilms in the MTPs were susceptible to both, DNase I- and proteinase K-treatment (Fig. 4). In comparison to the mock-treated control, significant reductions of biofilm formation were observed with proteinase K concentrations down to 1.9 µg / ml and DNase I concentrations down to 1.9 ng / ml. This paragraph was adapted from Kuehnast et al., 2018.

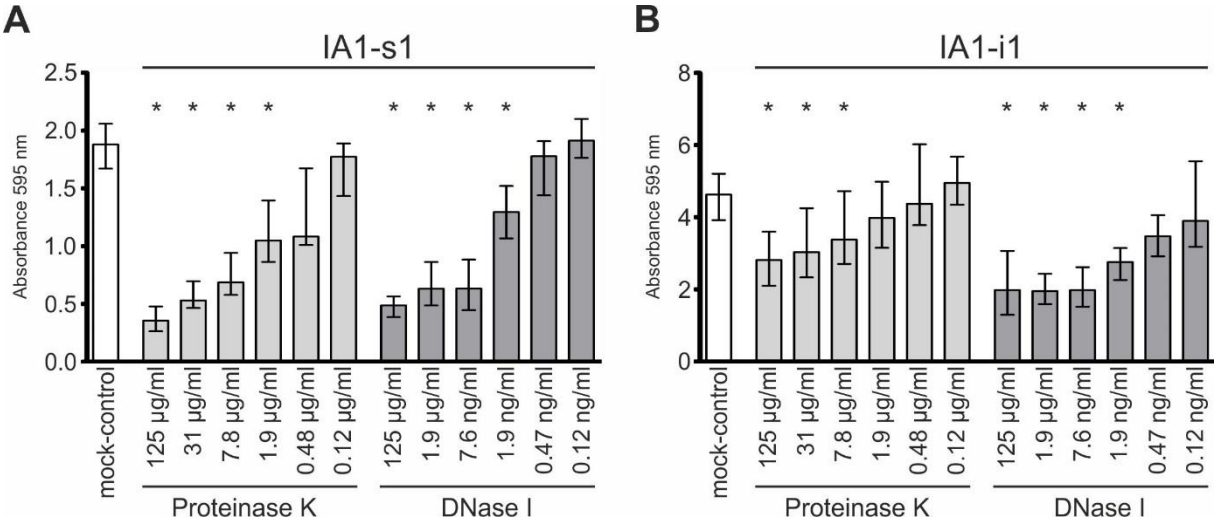

Figure 4: Impact of proteinase K and DNase I on *C. acnes* MTP biofilm quantification. 120 h old biofilms of reference isolates IA1-s1 (A) and IA1-i1 (B) were incubated for 4 h with serial dilutions of proteinase K (light gray), DNase I (dark gray,) or mock-treated control (open bars). Shown are the medians with interquartile range. At least 32 independent values were included for each data set. Significant reduction compared to the mock-treated control is indicated by an asterisk ($P < 0.05$, Kruskal-Wallis test followed by post hoc Dunn's multiple comparisons). Figure and legend were taken and modified from Kuehnast et al., 2018.

Biofilm integrity of IA1 strains essentially depended on proteins and eDNA. Removal of either led to its gradual collapse. These findings suggest that proteins of IA1 play a key role in biofilm formation of *C. acnes* and could be targeted for therapeutic intervention strategies. Furthermore, the MTP assay should be capable to reveal such effects.

1.4. Assay optimizations to reduce variation and increase quality

The basic assay was initially established to investigate phylotype and isolate specific biofilm formation. As biofilm formation between the phylotypes varied strongly, distinct significant differences could be revealed even through the given background of variations. However, to see more refined influences of antibodies on the same isolate and increase the quality of the assay, the variations were to be reduced.

The first step involved defining a test setup which would allow for identifying variations quickly. For this purpose, a 96-well plate was filled with the same *C. acnes* material and processed according to protocol. As the final protocol was supposed to compare a column of 8 wells with a specific condition to a neighboring column of 8 wells with a different condition, the 96-well plate of the test assay was split into 12 columns (8 wells each) as well. These 8 wells of each column were translated to quantitative values and combined to one median with interquartile range. As example, an early stage ("initial")

protocol showed a differential distribution of medians/interquartile range, following a curve with low values at the peripheral columns and higher values in the center (Fig. 5A). Starting from this point, most steps of the protocol were varied to find conditions with reduced deviation and increased stability (Fig. 6, optimizations).

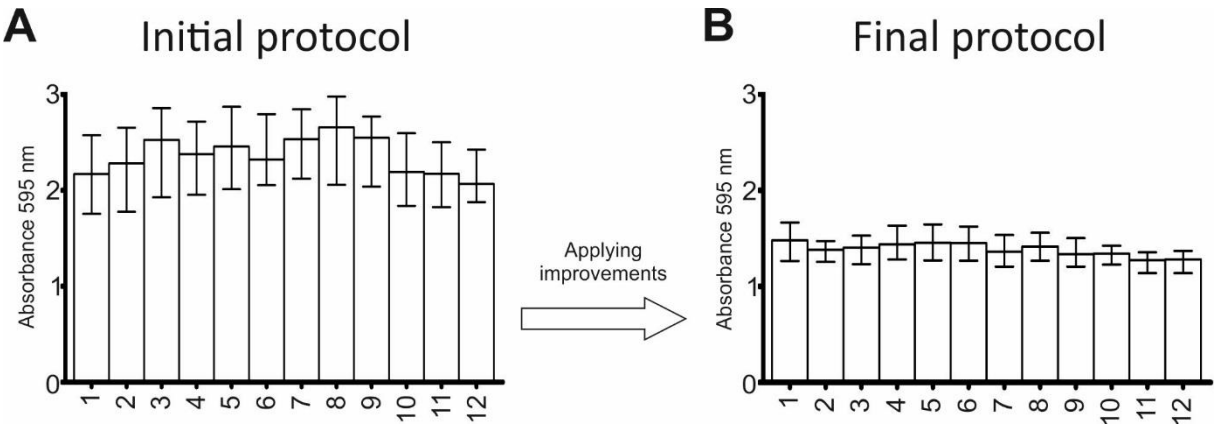

Figure 5: Optimizations of MTP biofilm quantification assay. IA1-s1 biofilm was quantified following the initial protocol (panel A, based on initial protocol in Fig. 6) or the final protocol after optimizations (panel B, optimizations in Fig. 6). 96-well microtiter plates were filled with bacterial resuspension from the same master mix, incubated and processed according to the respective MTP biofilm quantification protocol. Each column contains the biofilm values of 8 wells (in the lane corresponding to the numbers in the graph) on each plate from at least 6 plates, showing median and interquartile range. In total, the values were brought to relative absorbance values between 1 and 2 (which resembled the linear range of quantification) and deviation was reduced, increasing the assays accuracy.

For example, in order to reach the most intense fixation to the surface, drying times of step 10 were varied from 43°C to 100°C, while using a heat block or an incubator chamber. The resulting absorbance values were compared for variation and the one with the most stable result was chosen (in this case 50°C in the incubator). Another improvement incorporated experience from the immunocytochemistry into this protocol (Fig. 6, steps 5 and 6). Here it was shown that after 1 hour of incubation in rotation of anti-WCL serum (1 to 1000 dilution, rabbit immunized by *C. acnes* IA1-s1 whole cell lysate) and bacteria (OD_{600} = 0.4), full opsonization of the cells could be reached and verified by microscopy. Any adhesive protein targeted by anti-WCL serum would thus be covered by antibodies and possibly inhibit surface adhesion. Thus, instead of applying 10 µl serum on top of the 150 µl of *C. acnes* suspension in the well, the serum and suspension was mixed and incubated before pipetting into well.

Step	Scheme	Initial protocol	Optimizations	Improved protocol
1		Streaking from -80°C on BHI agar	Contamination control	Streaking from -80 on BHI agar
2		Incubation for 3-4 days	5 days for slow growing isolates	Incubation for 3-5 days
3		Resolving biomass in BHI by vortex	Vortex for maximum aggregate separation	Resolving biomass in BHI by vortex
4		Preparing batch with starting OD_{600}=0.1 in BHI	Varying starting OD_{600}: 0.0025, 0.025, to reach linear range (between 1-2 RAU)	Preparing batch with starting OD_{600}=0.01 in BHI
5			New. Incorporated from immunocytochemistry	Aliquoting 20 ml, addition of serum/saline (1.3 ml)
6	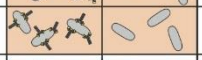		New. Incorporated from immunocytochemistry	Incubation 1h in rotation (1 spin per 2 seconds) for opsonization
7	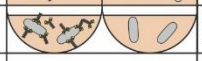	Pipetting one condition into 8 vertical rows by MP1/2, 150 µl total volume	Using calibrated MPX, addition to abiotic surface after complete opsonization	Pipetting one condition into 8 vertical rows by MPX, 160 µl total volume
8		Addition of 10 µl serum/saline, resuspending a few times	Testing 1, 2 and 4 replicates, to the point where trend stays the same	Creating 8 replicates
9	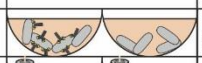	Incubation 3 days, for attachment and biofilm formation	Testing incubation of 1, 2, 3 days or 16 - 20h, trying to reach linear range (1-2 RAU)	Incubation 16-17 h, for attachment and biofilm formation, anaerobically, 37°C
10		Removal of supernatant by MP1/2, 8 wells per aspiration	Testing differential aspiration of platewasher or multichannel pipette	Removal of supernatant by platewasher
11		Drying on heatblock, 100°C, 30'	Testing heatblock vs heat incubatior, 43°C - 90°C and heat incubator positions	Drying in heat incubator, 50°C, 1h 15'
12		Addition of 100 µl methanol for 10'		Addition of 100 µl methanol for 10'
13	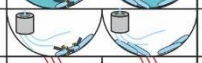	Removal of methanol by MP1/2, 12 well per aspiration		Removal of methanol by platewasher
14		Drying on heatblock, 100°C, 30'	Testing heatblock vs heat incubatior, at RT and 43°C - 90°C	Drying in heat incubator, 50°C, 10'
15		Staining 2' with crystal violet [0.1% (v/w) in H_2O]		Staining 2' with crystal violet [0.1% (v/w) in H_2O]
16		Washing 2x, submerging plate in fresh H_2O	Comparing rigid submerging to more gentle pipette washing	Washing 2x with H_2O, using MPX
17		Addition of 150 µl ethanol (96%)		Addition of 150 µl ethanol (96%)
18		Sealing plate surface by Parafilm		Sealing plate surface by Parafilm
19		Incubation ON, 4°C	Condensation of ethanol on Parafilm surface	Incubation for 3h - ON, RT
20		Resuspending biofilm by MP1/2	Investigating variation increase of resuspending due to volume change	Pipetting 50 µl to fresh 100 µl ethanol (96%)
21	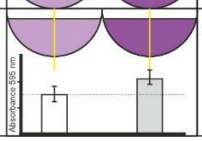	Measurement by platereader at 595 nm		Measurement by platereader at 595 nm

Figure 6: Protocol of MTP based quantification assays (initial and final). The main steps of the protocols of the initial assay and the final assay (after applying respective optimizations) are summed up. The scheme compares possible antibody mediated reducing effects on biofilm formation to an untreated control.

To investigate the linear range of detection of biofilm formation for this assay, a linear calibration curve was established. *C. acnes* suspensions ranging from an OD_{600} of 0.005 to 1 were prepared and centrifuged (2000 x g) against the surface of the 96-well plate. Afterwards, the biofilm assay protocol was performed beginning at step 10 (Fig. 6). When applying OD_{600} on the x-axis and the biofilm assay output RAU (relative absorbance units) on the y-axis, the linear range (where an increase in OD_{600} linearly correlated with an increase in RAU) could be defined to be between approx. 1 and 2 RAU, and 0.05 and 0.2 OD_{600} respectively. Thus, starting OD_{600} (Fig. 6, step 4) and incubation time (Fig. 6, step 9) were adapted to the point where the final RAU values lied between 1 and 2, optimally at 1.5.

1.5. Significant reduction of biofilm formation by anti-WCL serum

With all the variations tested (Fig. 6, optimizations), a sophisticated protocol was established (Fig. 6, improved protocol). Biofilm formation was reduced to stay within the linear range (~ 1.5 RAU – without blank subtracted), interquartile range was reduced and variation between columns brought to an insignificant level (Fig. 5, right panel). The improved protocol was used to test reducing effects of the anti-WCL serum (hyper-immune, HI) on biofilm formation compared to the respective pre-serum (serum which was taken from the same rabbit before immunization). A serial dilution of the HI and pre-sera in saline was applied ranging from 1:800 to 1:80,000 (Fig. 7). A control was added containing saline only. Significance was compared between HI- and pre-sera of the same dilution. Significant biofilm reduction could be detected for 4 out of 5 dilutions. Anti-22#1 serum was also tested for effects, but the results showed a dynamic change in biofilm formation effects depending on dilution levels. Significant reduction could be detected for low dilution levels (1:800) and an increase could be seen for dilution 1:16,000.

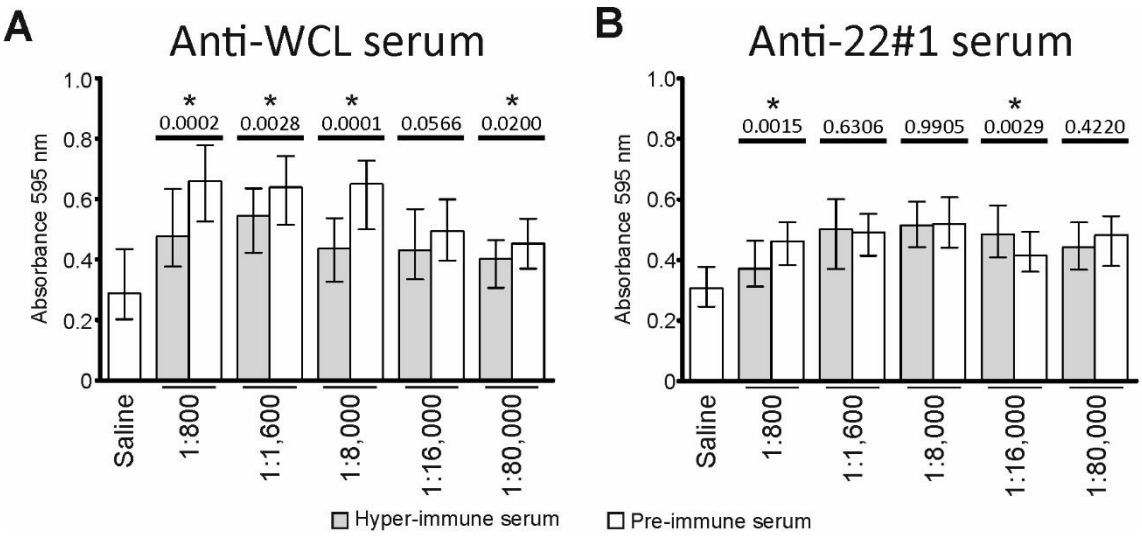

Figure 7: Effects of anti-WCL and anti-22#1 serum on MTP based biofilm formation. Strain IA1-s1 was incubated with a serial dilution of anti-WCL and 22#1 serum and their respective pre-sera (see Fig. 6 for optimized protocol). Significant reduction of the biofilm could be detected for hyper-immune anti-WCL serum in 4 of 5 dilutions. HI anti-22#1 serum seemed to reduce biofilm in high concentration and increase in lower concentration (1:16,000). Increased values of serum samples to saline control indicated possible serum based effects.

Theoretically, WCL based immunization should contain antibodies against all sorts of different epitopes of *C. acnes* including proteinous epitopes involved in initial and continued attachment, as well as in biofilm maturation. Shielding “sticky proteins” from the environment by antibodies would thus reduce biofilm formation in our assay. We

did see significant effects of the HI serum compared to the pre-serum. However, at this point these effects could either be due to “sticky” antibodies or due to serum compounds. On the one hand, if these effects were solely based on differential composition of HI- and pre-serum, it would be likely to see them for both, WCL and 22#1, which we didn’t. On the other hand, saline samples continuously showed lower biofilm formation than serum incubated samples, suggesting *C. acnes* increased biofilm formation upon contact with serum. OD_{600} values of these conditions did not differ, showing that truly the biofilm attachment was increased and not the total biomass. Nonetheless, to clearly pinpoint these effects to the antibodies, the serum was affinity purified.

1.6. Biofilm effects of anti-WCL affinity purified antibodies lay below detection threshold

Biofilm formation was quantified after opsonization with PBS, whole cell lysate derived serum (anti-WCL) or their affinity purified antibodies (purified anti-WCL serum, or “pAnti-WCL”), as well as the same samples (antiserum and affinity purified) but previously pre-incubated with *C. acnes* as antibody sink. Four different dilutions of antisera were performed: 1:1,000, 1:8,000, 1:10,000 and 1:80,000 (Fig. 8). Affinity purified antibodies were back-calculated to the same theoretical serum antibody concentration. As there was loss of antibody in the affinity purification process and limited avail of serum, experiments were limited to two independent runs. Although there seemed to be a slight tendency for increased serum effects, no significant defects could be detected for anti-WCL derived antibodies.

As we had evidence for protein based biofilm formation with reductions from 2 RAU (mock-control) to 0.4 RAU (maximum proteinase K effect, Fig. 4), it could be hypothesized that antibodies generally should have the capacity to affect *C. acnes* biofilm formation. As the anti-WCL derived antibodies didn’t mediate such effects, it is possible that either the immune response of the rabbit didn’t produce sufficient amounts of antibodies targeting “sticky proteins”, or reducing and increasing effects of biofilm formation weighted itself out. Biofilm increasing effects could base on interconnecting proteins from different cells or matrix compound, increasing robustness.

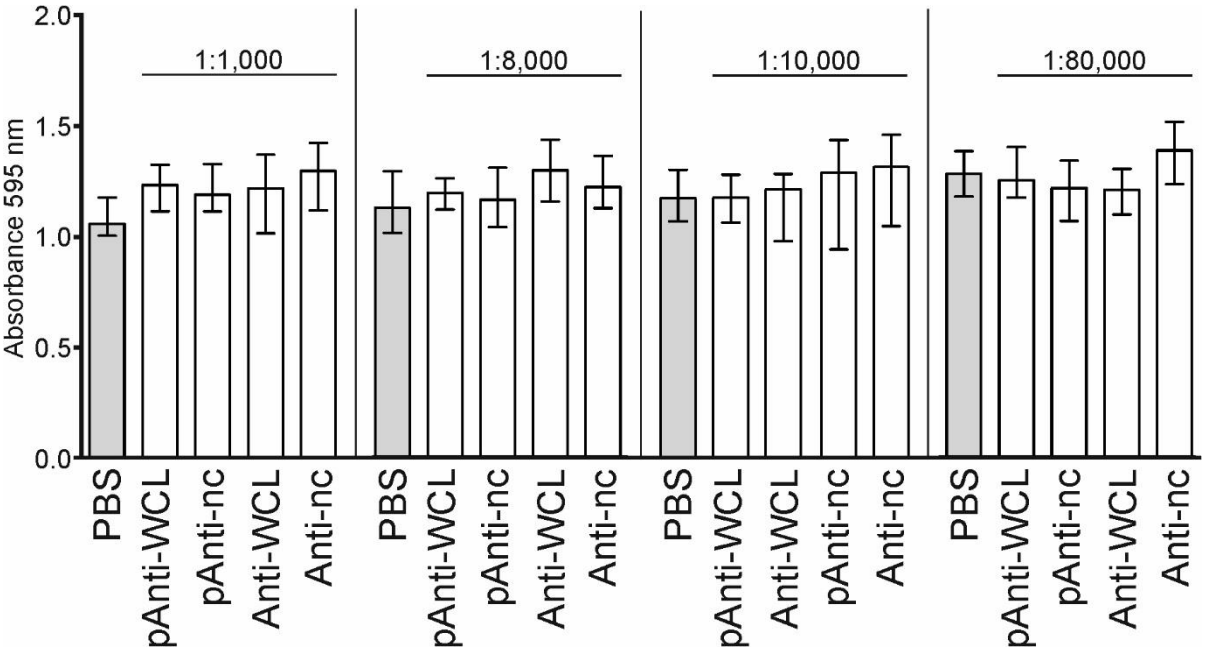

Figure 8: Effects of pAnti-WCL antibodies on MTP biofilm quantification. Strain IA1-s1 was incubated with different dilutions (1:1,000, 1:8,000, 1:10,000 and 1:80,000) of rabbit derived anti-WCL serum and affinity purified antibodies from anti-WCL serum ("pAnti-WCL"). Negative controls ("nc") were PBS, as well as anti-WCL serum ("Anti-nc") or pAnti-WCL antibodies ("pAnti-nc"), but previously pre-incubated with *C. acnes* as antibody sink. See Fig. 6 for optimized protocol. No significant effects could be detected under the applied conditions.

It has been reported for *S. epidermidis* that antibodies against specific protein target could either significantly reduce or increase biofilm formation in a flowcell model (Lam et al., 2014). In this work we were also able to show biofilm increasing effects on *S. epidermidis* by whole cell lysate derived antibodies. Even though no effects could be detected in the established assays for whole cell lysate derived antibodies with *C. acnes* under the given methods and conditions, the results showed that the MTP assay is capable of revealing *C. acnes* isolate specific differences, as well as connecting gradual protein reduction of phylotype IA1 extracellular matrices to gradually reduced biofilm quantity.

Possibly, to identify proteins involved specifically in biofilm attachment, the rabbit immunization process could be optimized to contain large quantities of biofilm derived fractions only (see section 3 for creation of biofilm mode and section 6 for a fractionation protocol for membrane-associated proteins). Furthermore, *C. acnes* is mostly surrounded by sebum lipids and extracellular matrices of keratinocytes in vivo. Attachment to these structures might be of elevated relevance (not regarding implant-associated infections, but in the context of acne). The assay could be improved by

coating the 96-well plates with either sebum, or epithelial extracellular matrix components.

1.7. Adaption of MTP assay to *S. epidermidis*

The protocol from *C. acnes* was adapted to *S. epidermidis* to quantify its biomass. Tryptic Soy Broth (TSB) was used in most laboratories as standard medium for *S. epidermidis*. To maintain comparability with literature, TSB was chosen instead of BHI. *S. epidermidis* as facultative anaerobic bacterium prospers in aerobic conditions, but can grow under anaerobic conditions as well. Therefor biofilm formation had to be investigated under both conditions. Anaerobic conditions were established by using the same method as for *C. acnes*. Incubation times for a mature biofilm were adapted to *S. epidermidis* growth speed (which is significantly faster) to approximately 20 h (from up to 7 days). As *S. epidermidis* lives on the skin, it is used to a range of temperatures (between 37°C and at least room temperature). To represent this, two incubation temperatures were tested: RT and 37°C. U-formed and flat-bottomed 96-well plates were available and literature showed no standardized form. To test which version worked optimally for *S. epidermidis*, both were tested.

1.8. *S. epidermidis* strains exhibited high diversity in biofilm quantity

Biofilm formation in flat-bottomed 96-well MTPs (under aerobic conditions at 37°C) showed increased variation and similar medians between strain #52 – #58 and #152, as well as between #51, #59, #150 and #151 (Fig. 9A). Results didn’t allow for strain specific quantification. U-formed wells on the other hand produced distinct differences and less variation under these conditions (Fig. 9B – F). #51, #53, #56 and #152 showed high values, #59, #150 and #151 low values (Fig. 9D). With these results at hand, U-formed wells were used for all further experiments. Generally, anaerobic biofilm reached levels close to aerobic conditions, indicating either very fast anaerobic growth speed or oxygen being present to some degree even beyond the start point of incubation. Interestingly, strain #51 seemed to have relatively high biofilm production under aerobic conditions (Fig. 9C and D, grey column) and low biofilm production under anaerobic conditions (Fig. 9B and E). Under RT conditions, strain #57 produced high amounts of biofilm, aerobically and anaerobically. At the same time strain #56 showed as low values as the negative control #150, even though it was the highest one at 37°C under all conditions.

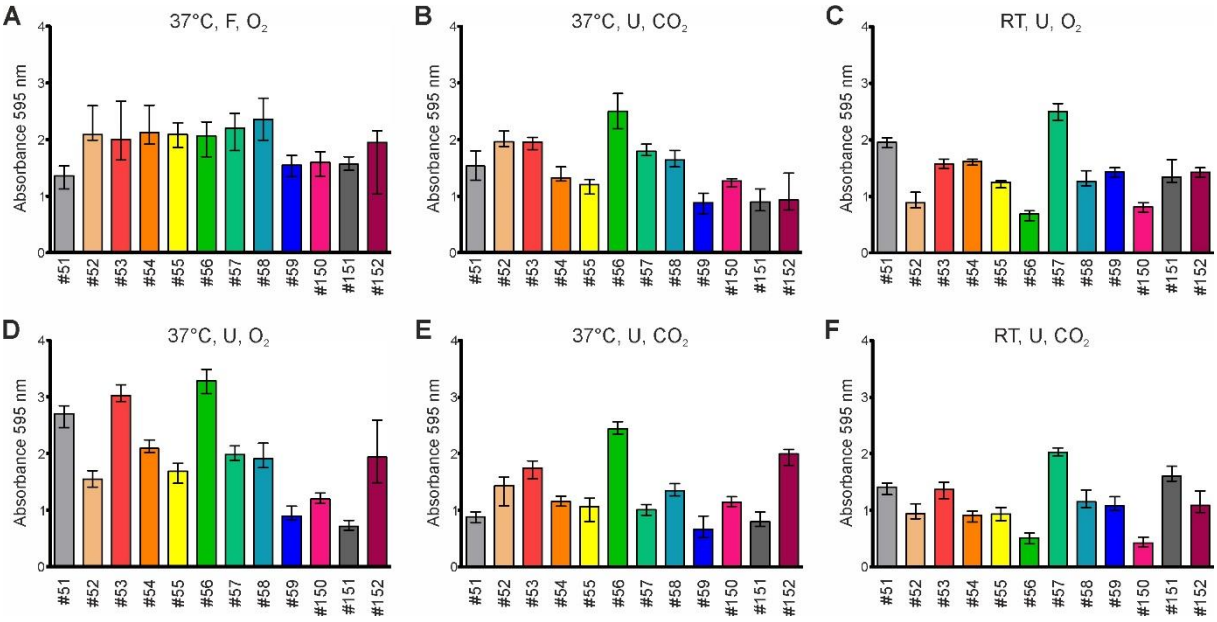

Figure 9: *S. epidermidis* biofilm formation under various conditions. Biofilm formation of 12 *S. epidermidis* strains was measured under following conditions: A) at 37°C aerobically in flat-bottomed wells, B) at 37°C anaerobically in U-formed wells, C) at RT aerobically in U-formed wells, D) at 37°C aerobically in U-formed wells, E) at 37°C anaerobically, U-formed wells and plates packed and incubated separately and F) at RT, anaerobically in U-formed wells. Each column stands for one strain under the specific conditions, incubated in 6 wells in 5 separate plates (n = 30 values). Plates were incubated approximately 20 h under different starting OD_{600} (see Methods for details). Shown are medians with interquartile range of the 595 nm absorbance of crystal violet.

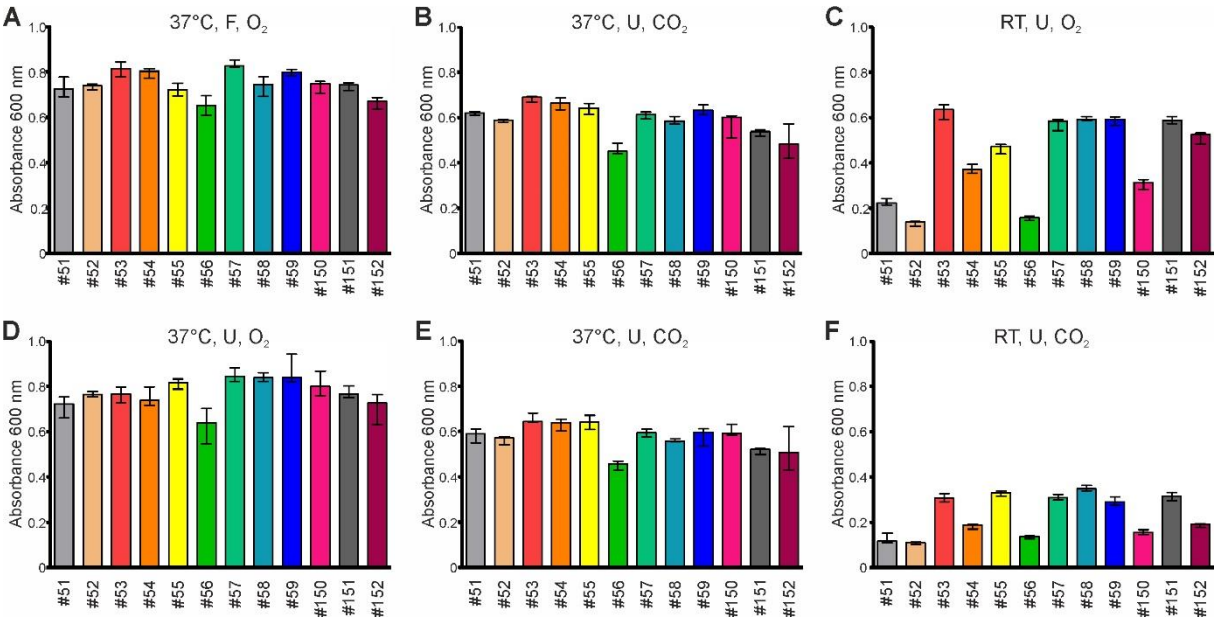

Figure 10: *S. epidermidis* growth under various conditions. Growth (OD_{600}) of 12 *S. epidermidis* strains was measured under following conditions: A) at 37°C aerobically in flat-bottomed wells, B) at 37°C anaerobically in U-formed wells, C) at RT aerobically in U-formed wells, D) at 37°C aerobically in U-formed wells, E) at 37°C anaerobically, U-formed wells and plates packed and incubated separately and F) at RT, anaerobically in U-formed wells. Each column stands for one strain under the specific conditions, incubated in 1 well in 5 separate

plates (n = 5 values). Plates were incubated ~ 20 h under different starting OD_{600} (see Methods for details). Shown are medians with interquartile range of 600 nm absorbance.

End-point growth varied little at 37°C for most strains, with #56 and #152 being the lowest ones (Fig. 10). Similar growth between U-formed and F-bottomed plates verified no growth artefact affecting the results. Generally, growth seemed to be stable and similar for all conditions.

The median of biofilm formation was divided by the median of the growth, determining the biofilm production per 1 OD_{600}. If comparing two strains with similar biofilm formation, but one strain having just half the OD_{600}, then this particular strain probably builds up a more robust biofilm structure. Strains with biofilm ratio between 3 and 5 were considered as good biofilm producers and strains with a ratio of 1 as the worst ones (Table 4)

Table 4: Biofilm per growth ratio. The median of the biofilm formation (Fig. 9) was divided by the median of the growth (Fig. 10) to calculate the biofilm per growth ratio for each strain. Strains with high values (green) were considered good biofilm producers. Temp.: incubation temperature, Atmos.: atmospheric conditions of aerobic (O_2) or anaerobic (CO_2), Form: form of MTP wells (U-formed or F-bottomed).

Temp.	Atmos.	Form	51	52	53	54	55	56	57	58	59	150	151	152
37°C	O_2	F	1.0	1.6	1.4	1.5	1.5	1.6	1.4	1.7	1.0	1.2	1.1	1.4
37°C	O_2	U	3.7	2.0	3.9	2.8	2.0	5.2	2.3	2.3	1.1	1.4	1.0	2.9
37°C	CO_2	U	1.7	2.4	2.0	1.5	1.3	3.7	2.1	2.0	1.0	1.6	1.3	1.8
37°C	CO_2	U	1.2	1.9	2.1	1.5	1.3	4.3	1.4	2.0	1.0	1.5	1.3	3.0
RT	O_2	U	4.0	3.2	1.1	2.0	1.2	2.0	2.0	1.0	1.1	1.1	1.1	1.3
RT	CO2	U	3.8	3.2	1.6	1.8	1.0	1.4	2.4	1.3	1.4	1.0	1.9	2.2

1.9. Anti-WCL serum's affinity purified antibodies increased biofilm formation in a modified assay

To test effects of affinity purified antibodies (based on rabbit immunization with *S. epidermidis* whole cell lysate) on biofilm formation, the aerobic condition at 37°C was chosen in the MTP assay. As affinity purified antibodies were limited, only the strong biofilm producers were picked: #56 (green) and #152 (purple). #150 (pink) served as control. The antibodies were compared to samples of the same antibody affinity purified stock, however previously pre-incubated with *S. epidermidis* and purified to get rid of any antibody binding *S. epidermidis*. Another control was addition of nothing. 7

wells were filled with the same sample combinations, whereas one was removed after incubation for OD_{600} measurement (Fig. 11).

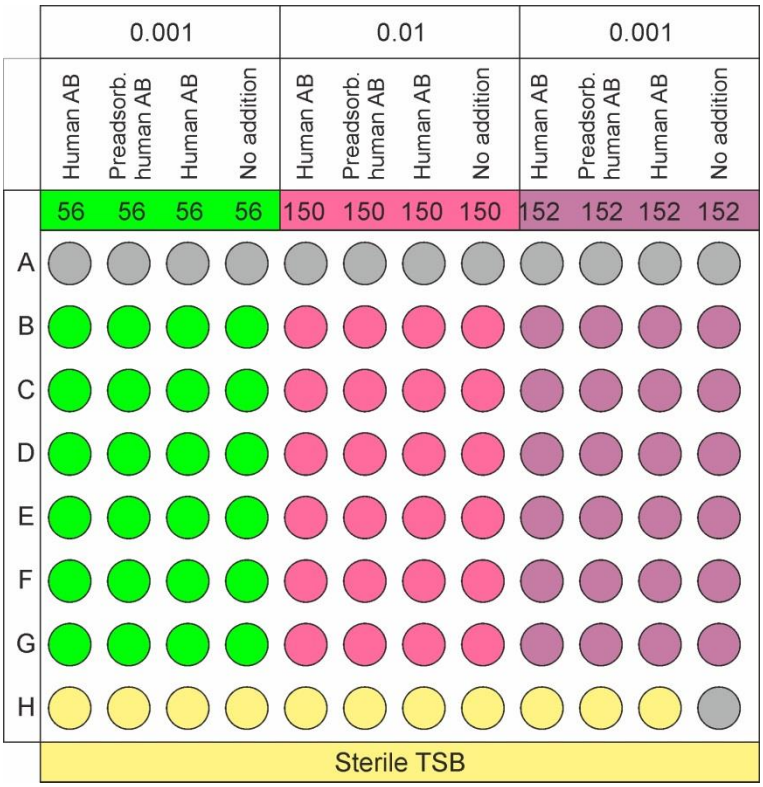

Figure 11: Scheme of 96-well plate for biofilm quantification of antibody effects. Different conditions of strain 56, 150 and 152 were pipetted into the plate according to the scheme from row A to G. To reach final biofilm values approx. within the range of 1 – 2 relative absorbance units, starting OD_{600} was set to 0.001 for #56 and #152, and 0.1 for #150. After incubation for ~ 20 h at 37°C aerobically, row A (grey) and the last well of row H (yellow) was removed and its OD_{600} was measured in the platereader (1:2 diluted). Row H (yellow) was initially filled with sterile TSB as blank and sterile control. The remaining wells (yellow, green, magenta and violet wells) were further processed according to the MTP biofilm assay. Six replicates of the plates were analyzed, whereas four were used with standard aspiration protocol and two were washed between incubation and aspiration.

Growth of all strains was on similar levels, aside of #56 K+ (Fig. 12C). As was found out later, the biofilm was attached so tightly to the surface that it could resist the defined 10 times resuspension by pipetting. Therefor not all biomass was removed from the well, leading to lower values.

Four replicates were treated according to the regular protocol investigating biofilm reduction. Even though there seemed to be a tendency for a difference between the different sample combinations, no significant values could be identified.

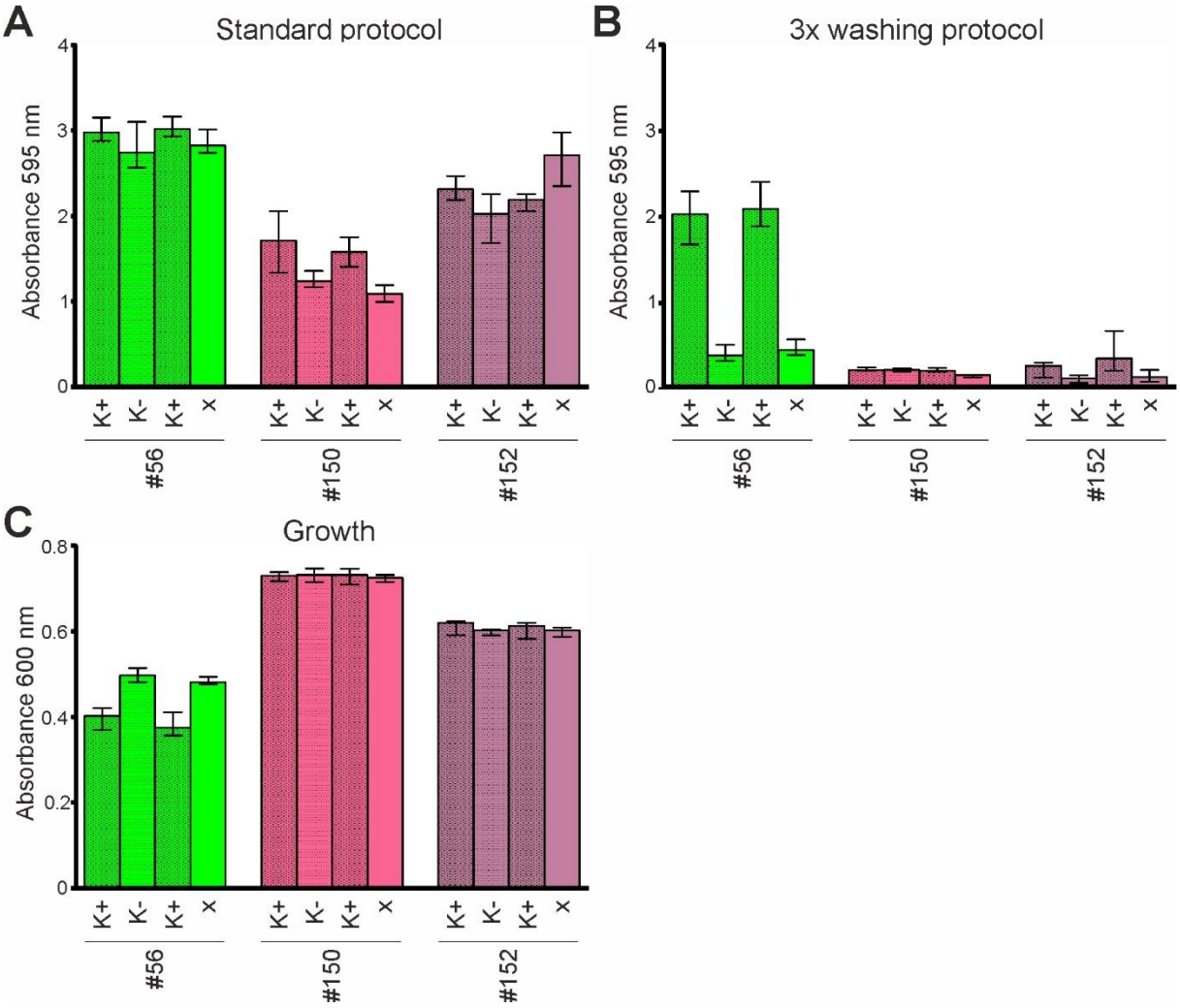

Figure 12: Antibody effects on *S. epidermidis* biofilm of #56, #150 and #152. Affinity purified antibodies of the anti-WCL serum (K+, 100 µg / ml) were compared to samples of the same antibody affinity purified stock, however previously pre-incubated with *S. epidermidis* as sink and purified (K-, 50 µg / ml). Another control was the addition of nothing (x). The different conditions of strain #56, #150 and #152 were incubated for ~ 20 h at 37°C aerobically in a MTP. Shown are medians and interquartile range. (A) In the standard protocol the supernatant was instantly removed by aspiration. The data set contained 6 wells from 4 plates (n = 24) for each column. Results indicated antibody effects for #150 K+ and #56 K+, however not significant. (B) In the washing protocol, the supernatant was removed, washed 3 times with H_2O by pipette and then proceeded according to the protocol. 6 wells from 2 plates (n = 12) were measured. Antibody incubated strain #56 showed more than 4-fold increase in biofilm formation. (C) One well per plate was removed after incubation and the OD_{600} was measured. On a side-note, although #56 K+ indicated reduced growth, this happened due to a technical issue.

The two other replicates of the initially 6 ones were treated with additional washing steps (“washing protocol”) after incubation and before starting the first aspiration and drying step of the MTP assay (Fig. 6, MTP optimized protocol step 10). All wells were washed trice with H_2O_{ve} using a multichannel pipette. Afterwards, the plates were processed together with the 4 replicates (from above). Surprisingly, the biofilm

formation of #56 incubated with antibodies *increased* biofilm formation from ~ 0.4 relative absorbance units (RAU) to 2 RAU (Fig. 12B, strain #56 K+ vs K- or x). A similar tendency could be seen also for #152 after one or two washing steps (laboratory observation).

The results showed that the total pipeline of biofilm quantification reached a sophisticated point. At the same, as biofilms of different species and strains reached different rigidity, the washing steps allowed additional fine-tuning and adaptions to more or less rigid biofilms. As example, three additional washing steps used for the more stable biofilm of *S. epidermidis* #56 revealed increased rigidity mediated by antibodies. Tweaking the protocol at step 10 to use three, two, one or no washing steps could reveal shades of different biofilm formation capacities for at least two species.

2. Fluorescence Microscopy

To gain a second perspective on *C. acnes* biofilms, differential biofilm structures and attachment capacities of *C. acnes* phylotypes (skin and implant) were visualized and quantified by fluorescence microscopy and Comstat2 software (Heydorn et al., 2000; Vorregaard, 2008). Similar to the MTP based investigation, effects of proteinase K and DNase I were tested on mature biofilms and attachment. Finally, the protocol was adapted to visualize, characterize and quantify *S. epidermidis* biofilms. Sub-sections 1, 2 and 3 were previously published in the International Journal of Medical Microbiology (Kuehnast et al., 2018) and either taken as a whole or modified for this thesis.

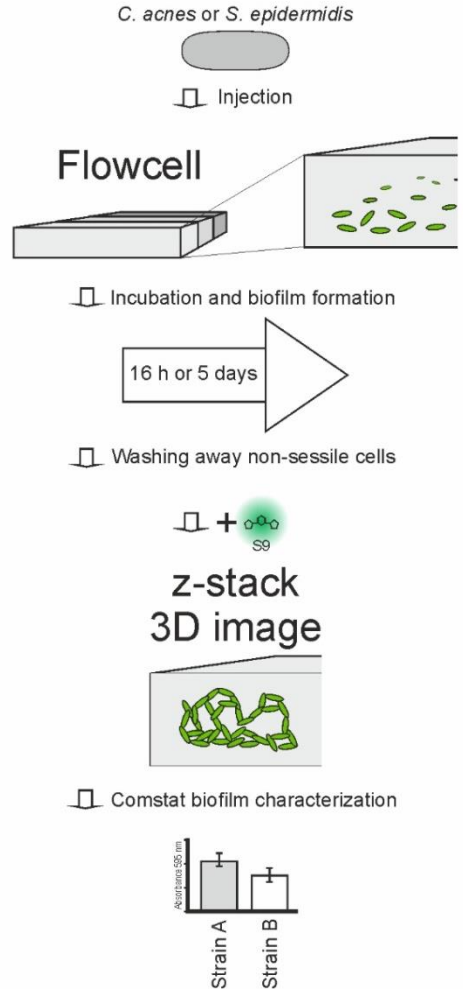

Figure 13: Overview of fluorescence microscopy protocol. *C. acnes* or *S. epidermidis* was injected into a flowcell chamber which sedimented to the cover glass and grew as biofilm into the volume of the chamber. Incubation times were 20 h (*S. epidermidis*, aerobically and anaerobically) or 5 days (*C. acnes*, anaerobically). After washing away non-sessile cells and staining cells with SYTO9 (staining DNA), cells were microscoped in the FITC channel and signal intensities were quantified using Comstat software (Heydorn et al., 2000; Vorregaard, 2008).

2.1. *C. acnes* phylotypes showed characteristic biofilm morphology

Whereas the MTP based assay (section 1) is applicable for high-throughput analyses, microscopic analyses are more labor-intensive and time consuming. Therefore, the focus was laid on reference strains as representatives of the six phylotypes and two anatomical isolation sites. Each reference strain was selected based on the individual dynamic biofilm formation which matched the corresponding median values of the respective phylotype best (Fig. 2). As the majority of *C. acnes* isolates' biofilm levels reached a plateau or peaked at 120 h (Fig. 2), this end point was chosen also for fluorescence microscopy. The cells were injected into the flowcell system, containing three microscopic chambers of ~ 200 µl volume. The cells would sediment to the bottom and build the biofilm on the cover slip glass, allowing microscopy of biofilm up to 50 µm into the volume. The non-sessile cells were washed away and the biofilm was stained using SYTO9 fluorescence dye (targeting DNA). This paragraph was adapted from Kuehnast et al., 2018.

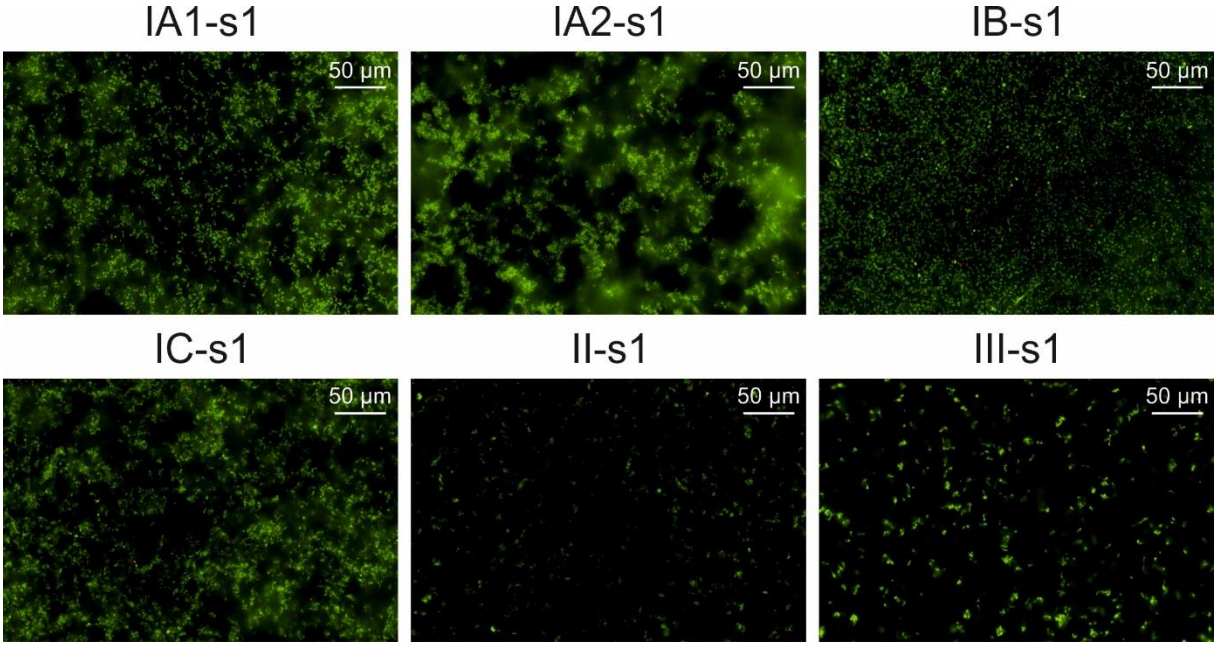

Figure 14: Mature biofilm showed viability after 120 h. *C. acnes* reference isolates from the skin were grown in flowcells for 120 h in BHI and stained with the LIVE/DEAD viability kit. The height of imaging lay 1.2 µm above the cover glass. Green color indicated viability, red ones indicated lysis. Figure was taken from Kuehnast et al., 2018.

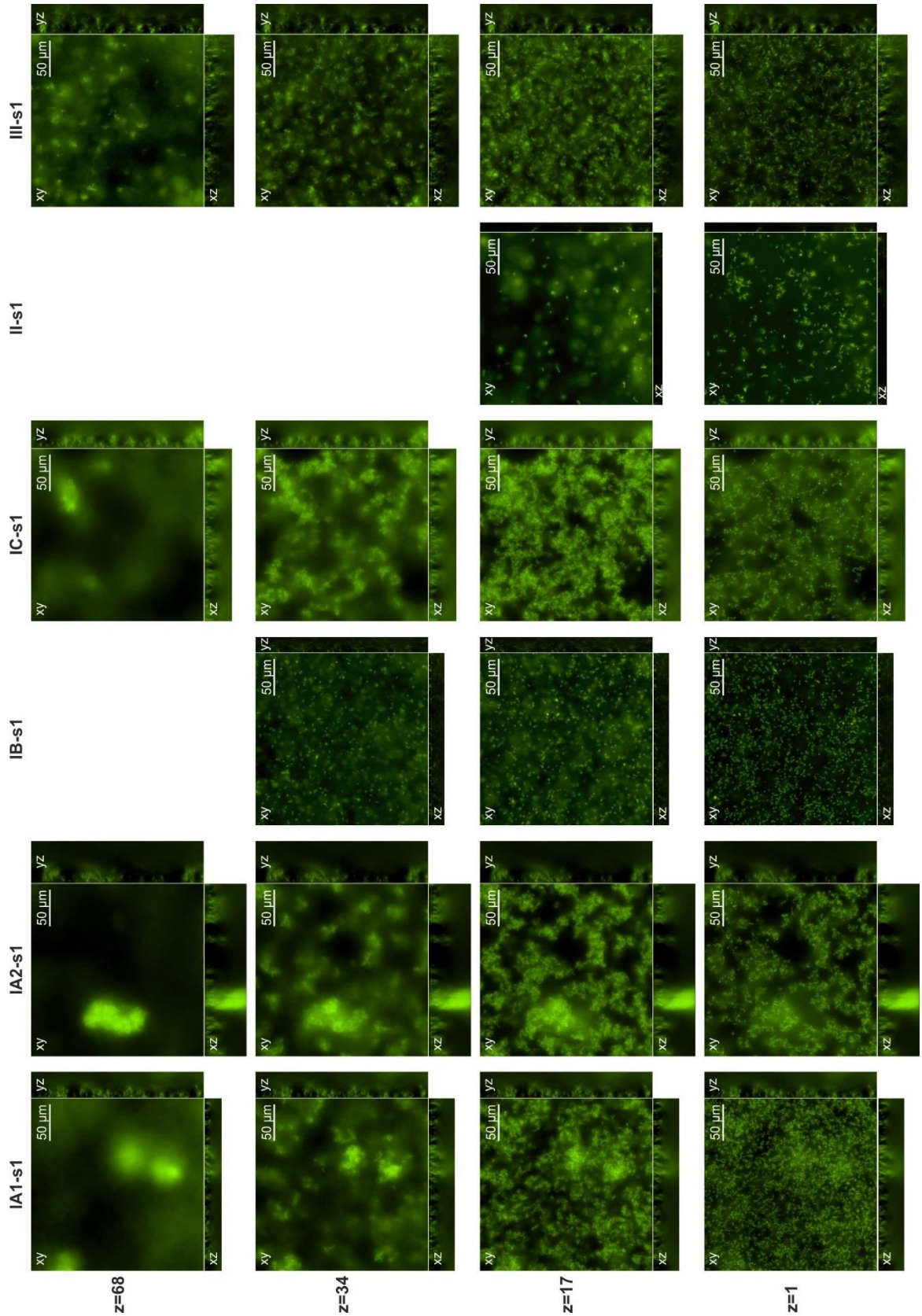

Figure 15: Biofilm visualization of skin *C. acnes* strains revealed phylotype-dependent architecture. Shown are fluorescent microscopy images of SYTO9 stained *C. acnes* biofilms as horizontal (xy) and vertical (xz and yz) projections (large and side panels, respectively). Each strain used as representative of the phylotype is indicated on top of each stack. Biofilms were grown for 120 h in flow-cell chambers with BHI broth. Large panels represent selected

single optical sections through the acquired three-dimensional data sets at the indicated z position. Optical sectioning was performed in 0.3 µm steps. Figure and legend were taken from Kuehnast et al., 2018.

Firstly, the viability of the biofilm was determined by using propidium iodide (PI) and SYTO9 fluorescent dyes. SYTO9 penetrates impermeable (living) cell membranes, intercalates into DNA and starts fluorescing green. PI can migrate through permeable (dead) membranes only, intercalate into DNA and start fluorescing red. Furthermore, PI quenches SYTO9 fluorescence, which is why cells become red and not an overlay of both signals resulting in yellow. Screening the biofilm of skin isolates showed that aside of a few red cells at the bottom the great majority of cells were green, verifying a viable biofilm for all phylotypes (Fig. 14). Representative images of biofilms formed by skin and implant derived reference strains of all six phylotypes are provided in Fig. 15 and 16, respectively. Image stacks of independently grown biofilms of each reference strain were also evaluated for defined biofilm parameters by COMSTAT 2 software (Fig. 17) (Heydorn et al., 2000; Vorregaard, 2008). Skin and implant derived reference strains of the phylotypes IA1, IA2 and IC formed well-structured three-dimensional biofilms with distinct pillars and fluid-filled caverns and channels (Figs. 15 and 16). Defined multicellular aggregates are highlighted by relatively high average diffusion distances (Fig. 17C), providing a measure for the shortest average distance from a cell in the biofilm to a fluid-filled channel. Reference strains of phylotype III formed biofilms with similar thickness and biomass, but less defined cell aggregates and pillars indicated by a reduced average diffusion distance compared to IA1, IA2 and IC (Fig. 17). Biofilms of IB and II phylotype strains showed the least structured three-dimensional morphology with almost no cell aggregates, relatively low biomass and thin biofilms (Figs. 15 - 17). This paragraph was adapted from Kuehnast et al., 2018.

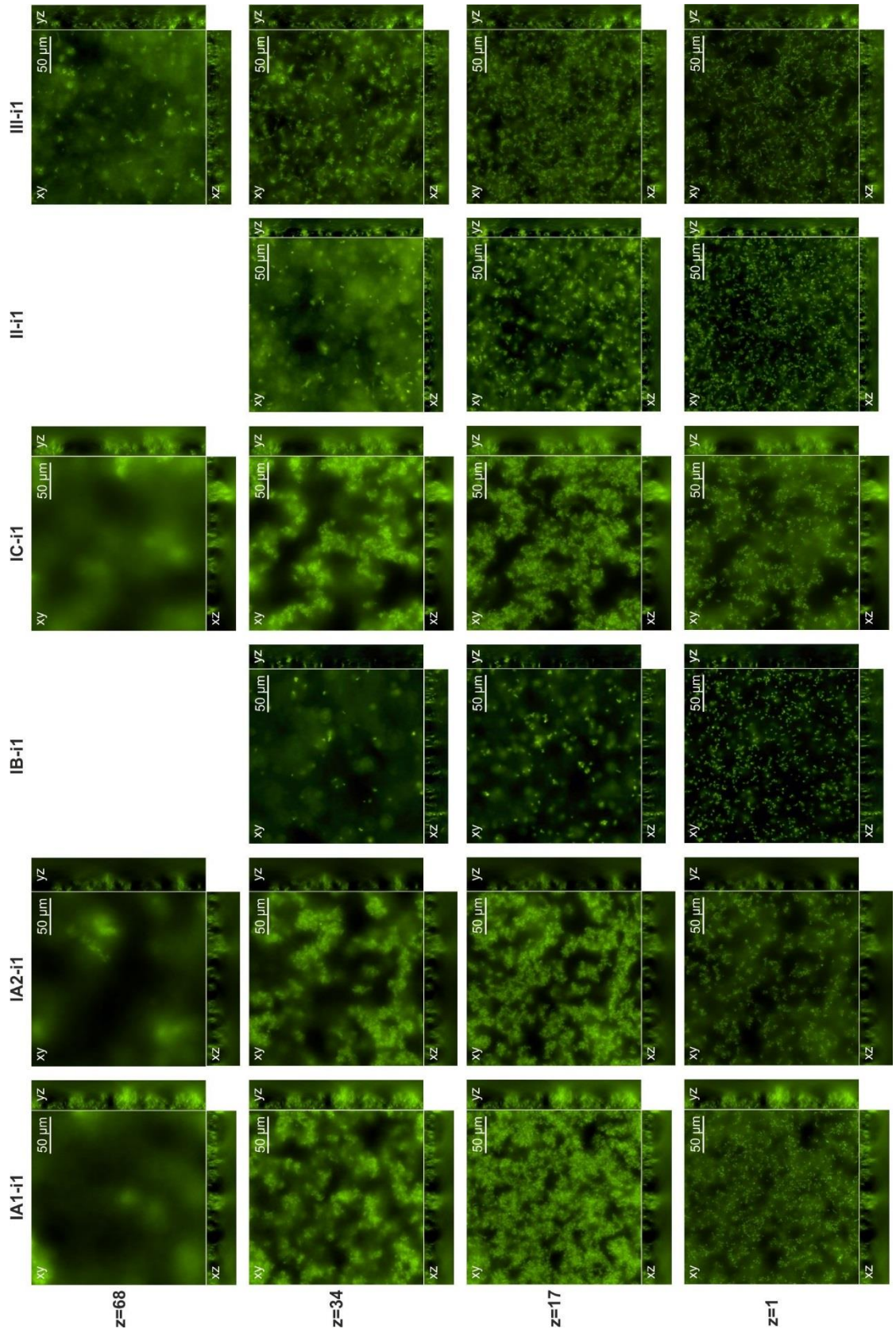

Figure 16: Biofilm visualization of implant-associated *C. acnes* strains revealed phylotype-dependent architecture. Shown are fluorescent microscopy images of SYTO9 stained *C. acnes* biofilms as horizontal (xy) and vertical (xz and yz) projections (large and side panels, respectively). Each strain used as representative of the phylotype is indicated on top of each stack. Biofilms were grown for 120 h in flow-cell chambers with BHI broth. Large panels

represent selected single optical sections through the acquired three-dimensional data sets at the indicated z position. Optical sectioning was performed in 0.3 µm steps. Figure and legend were taken from Kuehnast et al., 2018.

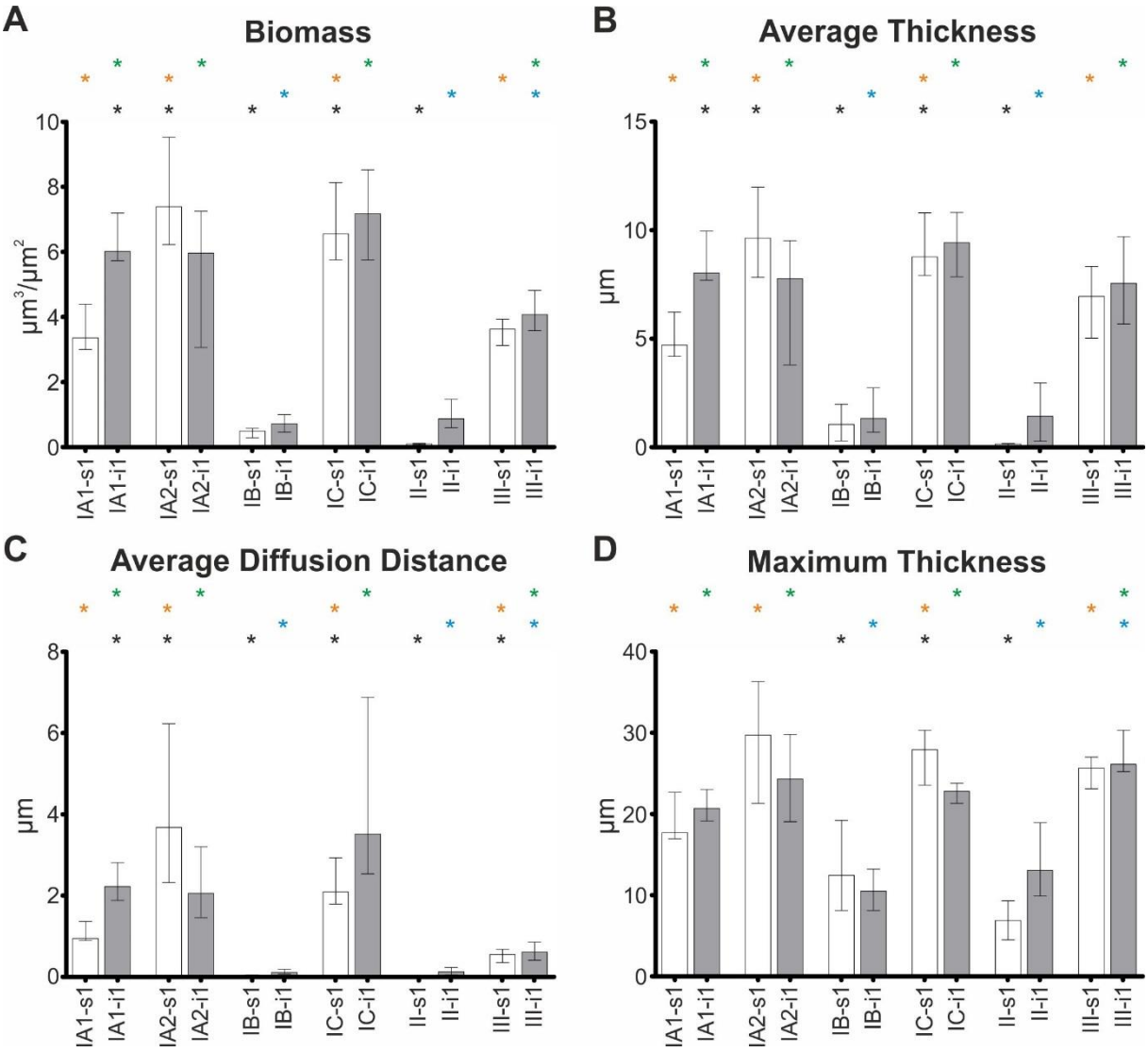

Figure 17: Analyses of the *C. acnes* biofilm morphology by COMSTAT revealed phylotype-dependent characteristics. Image stacks of respective isolates were analyzed for the biomass (A), the average thickness (B), the average diffusion distance (C) and the maximum thickness (D) using the COMSTAT 2 software (Heydorn et al., 2000; Vorregaard, 2008). Shown are the medians of at least ten image stacks from at least four independent experiments for each strain. The error bars indicate the interquartile range. Significant differences are indicated by asterisks for the following comparisons ($P < 0.05$, Kruskal-Wallis test followed by post hoc Dunn's multiple comparisons): Significant differences of IA1-s1 to IA1-i1 or other skin-derived isolates (open bars) are indicated by black asterisks, significant differences of IA1-i1 to other implant-derived isolates (grey bars) are indicated by blue asterisks, significant differences of IB-s1 to IB-i1 or other skin-derived isolates are indicated by orange asterisks, significant differences of IB-i1 to other implant-derived isolates are indicated by green asterisks. Figure and legend were taken from Kuehnast et al., 2018.

The microscopic analyses allowed for a more refined characterization of the capacity for biofilm formation. While the MTP assay incorporated several stringent washing

steps to remove unattached cells and remaining traces of crystal violet, the processing of mature biofilms for the microscopic evaluation was more gentle. After growth and biofilm maturation, the cells were washed with a constant but gentle flow of BHI. IA1, IA2, IC isolates could resist this flow (in contrast to IB and II), but only IA1 was able to resist the MTP based, stringent washing protocol. Thus, fragile biofilms with low adhesive properties are better preserved in the microscopy chamber, but more likely to be destroyed in the microtiter plate assay. This could explain the relatively high biofilm levels of IA2, IC and III isolates observed only by the microscopic analyses and emphasizes the necessity to investigate biofilm formation via different approaches. Consistent with the results of the MTP assay, the biofilm morphology correlated more with the phylotype than with the anatomical isolation point. Implant derived IA1-i1 isolate exhibited slightly increased biomass, average thickness and diffusion distance values compared to the skin-derived IA1-s1 (Fig. 17, comparing open and grey bars). A similar result could be observed for phylotype II. It could be hypothesized that implant-derived IA1 and II isolates have a slightly increased biofilm formation capacity compared to skin isolates of the same phylotype. Interestingly, Holmberg et al. reported that invasive isolates of *C. acnes* produce more biofilm compared to superficial skin isolates (Holmberg et al., 2009). Although this study used a less comprehensive phylotyping scheme, more than 50% of their isolates were categorized in the IA group followed by group II with approximately 30%. Thus, the study likely investigated predominantly IA1 and II isolates. Furthermore, the results of both studies might indicate that invasive, implant-derived IA1 and II isolates have an increased biofilm formation capacity compared to skin-derived IA1 isolates or that their biofilm formation capacity may be differentially modulated in specific environments, showing more biofilm formation under the conditions applied in these studies (i.e. BHI broth). The pathophysiological relevance of these findings requires further investigation. This paragraph was taken from Kuehnast et al., 2018.

2.2. Abiotic attachment of *C. acnes* isolates correlated with the phylotype classification

As attachment to abiotic surfaces is considered to be the first step in biofilm formation, the ability to cover an abiotic surface within 1 h was assessed for the skin and implant derived reference strains (Figs. 18 and 19). IA1, IA2 and IC isolates, which formed a well-structured three-dimensional biofilm (Figs. 15 - 17), showed a similar, relatively

high median surface coverage of ~15% (Fig. 18B). In contrast, isolates of groups IB, II and III exhibited low attachment properties with a median surface coverage of 5% or less. No obvious differences between skin and implant derived isolates within the same phylotype could be observed. This paragraph was taken from Kuehnast et al., 2018.

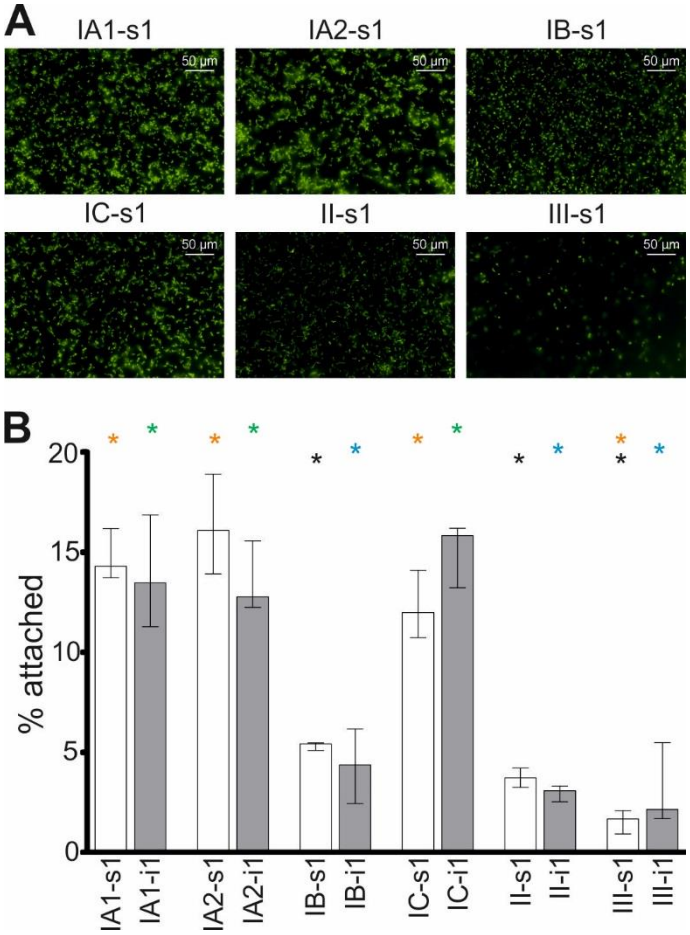

Figure 18: Adhesive properties of *C. acnes* isolates to abiotic surfaces depended on phylotype. Shown are representative microscopic images of skin-derived reference strains (A) and median surface coverage (B) determined by the COMSTAT 2 software (Heydorn et al., 2000; Vorregaard, 2008) for all twelve reference strains. *C. acnes* cells were allowed to attach for 1 h, before non-attached cells were removed and the attached cells were stained with SYTO 9. Micrographs represent a single optical section to visualize the surface coverage on the cover slip. For each isolate at least ten images from four independent experiments were analyzed. The error bars indicate the interquartile range. Significant differences are indicated by asterisks for the following comparisons ($P < 0.05$, Kruskal-Wallis test followed by post hoc Dunn's multiple comparisons): Significant differences of IA1-s1 to IA1-i1 or other skin-derived isolates (open bars) are indicated by black asterisks, significant differences of IA1-i1 to other implant-derived isolates (grey bars) are indicated by blue asterisks, significant differences of IB-s1 to IB-i1 or other skin-derived isolates are indicated by orange asterisks, significant differences of IB-i1 to other implant-derived isolates are indicated by green asterisks. Figure and legend were taken from Kuehnast et al., 2018.

Surface coverage (and with it attachment to abiotic surfaces) correlated with the microscopic biofilm formation capacities (Fig. 17) for IA1, IA2, IC, IB and II

representative strains. Only the isolates III-s1 and III-i1 could resist the induced flow after 5 days of maturation to some degree, while possessing the lowest initial attachment capacities. Type III seemingly started to fortify its attachment capacity over time, however not by building clear biofilm typical structures.

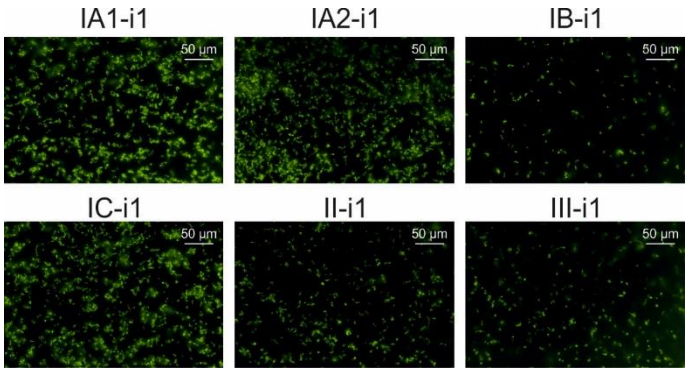

Figure 19: Adhesive properties of implant-associated isolates to abiotic surfaces depended on phylotype. Shown are representative microscopic images of skin-derived reference strains. *C. acnes* cells were allowed to attach for 1 h, before non-attached cells were removed and the attached cells were stained with SYTO 9. Micrographs represent a single optical section to visualize the surface coverage on the cover slip. Figure and legend were taken from Kuehnast et al., 2018.

2.3. *C. acnes* biofilms and attachment to abiotic surfaces depended on extracellular DNA (eDNA) and proteins

Proteins and eDNA may not only be important as structural components for mature biofilms, but can also play critical roles in the initial surface attachment. The flowcell chamber assays established in this study were used to investigate the impact of proteinase K or DNase I-treatment on biofilm structure and surface attachment of reference strains for the six *C. acnes* phylotypes from the skin, as well as implant-associated strains from phylotype IA1 and IB. The concentration of both enzymes was adjusted to 1 mg / ml to ensure effective degradation of accessible protein or DNA without adverse effects on cell viability. The latter was verified by performing a CFU viability assay, where cells were exposed to DNase I and proteinase K for 4 h at 37 °C, simulating the same condition used in the biofilm or attachment assays. No significant decrease in the CFU count of DNase I or proteinase K-treated cells was observed in comparison to the mock-treated control for any reference *C. acnes* strain (Fig. 20).

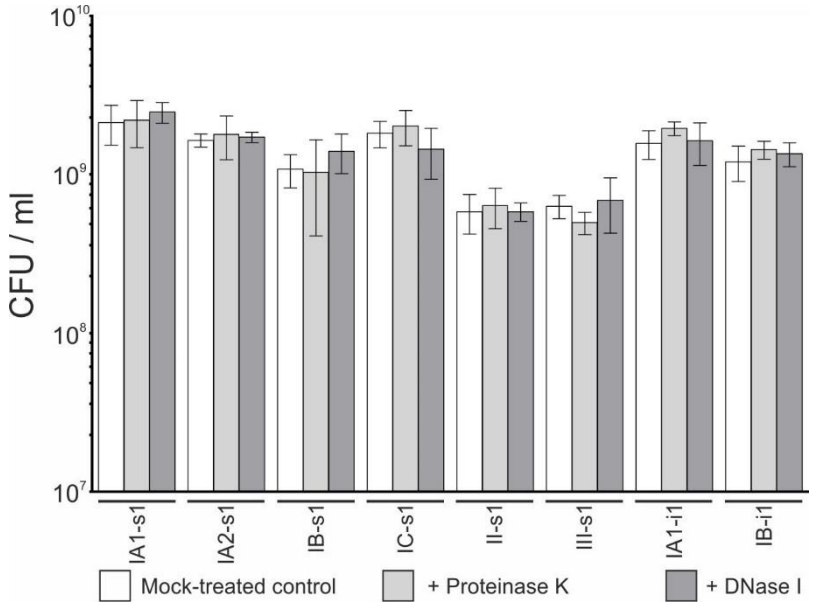

Figure 20: Proteinase K and DNase I does not impair growth of *C. acnes*. Strains were treated with 1 mg / ml (in BHI) proteinase K or DNase I for 4 hours at 37°C (to simulate conditions for experiments shown in Fig. 21) and plated in serial dilutions to compare colony forming units (CFU per 1 ml). Mock-treated control was incubated with BHI only. No reduction of CFU could be detected, indicating proteinase K and DNase I having no effects on viability and proliferation speed. Figure and legend taken from Kuehnast et al., 2018.

Treatment of mature biofilms with proteinase K resulted in significant reduction of the biofilm biomass (Fig. 21A). In the majority of cases, the biofilm was completely degraded. Only for II-s1, which generally produced almost no detectable biofilm, no significant reduction of the biofilm biomass upon proteinase K-treatment could be observed. In contrast, treatment with DNase I was only effective against mature biofilms of IB, IC and III, whereas IA1 biofilms were fairly resistant to DNase I activity. Thus, the results indicate a phylotype-dependent difference in DNase I-sensitivity of mature *C. acnes* biofilms.

With regard to the surface adhesion, proteinase K- and DNase I-treatment significantly impaired attachment properties of almost all *C. acnes* strains independent of the phylotype (Fig. 21B). Hence, proteins and eDNA seemed to contribute to the initial surface attachment of *C. acnes*. This paragraph was modified from Kuehnast et al., 2018.

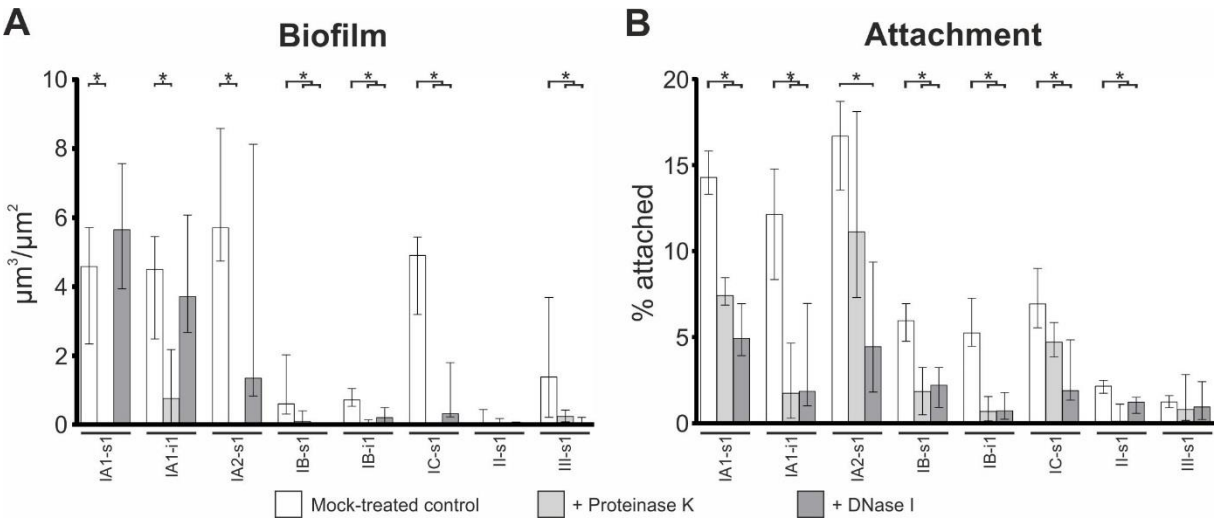

Figure 21: Impact of proteinase K and DNase I-treatment on biofilms and abiotic surface adhesion of *C. acnes.* (A) Biofilms were grown for 5 days in microscopical chambers with BHI broth and subsequently incubated for 4 h with 1 mg / ml proteinase K (light gray), 1 mg / ml DNase I (dark gray,) or mock-treated with BHI broth (open bars), before non-attached cells were removed and the attached cells were stained with SYTO9. Fluorescent image stacks were acquired to analyze the biomass using the COMSTAT 2 software (Heydorn et al., 2000; Vorregaard, 2008). Shown are the medians of at least ten image stacks from at least four independent experiments for each strain. The error bars indicate the interquartile range. (B) *C. acnes* cells were incubated for 4 h with 1 mg / ml proteinase K (light gray), 1 mg / ml DNase I (dark gray) or mock-treated with BHI broth (open bars), before they were allowed to attach for 1 h in microscopical chambers. Subsequently, non-attached cells were removed and the attached cells were stained with SYTO9 to acquire representative microscopic images for analysis of the median surface coverage using the COMSTAT 2. Shown are the medians of at least ten images from at least four independent experiments for each strain. The error bars indicate the interquartile range. (A and B) Significant differences in biomass or attachment between mock-treated control and proteinase K- or DNase I-treated samples are indicated by asterisks ($P < 0.05$, Kruskal-Wallis test followed by post hoc Dunn's multiple comparisons). Figure and legend taken from Kuehnast et al., 2018.

2.4. Successful translation to *S. epidermidis* and biofilm characterization

Six reference strains were grown according to the flowcell protocol, stained with SYTO9 (5 µM final concentration) and z-stack images recorded (Figs. S15 - S20). Strain #56 with high biofilm formation in the MTP assay (Fig. 9) also showed the highest biofilm thickness under the microscope (Fig. 22). Strain #150 biofilm was not able to withstand the applied flow and lost most of its biomass. A monolayer of cells remained on the surface of the cover glass without a three dimensional structure (Fig. 22).

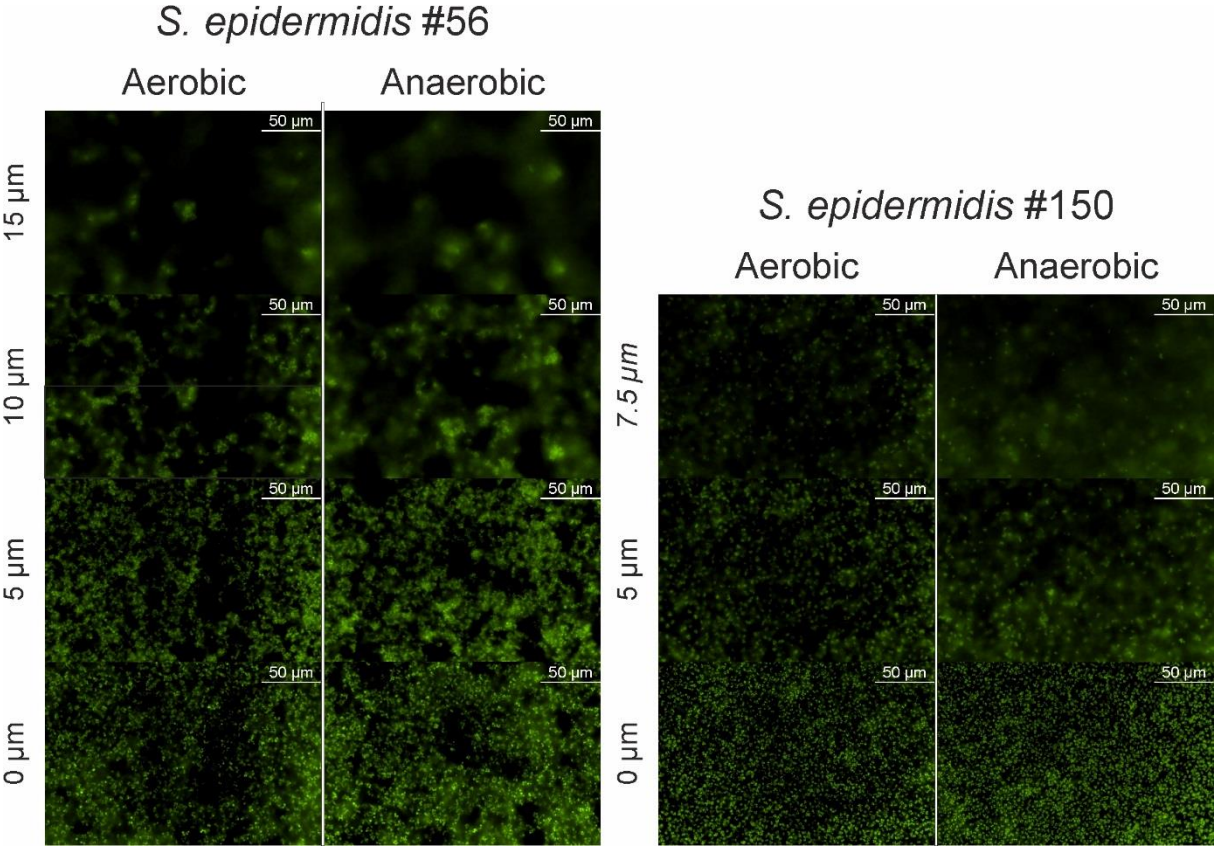

Figure 22: Biofilm morphology of *S. epidermidis* strain #56 and #150, aerobically and anaerobically. The strains were grown in microscopical chambers under anaerobic and aerobic conditions for ~20 h at 37°C. After washing away non-sessile cells, bacteria were stained with SYTO9 (targeting DNA) and image stacks were created. Representative images are shown every 5 µm in height, starting from the cover glass (z-axis). Whereas strain #56 grew into a flow resistant biofilm for up to 15 µm, everything but a mono-layer was washed away from strain #150.

Two z-stacks from three independent flowcell chambers each were quantified by Comstat2 and properties such as biomass, average and maximum thickness and average diffusion distance were calculated (Fig. 23).

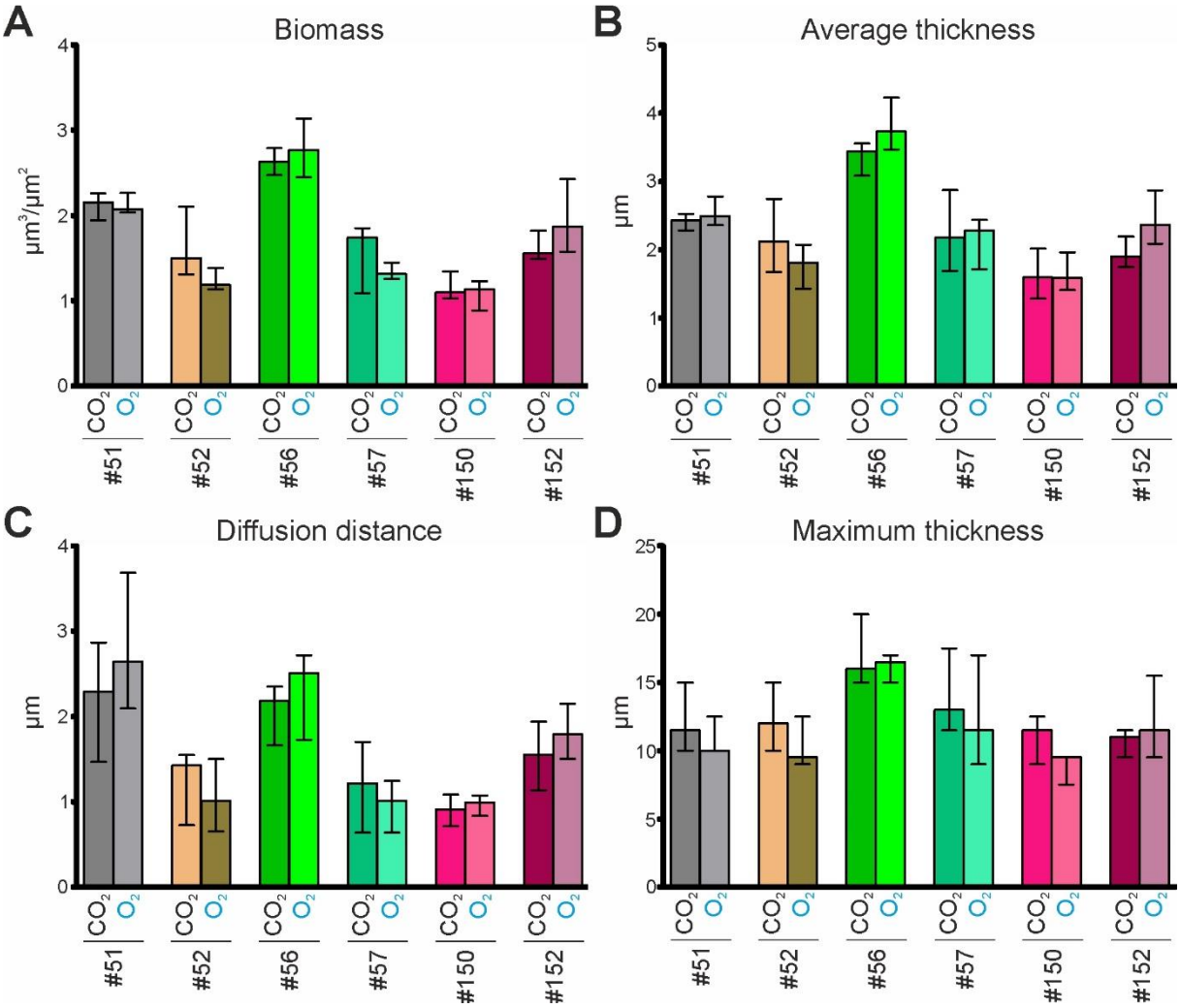

Figure 23: Comstat characterization and quantification of *S. epidermidis* biofilm morphology. Six reference strains of *S. epidermidis* were grown in flowcell chambers under anaerobic and aerobic conditions for ~ 20 h at 37°C. After washing of non-sessile cells, bacteria were stained with SYTO9 (targeting DNA) and image stacks were created (with steps of 0.5 µm). These were analyzed for the biomass (A), the average thickness (B), the average diffusion distance (C) and the maximum thickness (D) using the COMSTAT 2 software (Heydorn et al., 2000; Vorregaard, 2008). Shown are the medians of at least two image stacks from at least three independent experiments for each strain. The error bars indicate the interquartile range.

Strain #56 and #152 showed highest biomass and biofilm thickness in the microscopical chamber (Fig. 23), correlating with the results from the MTP assay (Fig. 9D, B and E) and verifying correct depiction of biofilm quantities from two independent perspectives.

3. Planktonic and Biofilm Stage Characterization

The definition of a biofilm stage, as described in the introduction, consists of attachment to a surface, building of an extracellular matrix scaffold, reduction in proliferation speed, directional growth into aggregates and water corridors, until at a late stage cells detach from the colony to find new niches. This definition, however, varies strongly from species to species, even from sub-group to sub-groups. *Vibrio cholerae*, for example, switches from the biofilm stage to a planktonic stage by formation of flagella for motility and turning into a singular cell living stage. *C. acnes* on the other hand was observed to form aggregates in almost all, so far investigated conditions. The subject of this section was the investigation and establishment of a non-biofilm condition called planktonic. Subsequently, the planktonic and the biofilm derived cells were compared from different perspectives, such as attachment and aggregation, as well as protein composition and function.

3.1. Comparative protein profile analyses of *C. acnes* isolates revealed distinct differences in biofilm-derived samples

Recently, Jahns et al. reported that the planktonic or biofilm mode can be enriched by cultivating a *C. acnes* IB isolate for short or long durations, respectively (Jahns et al., 2016). Other publications went for a similar direction, whereas planktonic mode was correlated more to exponential growth phase, and biofilm stage to stationary growth phase (Brzuszkiewicz et al., 2011). Based on these publications and preliminary results within this work, a general protocol applicable for all phylotypes was established.

C. acnes isolates were grown for either 18 h or 75 h to isolate planktonic or biofilm mode enriched cells, which was monitored by microscopic evaluation. Microscopic analyses visualized planktonic *C. acnes* cultures (PL) as dispersed cells with small aggregates of a few cells only (Fig. 24). In contrast, biofilm cultures were visualized as multi-cellular aggregates of up to 200 µm. Similar to the biofilm formation, the aggregation phenotype was phylotype dependent and showed most pronounced differences for IA1, IA2, IB and IC isolates. This suggests that biofilm derived cells had a higher inter-cellular surface adhesion capacity compared to planktonic cells.

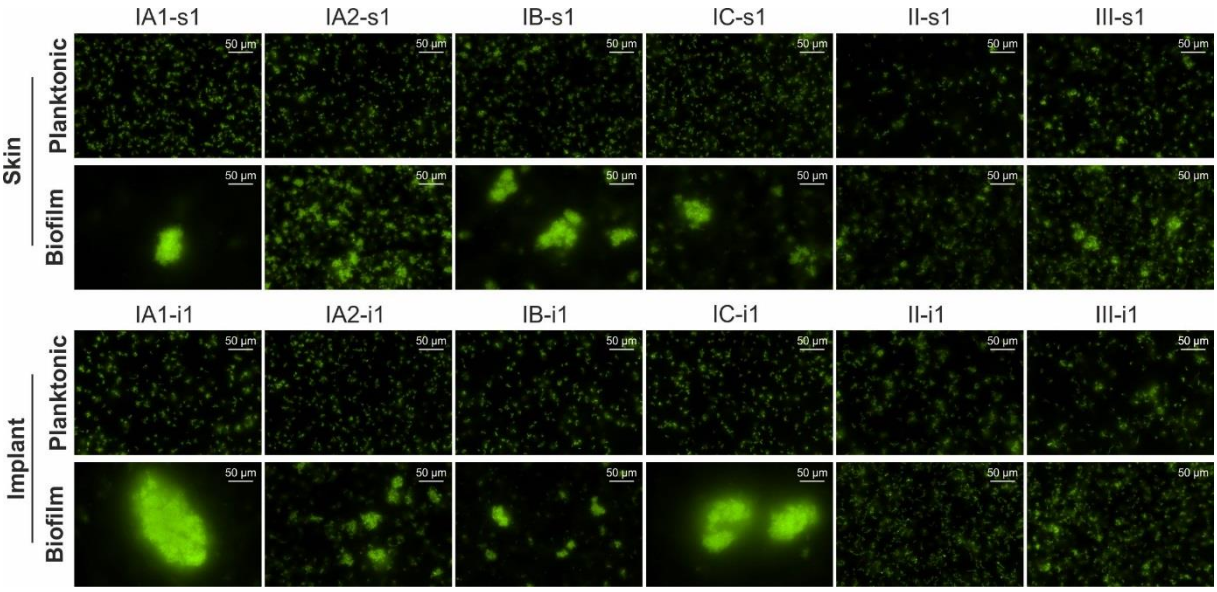

Figure 24: Microscopic visualization of planktonic and biofilm aggregation. Reference strains from all phylotypes and anatomic sites of infection (skin vs implant) were grown according to the rpm based planktonic and biofilm protocol. After harvesting, cells were mixed with SYTO9 (DNA staining fluorescence dye), injected into the flowcell and visualized in the FITC channel. Planktonic cells showed low cell aggregates of maximum of a few cells in all cases, whereas biofilm cells showed phylotype dependent intercellular binding capacity, forming aggregates of up to 200 µm (implant-associated strain IA1-i1).

Using this protocol, whole cell lysate and membrane-associated protein samples were isolated from planktonic and biofilm derived cultures of all twelve reference strains (six from the skin and six from implant associated isolates) and subjected to a comparative protein profile analysis by SDS-PAGE (Figs. 25 and 26). Despite some phylotype heterogeneity, all of the twelve reference strains exhibited similar protein profile patterns during the planktonic state (Fig. 25A and E, as well as B and F). This suggests that different *C. acnes* isolates had a comparable expression of abundant cytosolic and membrane-associated proteins during the planktonic state. This correlated with the similarities of the planktonic microscopical phenotypes (Fig. 24). In contrast, protein profiles of whole cell lysates and membrane-associated fractions from biofilm derived cultures exhibited more heterogeneity between the twelve *C. acnes* isolates (Fig. 25C and G, as well as D and H). Especially in the membrane-associated fractions representing the surface-associated proteins distinct alterations in defined bands between the phylotypes could be observed (Fig. 25D and H). In general, the heterogeneity in protein profiles was more pronounced between isolates from different phylotypes than between skin and implant derived isolates of the same phylotype. However, some defined differences between skin and implant derived isolates of the same phylotype could also be observed, e.g. an abundant band at ~20kDa in BF^{MF}

sample of IB-s1, which was missing in the BF^{MF} sample of IB-i1 (Fig. 25F, D and H). This suggests that the diverse *C. acnes* isolates exhibited distinct differences in protein expression during the biofilm state.

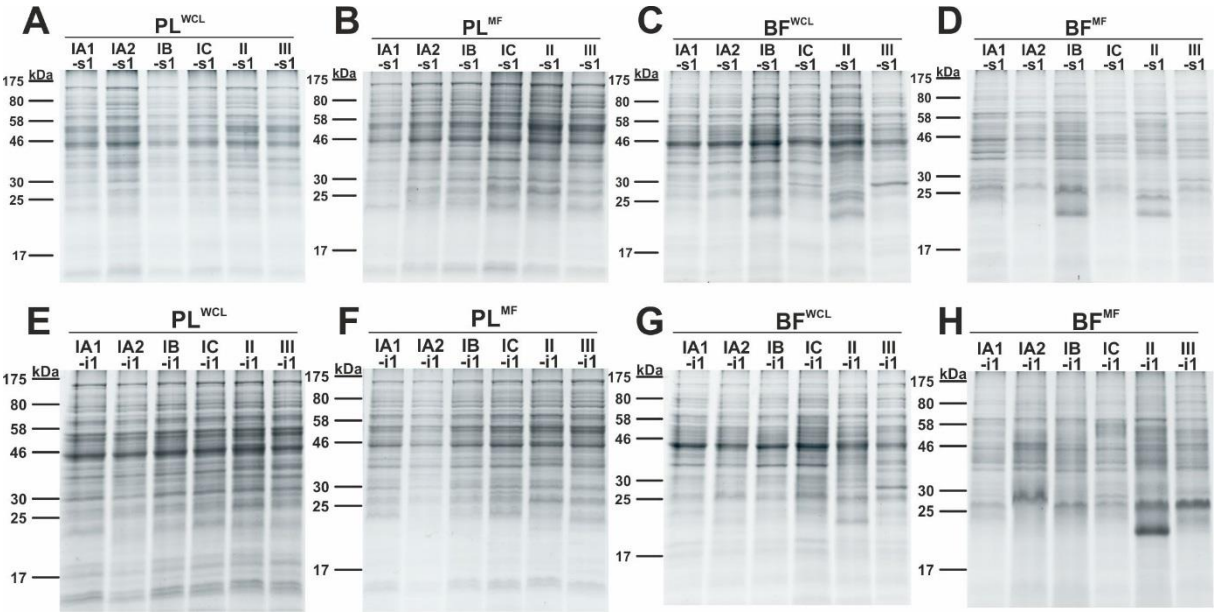

Figure 25: Protein profile comparison of *C. acnes* reference strains. Shown are Coomassie-stained gels of whole cell lysates (WCL) and membrane-associated fractions (MF) obtained from *C. acnes* reference strains representing the six phylotypes (IA1, IA2, IB, IC, II and III) categorized by anatomical site of isolation [-s=skin (A to D) and -i= implant (E to F)] and the cultivation condition [PL=planktonic (A, B, E, F) and BF=biofilm (C, D, G, H)]. Cells were cultivated in (PL, A, B, E and F) or biofilm (BF, C, D, G and H) mode. Horizontal lines to the left indicate the molecular masses of the protein standards in kDa.

This consequently implied that the protein profile of a specific *C. acnes* isolate exhibited defined changes between the planktonic and biofilm mode. To visualize these differences for every reference strain in more detail, whole cell lysates and membrane-associated fractions obtained in the planktonic or biofilm mode were directly compared by SDS-PAGE (Fig. 26). For all strains analyzed, most pronounced differences were between the membrane-associated fractions obtained in the planktonic or biofilm mode. Thus, planktonic and biofilm derived *C. acnes* differed mostly in their surface-associated protein expression.

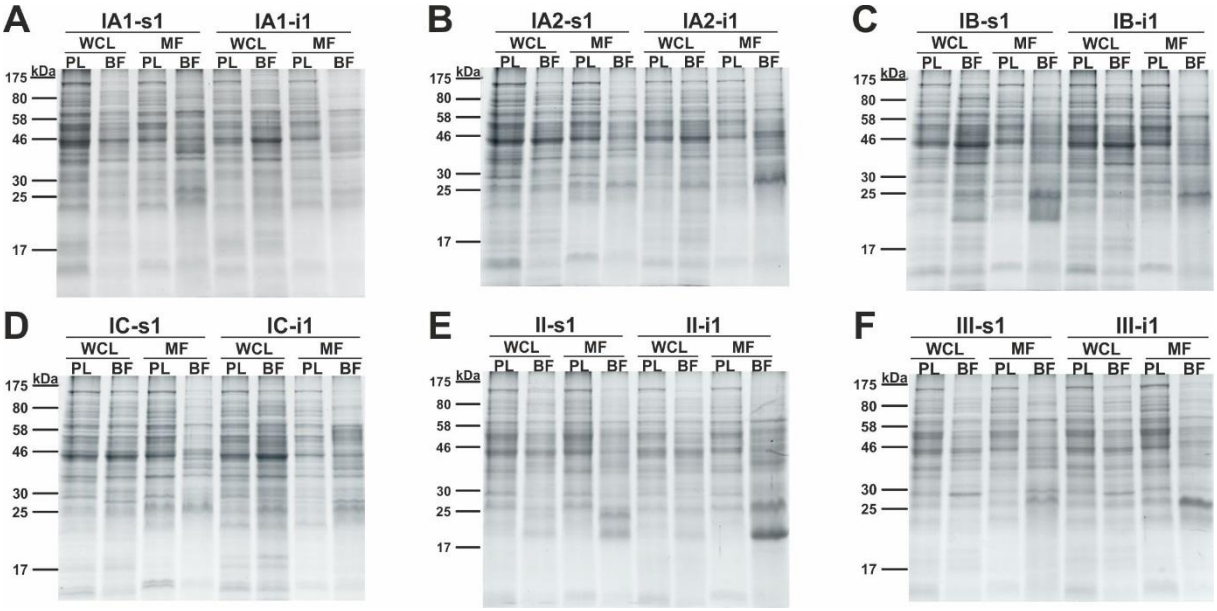

Figure 26: Strain-specific protein profile alterations of *C. acnes* isolates in the planktonic (PL)- and biofilm (BF)-mode. Shown are Coomassie-stained gels of whole cell lysates (WCL) and membrane-associated fractions (MF) obtained from *C. acnes* reference strains cultivated in the planktonic (PL)- or biofilm (BF)-mode. *C. acnes* reference strains comprised skin (s)- and implant (i)- derived isolates of the phylotypes IA1 (A), IA2 (B), IB (C), IC (D), II (E) and III (F). Horizontal lines to the left indicate the molecular masses of the protein standards in kDa.

3.2. Identification of proteins with differential abundance during planktonic and biofilm mode

Membrane-associated fractions of *C. acnes* isolates IA1-s1 and IB-s1 were chosen to identify differentially expressed proteins in the planktonic and biofilm mode by mass spectrometry analysis (Fig. 27). IA1-s1 represented the IA1 phylotype with acne association and high biofilm formation capacity. In contrast, IB-s1 represented phylotype IB, which showed low biofilm production (Fig. 3 and 17), lack of distinct biofilm structure (Fig. 15) and weak surface attachment (Fig. 18).

Several proteins of both isolates found to be more abundant in the planktonic-mode were involved in nutrient acquisition and metabolism, suggesting that the planktonic and biofilm mode might reflect different metabolic states. Based on in silico analyses, the majority (62%) of the proteins identified were integral membrane or membrane-associated proteins, confirming the membrane enrichment in these samples. In addition, some cytosolic proteins were identified. For example, the RNA polymerase beta- and beta‘-subunit were independently identified in samples of both strains, the beta-subunit to be abundant in biofilm derived samples of both isolates. At the moment we cannot exclude that these arose from contaminations of the membrane-associated

fractions. However, moonlighting proteins with DNA-binding activity have been found in biofilms of other Gram-positive bacteria, such as *Staphylococcus aureus* and *Streptococcus pneumoniae* (Domenech et al., 2013; Foulston et al., 2014).

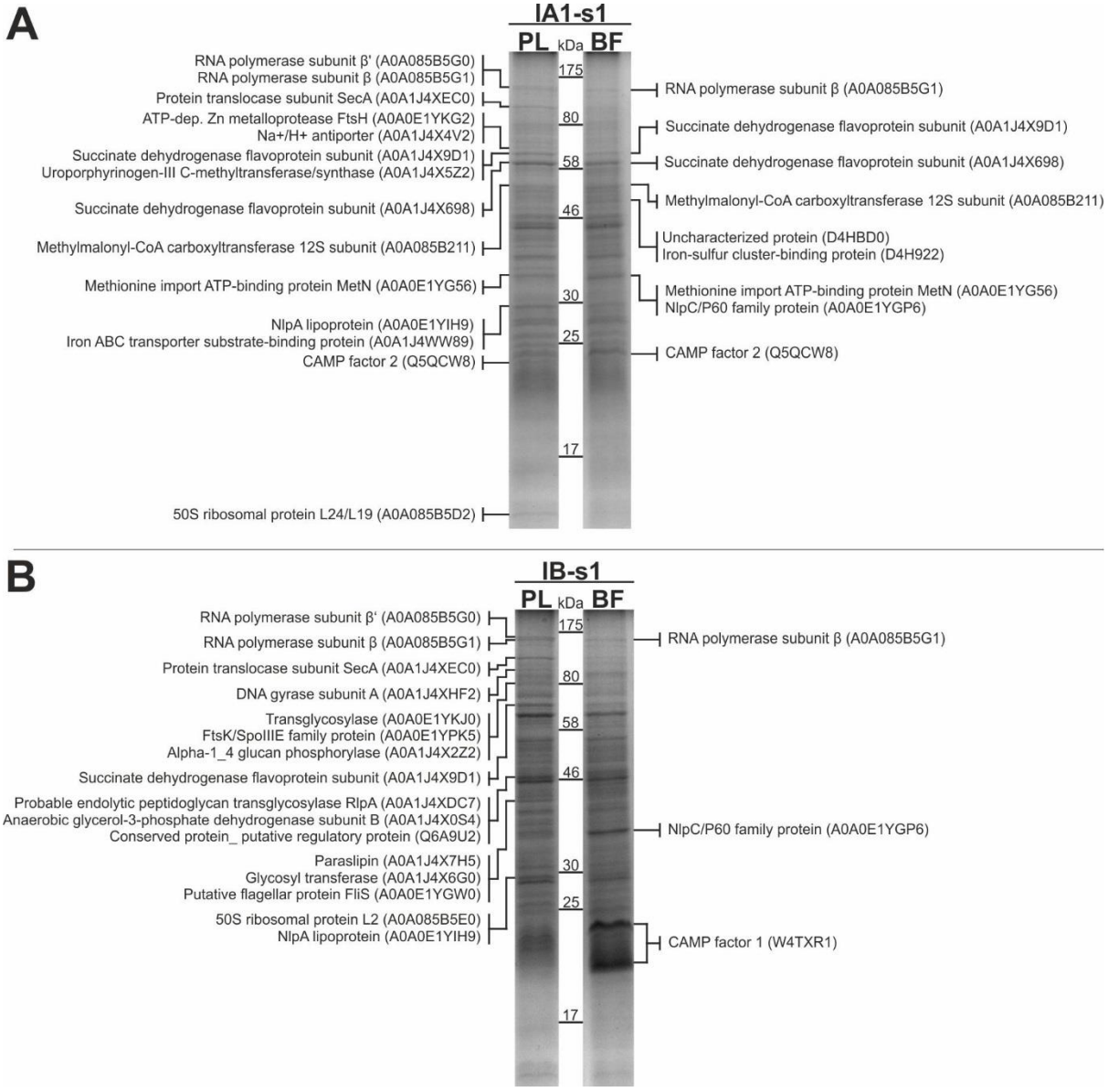

Figure 27: Mass spectrometry analysis of protein candidates differentially expressed in planktonic (PL)- and biofilm (BF)-mode. Shown are Coomassie-stained gels of membrane-associated fractions obtained from *C. acnes* isolate IA1-s1 (A) and IB-s1 (B) during planktonic (PL) and biofilm (BF) mode. Protein bands with differential appearance or intensity between planktonic and biofilm mode were identified by mass spectrometry. After in silico analysis the predictions were indicated at their respective position on the gel, showing protein identities and accession numbers. Horizontal lines in the middle indicate the molecular masses of the protein standards in kDa. Generally, planktonic proteins were identified to be more closely associated to metabolism and proliferation, whereas biofilm-associated proteins showed increased abundance in proteins coping with starvation (iron-sulfur cluster-binding protein), inducing virulence (CAMP factor) or possible biofilm regulation (NlpC/P60 family protein).

The NlpC/P60 family protein (A0A0E1YGP6) was identified in biofilm derived samples of IA1-s1 and IB. Interestingly, the cut-out band of planktonic proteins of IA1-s1 on the same height did not include any traces of it under the given sensitivity, possibly indicating an upregulation in biofilm mode. Generally, NlpC/P60 proteins are involved in murein degradation, acyl transfer or amide hydrolysis (Anantharaman and Aravind, 2003). In *Mycobacterium tuberculosis* a NlpC/P60 protein facilitated biofilm formation (Padhi et al., 2016). While the exact function for this particular protein remains to be unraveled, cell wall-associated hydrolases (to which NlpC/P60s belong) can be involved in cell division, modulation of immune activation and regulation of latency (Wyckoff et al., 2012).

Furthermore, in the biofilm mode both *C. acnes* isolates showed high abundance of the Christie-Atkins-Munch-Peterson (CAMP) factors, which were initially considered as virulence factors of *C. acnes* (Nakatsuji et al., 2011). The genome of *C. acnes* encodes five CAMP factors (CAMP 1 to 5) with a homology ranging between 33% and 99% (compared to CAMP 1) and diverse activities (Lheure et al., 2016; Valanne et al., 2005). As an example, CAMP 1 exacerbated immune reactions by binding to the TLR-2 receptor (Lheure et al., 2016), while CAMP 2 had a potent co-hemolytic activity (Sörensen et al., 2010; Valanne et al., 2005). Concordant with previous studies demonstrating phylotype specific expression of the different CAMP factors (Lheure et al., 2016; Valanne et al., 2005), CAMP 2 was only found in IA1-s1, while CAMP 1 was only detected in IB-s1. This is consistent with our data, as well as with a recent report by Jahns et al. indicating that CAMP 1 is transcriptionally upregulated during biofilm formation of a IB isolate (Jahns et al., 2016). Notably, band intensities reflecting the CAMP factors differed in the biofilm derived samples of IA1-s1 and IB-s1, indicating differential expression levels. Another study performed mass-spectrometry of proteins secreted in healthy and acne-associated follicles. They found a reduction of detectable CAMP1 factor from 72% of all follicles in healthy individuals compared to 10% in acne-associated follicles. CAMP2 was only found in 10% of the samples, which was reduced to 0% in acne-associated follicles (Bek-Thomsen et al., 2014). From this perspective, CAMP factors either don’t seem to play a key role in virulence, or the immune system at some point is forced to and capable of reacting to CAMP factors and mediating its degradation.

4. Immunocytochemistry

Within an industrial collaboration with Origimm Biotechnology (Vienna, Austria), we were provided with (mouse or rabbit) antisera, containing antibodies against possible surface-associated protein candidates of *C. acnes*. To identify whether the protein candidates were accessible for antibodies on the surface at all and if yes, in which manner (full opsonization or partial cell coverage), an immunocytochemistry assay was established. Herein, viable *C. acnes* cells in planktonic and biofilm mode were opsonized by the respective antisera, incubated with an anti-Fc secondary antibody which was fluorescence dye-conjugated and visualized under the microscope.

4.1. Establishment of a protocol for microscopical visualization of *C. acnes* surfaces

To visualize binding of primary antibodies within the antiserum on *C. acnes* surfaces, a protocol was established similar to an immunoblot. A fluorescent secondary antibody was bound to the Fc-part of the primary antibody (from the antiserum) and the cells were fluorescence microscoped in situ (Fig. 28). Cy3 with an excitation (Ex) peak at 550 nm and an emission (Em) peak at 570 nm was chosen, as it delivered a strong and stable (orange) signal, supposedly out of the emission range of SYTO9 (Ex 485 nm, Em 498 nm). In the fluorescence microscopy section (2) SYTO9 was used as DNA staining dye. Generally, SYTO9 offered clear images of bacterial cytosolic DNA and extracellular DNA with low bleaching effects. Unfortunately, when using the lamp on maximum intensity with the TRITC or TexasRed filter active, a weak fluorescence leakage of SYTO9 into these channels could be detected. To avoid background signals being mistaken for antibody fluorescence, a DNA staining dye with lower excitation/emission wavelength was chosen: DAPI (Ex 350 nm, Em 470 nm). In a follow-up test, cells stained by DAPI could not be detected by microscopy when applying the Cy3 visualizing filters with maximum lamp intensity.

Antisera were harvested from rabbits after immunization with each individual protein candidate (one rabbit for one protein candidate). To make sure that the rabbits did not possess antibodies against the respective protein antigen, serum prior to immunization was taken (“pre-serum”) and tested in parallel to all immunocytochemistry and immunoblot experiments. Rabbits with pre-serum signal were excluded from the experiments. As mice did not allow pre-serum extraction, a control group of ten mice

was instead immunized with PBS. No signal was detectable from their serum. Sometimes aggregates of high fluorescence intensity (possibly protein aggregation) could be detected also for the pre-serum control. To reduce Cy3-background fluorescence in the pre-serum, optimization steps were included into the protocol. These included lower dilutions of serum, addition of BSA through all incubation steps, a blocking step with BSA and additional washing steps. In the end, fluorescence aggregates in the pre-serum mostly disappeared and signal background was lowered to a peak of approximately 395-410 relative intensity units (RIU). The protocol was summed up in Fig. 28.

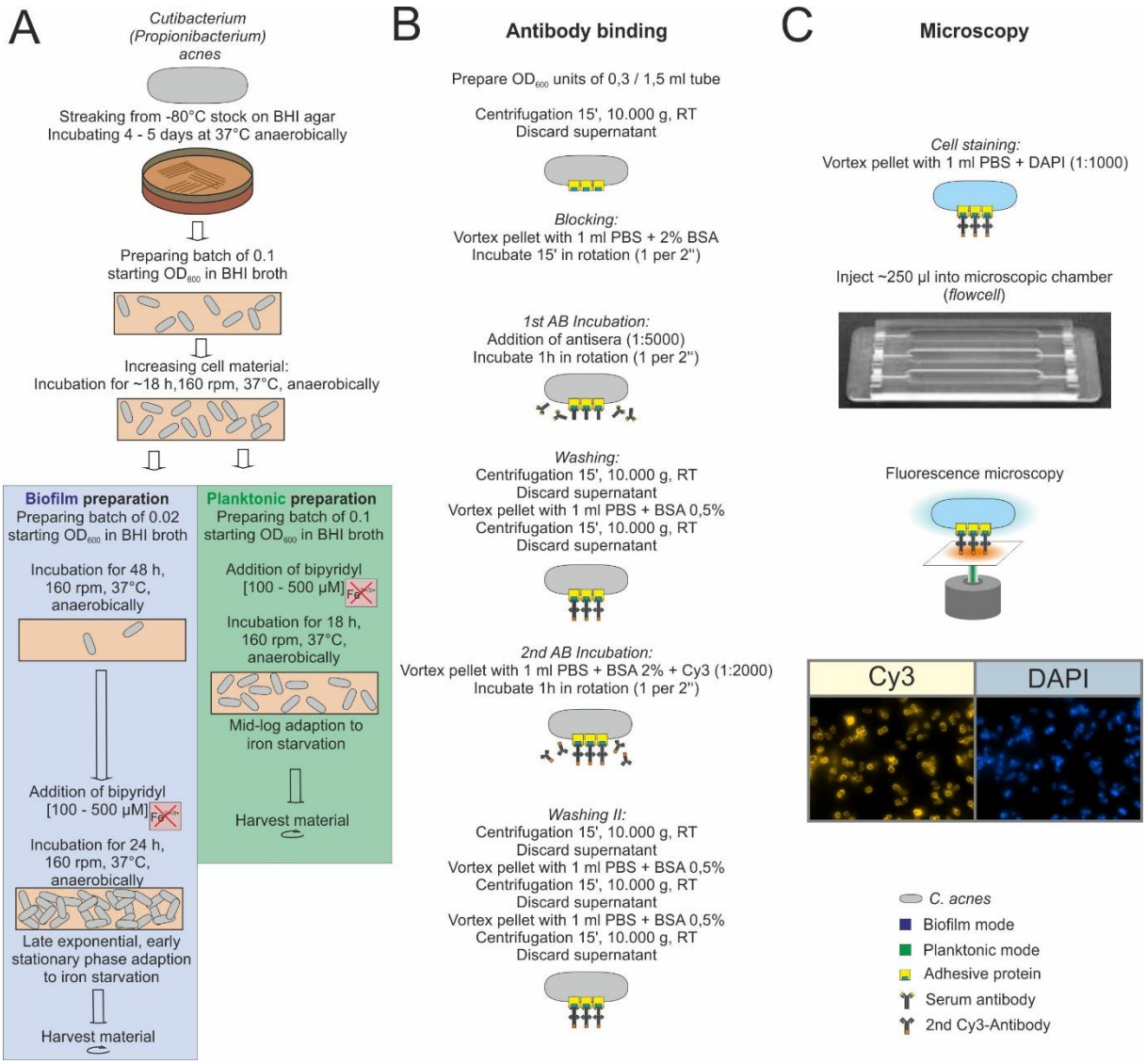

Figure 28: Overview immunocytochemistry protocol. (A) The protocol shows the major steps from streaking from -80°C stock to deriving planktonic and biofilm cells in iron starvation. (B) Subsequently, these cells were opsonized by primary (antiserum) and secondary antibodies (Cy3-conjugated), alternated by washing steps. (C) Surface covered *C. acnes* cells were fluorescence stained by DAPI, injected into the flowcell and microscoped in DAPI channel

(for DAPI dye showing mostly cytosolic DNA) and FITC channel (Cy3-dye showing *C. acnes* surface).

4.2. Binding of anti-22#1 serum to *C. acnes* surfaces showed qualitative and semi-quantitative possibilities of analysis

ICC (antibody) based fluorescence microscopy offered three interpretations of its fluorescence signals: a) answering the question whether the target protein is accessible for the antibodies at all in planktonic and biofilm state in situ, b) a qualitative visualization of the binding pattern (full coverage, partial hotspot binding) and c) a semi-quantitative judgement of its binding abundance.

In an example, images from anti-22#1 serum on the reference strains in biofilm and planktonic stage were cropped in their contrast and brightness to reach a point which visualized binding patterns in the best way (Fig. 29). Surface coverage could be visualized, interpreted and compared for all antisera and strains, in planktonic and biofilm mode. The IA1-s1 strain showed full coverage of the cells by a single antibody, verifying that protein 22 was present all over each single cell. In case of the type III strain, the protein seemed to be differentially expressed in a clustered way, leading to hotspots instead of full coverage (Fig. 29, last row). These results answered questions a) accessibility and b) surface coverage.

The signal intensity in Fig. 29 indicated similar abundance of antibodies, covering all strains similarly. However, when changing the applied method to crop for best contrast to a method where intensity cropping was precisely the same for all strains, then signals could be semi-quantitatively analyzed (Fig. 30). In that way the signal intensities changed noticeably. To visualize this, the same design as for Fig. 29 was chosen, but instead signal intensity cropping range of 700 to 2000 relative intensity units (RUI) was determined for all.

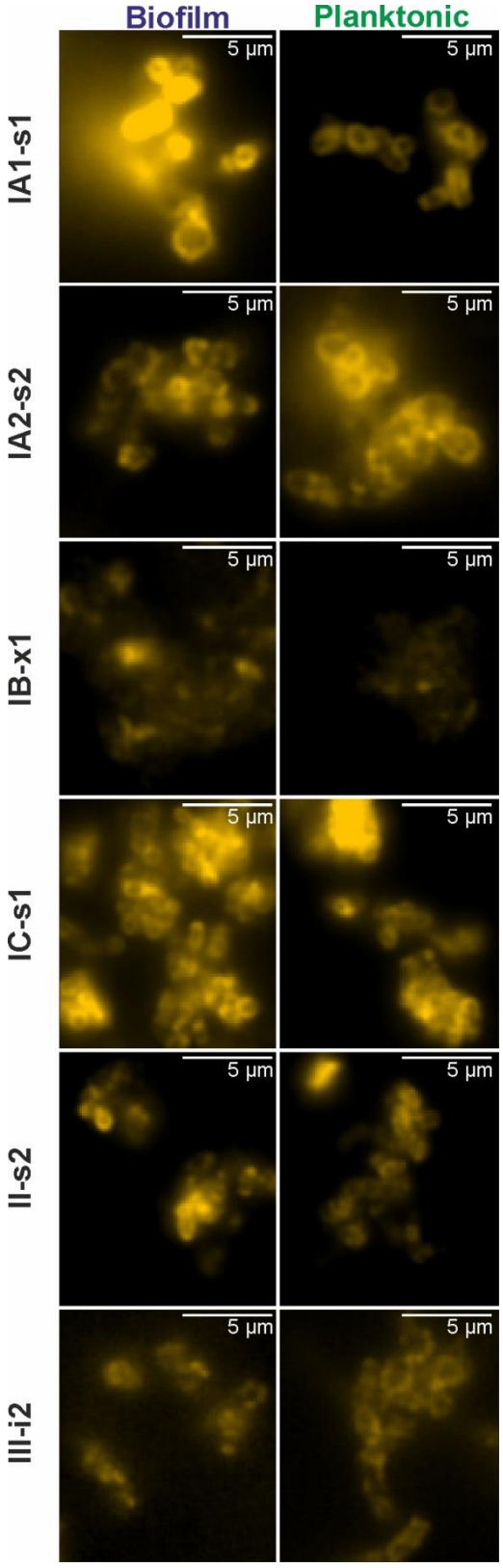

Figure 29: Visualization of antiserum 22#1 mediated surface coverage on 6 reference strains in planktonic and biofilm mode. The skin reference strains were brought to planktonic and biofilm mode and surface covered by rabbit antiserum 22#1and Cy3 according to the protocol (see Fig. 28 for details, but without addition of an iron chelator). Brightness adjustments followed the intention of best contrast for best surface coverage visualization, at the prize of semi-quantitative interpretation. See Fig. 30 for emphasis on semi-quantification.

Serum 22#1 showed binding to surfaces in all cases and ranged from full coverage to a spotty phenotype.

From this particular perspective the type III isolate could no longer be seen, stating that semi-quantitatively the antibody binding was weaker (but not how much). At the same time, the signal of type IC representative was too strong in planktonic and biofilm stage to still detect and analyze surface phenotypes. To detect surface coverage, the signal visualization window had to be enlarged from 700-2000 RUI to 850-5000 RUI (Fig. 30, arrow with decreasing detection sensitivity). Now surface binding could be seen. At the same time type III isolate's signal was too low to be detected under these conditions. So the signal could be increased (to 500-1000 RUI) to reveal that antibodies are binding, however with weaker affinity (Fig. 30, arrow with increasing detection sensitivity).

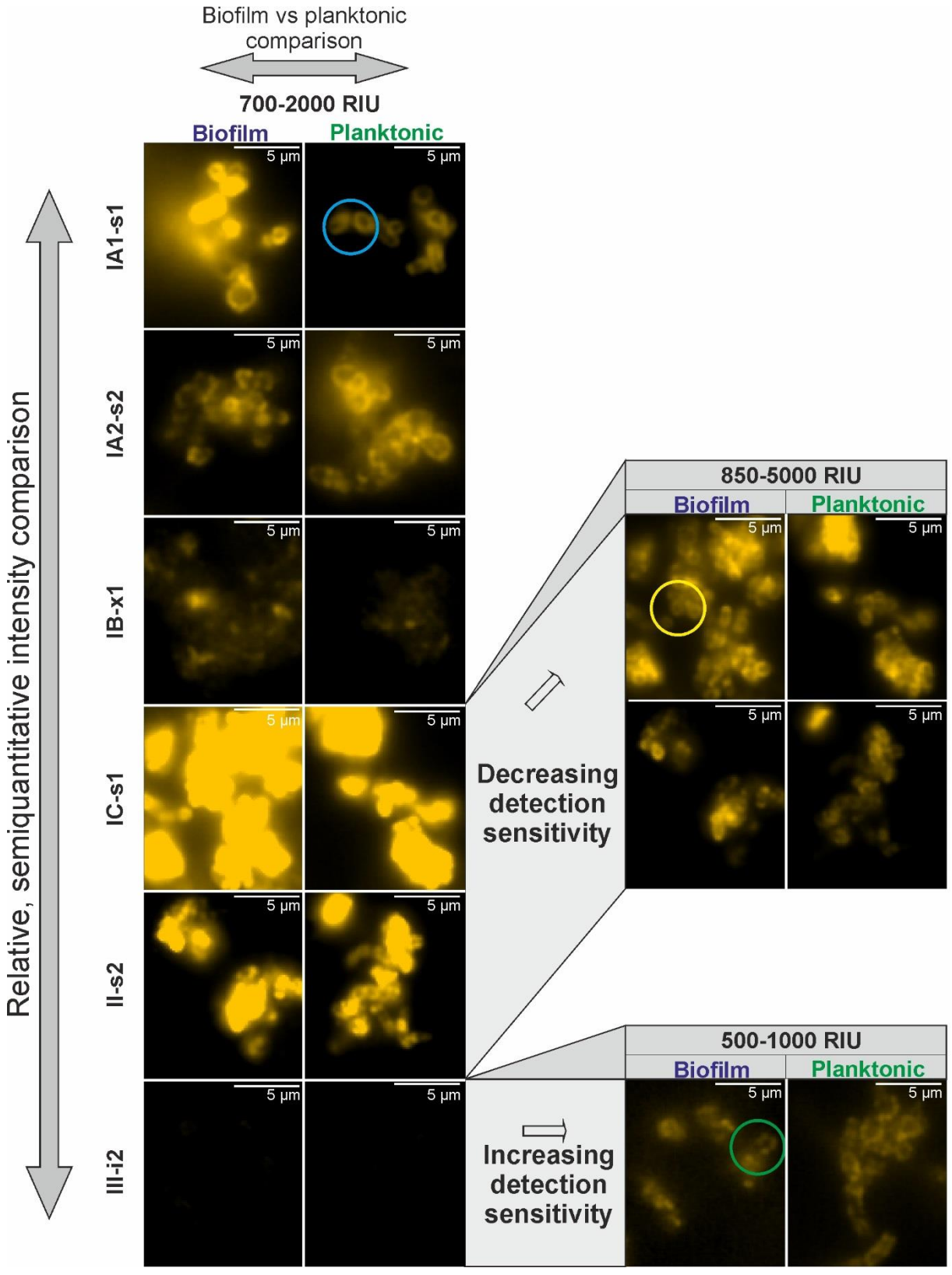

Figure 30: Semi-quantitative visualization of antiserum 22#1 mediated surface coverage on 6 reference strains in planktonic and biofilm mode. The skin reference strains were brought to planktonic and biofilm mode and opsonized by rabbit antiserum 22#1and Cy3 according to the ICC protocol (see Fig. 28 for details, but without addition of an iron chelator). The signal corridor was set to an equal signal range for all images (700-2000 relative intensity units [RIU]), allowing semi-quantitative interpretations of the results. Signal from IC-s1

overexposed the signal corridor, indicating relatively greater abundance of this epitope on the surface than the other strains. III-i2 on the contrary showed no signal in this range, visualizing lower antibody binding capacities of antiserum 22#1 against this strain. According to these results, protein 22#1 seemed to be in greatest abundance on IC and II, good abundance on IA1, IA2 and IB and in low abundance on phylotype III. Anti-22#1 serum showed binding to surfaces in all cases and ranged from full coverage to a spotty phenotype.

As Origimm had more sophisticated, internal methods for screening and quantifying antibody abundance on cell surface and quantification constituted a major part of the immunoblot section, this part of the work focused on answering question a) and b) and used semi-quantification only in special experiments as a second option (like interpretation of bipyridyl effects on protein 28 expression).

4.3. Iron chelator bipyridyl induced increased protein 28 expression

In vivo, iron is essential for all bacteria. As defense mechanism the human host secrets high-affinity iron binding proteins like lactoferrin to reduce its avail. BHI on the other hand contained iron, liberated from brain, heart and other bovine cells. At the same time, protein 28 was predicted to be involved in iron metabolism. To acknowledge both prerequisites, iron concentration was reduced in the system by the addition of the iron chelator 2,2'-bipyridyl. The features of bipyridyl were previously reported to include high affinity for both ferric (Fe^{3+}) and ferrous (Fe^{2+}) forms of iron, as well as membrane permeability and in further consequence its ability to attack intracellular iron reserves (Thompson and Carabeo, 2011).

To investigate the effects of different grades of iron starvation on protein 28 expression, a serial dilution of bipyridyl was prepared and added to the planktonic growth protocol in the last 17 h of incubation. Afterwards, cells were washed, opsonized by anti-28#1 serum and visualized by Cy3-conjugated antibodies (Fig. 31). As control, the same samples were instead opsonized by anti-27#1 serum (Fig. 32). Cy3-mediated fluorescence was characterized for surface binding location and abundance (semi-quantitatively).

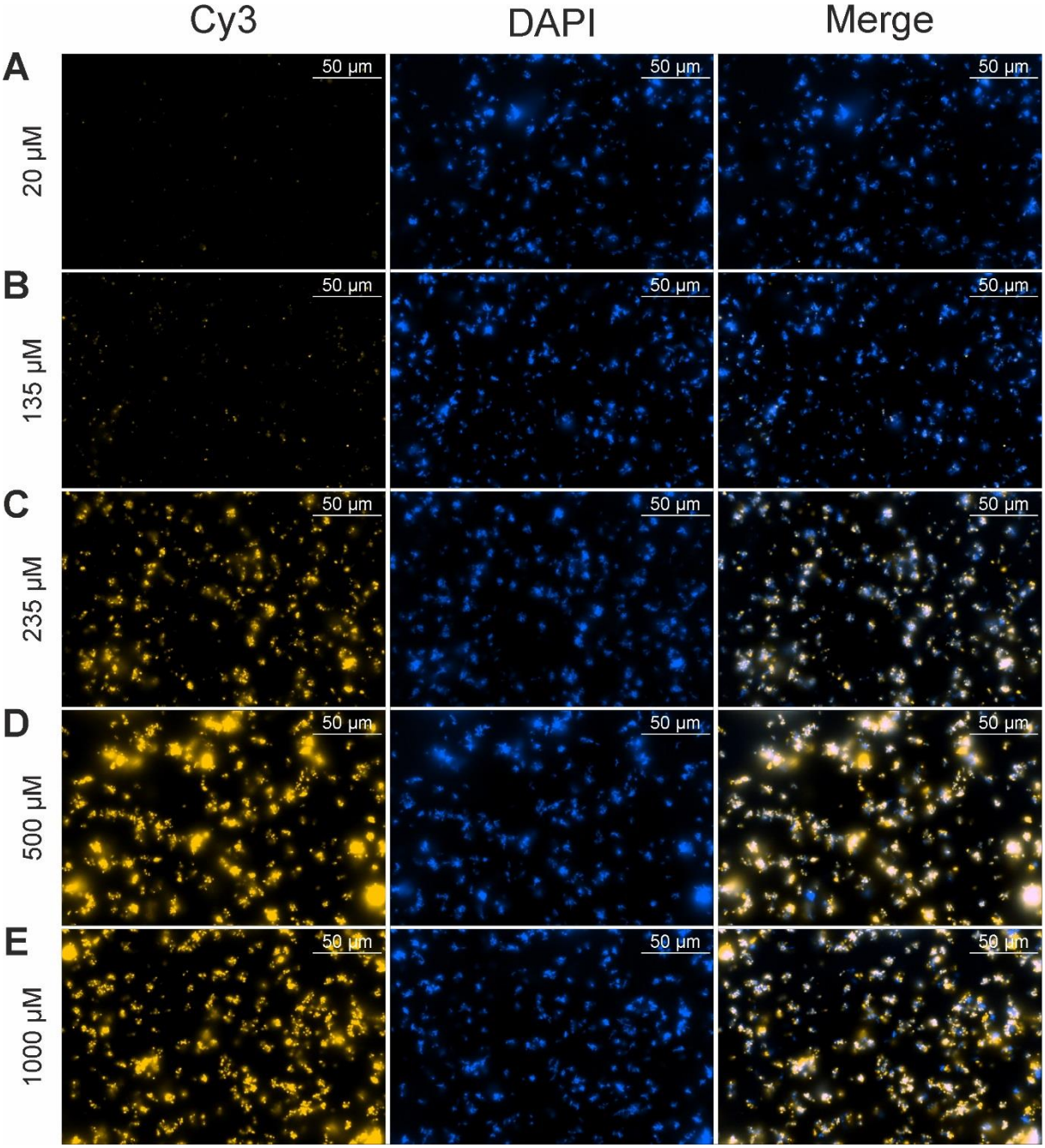

Figure 31: Anti-28#1 serum mediated signal intensity correlated with bipyridyl concentration. *C. acnes* strain IA1-s1 was grown according to the planktonic protocol (see Fig. 28 or Materials and Methods). Cells were opsonized by rabbit antiserum immunized with protein 28 and fluorescence tagged by Cy3-conugated antibodies (orange, TRITC channel). The same cells were visualized by DAPI staining DNA (blue, DAPI channel). Bipyridyl concentrations varied between (A) 20 µM and (E) 1000 µM. The signal corridor was set to an equal signal range for all images, allowing semi-quantitative interpretations of the results. Surface coverage increased with increased bipyridyl concentration, suggesting gradually increased protein 28 expression upon iron starvation.

According to these results, protein 28 was expressed in low abundance under high iron concentrations. The higher the bipyridyl concentration and with it the lower the iron

supply got, the more protein 28 was expressed, translocated to the surface and targeted by protein 28 antibodies (Fig. 31).

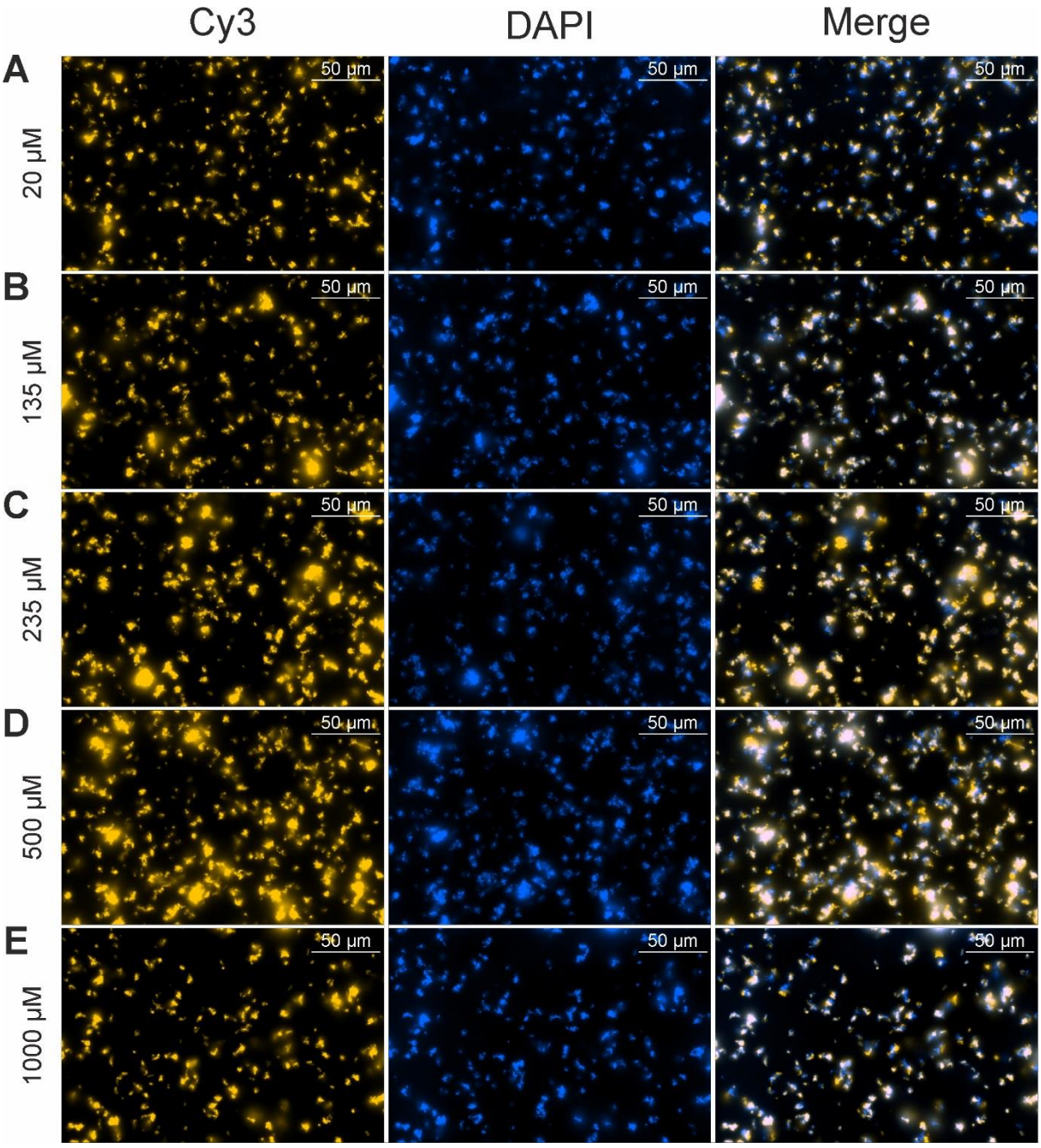

Figure 32: Anti-27#1 serum signal remained the same on bipyridyl concentration variation. *C. acnes* strain IA1-s1 was grown according to the planktonic protocol (see Fig. 28 or Materials and Methods). Cells were opsonized by rabbit antiserum immunized with protein 27 and fluorescence tagged by Cy3-conugated antibodies (orange, TRITC channel). The same cells were visualized by DAPI staining DNA (blue, DAPI channel). Bipyridyl concentrations varied between (A) 20 µM and (E) 1000 µM. The signal corridor was set to an equal signal range for all images, allowing semi-quantitative interpretations of the results. Surface coverage stayed similar even upon increased bipyridyl concentration, suggesting no effects on protein 27 expression by iron starvation. As samples were performed in parallel to protein 28 investigations and relied on same sample material (Fig. 31), the results herein made it unlikely that general technical artefacts caused the protein 28 gradual phenotype.

As control, antiserum 27#1 targeting protein 27 expression was visualized and no change in phenotype could be seen, indicating signal change of protein 28 was not due to artificial side effects like differential cell concentration or washing effects (Fig. 32). To compare semi-quantitative levels of (low) 20 µM bipyridyl and (almost bacteriostatic) 1000 µM bipyridyl, the fluorescence signal intensity window was compared for both conditions (Fig. 33).

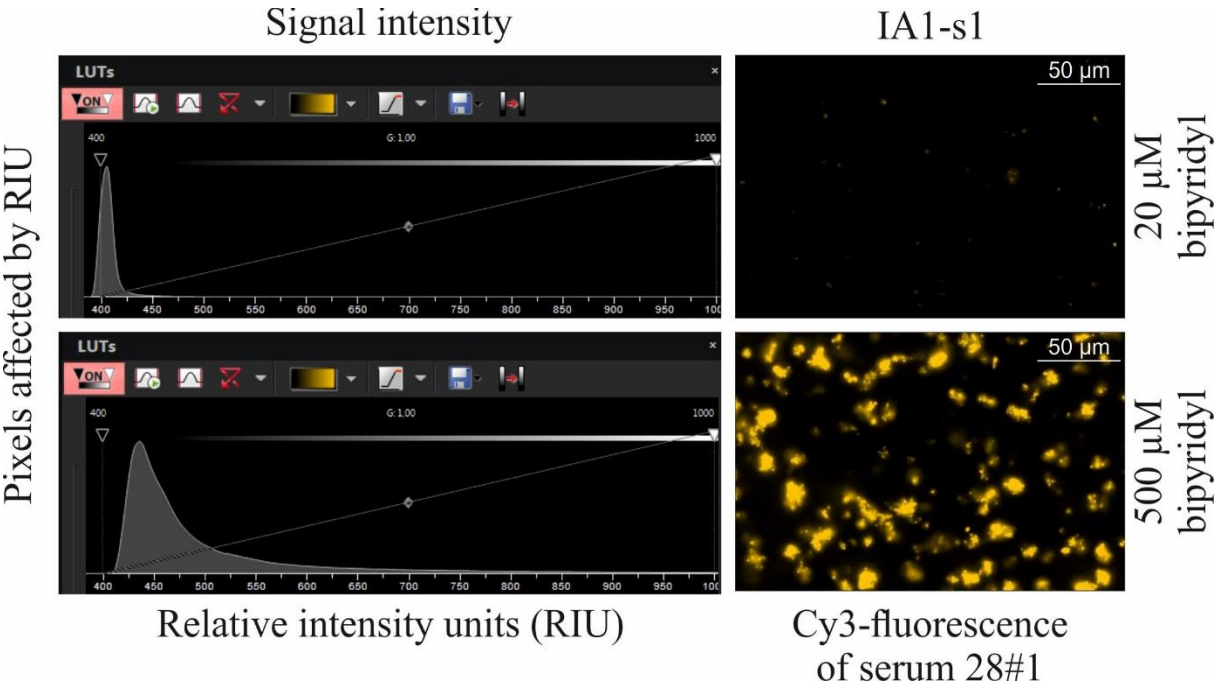

Figure 33: Semi-quantitative analysis of differential bipyridyl signal strength. The signal corridor for comparison of protein 28 data (Fig. 31) was set to an equal signal range for both images (400 – 1000 RUIs). The 20 µM bipyridyl sample showed a signal peak at approx. 405 RUIs. The 500 µM sample on the other hand peaked at 425 with larger areas under the curve. Fluorescence image and signal area under the curve support semi-quantitative interpretation.

The signal intensity with low bipyridyl concentrations ranged from approximately 390 to 425 RIU (Fig. 33, upper panel). The sample incubated with high bipyridyl concentrations exhibited increased signal intensity of 425 – 750 RIU (from 390-425). Intermediate bipyridyl concentrations showed intermediate signal intensities.

Taken together, bipyridyl served as functional iron chelator and gradually increased protein 28 expression of *C. acnes* under iron starvation conditions. As the in vivo situation is reflected by iron starvation, the physiological situation of *C. acnes* on the skin and its protein 28 expression is more likely resembled by high quantities of bipyridyl, verifying its importance for further analysis. Bipyridyl effects on protein 28 expression were also monitored in an immunoblot (section 6), getting to similar results

(Fig. 39). With these results in mind, final analyses on protein 28 were done with bipyridyl concentration of 100 – 500 µM depending on the phylotype: 100 µM for type III, 500 µM for type IA1 and II and 250 µM for type IA2, IC and IB.

4.4. Antibodies against protein 22, 27, 28 and H4 revealed full surface coverage for phylotypes IA1, IA2 and IC

As mentioned in the subsection above, the main goal of immunocytochemistry was to answer the question whether the target protein is accessible for the antibodies at all in planktonic and biofilm state and if yes, show qualitative visualization of the binding pattern (full coverage or partial hotspot binding).

In close collaboration with Origimm the selection process of over 60 lead candidates was narrowed down to the proteins 22, 27, 28 and H4. Summarizing images, showing combined DAPI (DAPI dye) and TRITC (Cy3 dye) channels of biofilm and planktonic cells of all phylotypes, can be found in the supplemental part (Figs. S1 – S6).

Serum H4 showed complete surface covering opsonization for IA1, IA2 and IC phylotypes in both physiological states (Fig. S1). Blue DAPI signal, showing *C. acnes* cytosolic DNA, was surrounded by an orange halo, mediated by H4 based epitopes on *C. acnes* surface. IB and III however remained mostly blue, suggesting weak surface binding or lack of target protein on the accessible surface. Type II in planktonic mode occasionally contained small cell aggregates without visible surface coverage. In biofilm mode this ratio seemed to have been reduced. All runs were additionally tested with *C. acnes* anti-WCL serum. In all cases full opsonization and typical *C. acnes* morphology from all cells was visible, suggesting no contamination.

Two antisera 22#1 and 22#2 (from two independent rabbit immunizations) were evaluated, revealing generally high similarity in the data (Figs. S2 and S3). Similar to the results of H4, IA1 and IA2 showed full opsonization. IA1 had somewhat weaker but similar phenotype, and in less abundance for planktonic mode. Full opsonization binding could be seen for IB and III, interestingly though only for a few cells. The rest remained unmarked. Type II cells were gradually surface covered, ranging from full coverage to no visible coverage.

In comparison of serum 27#1 and 27v1 patterns looked similar, although signal from 27#1 seemed to be more pronounced (Figs. S4 and S5). Full opsonization could be

visualized for the IA1, IA2 and IC phylotype representatives. Cells were gradually opsonized for II, but here the weakest opsonization still showed mild but complete surface coverage. IB in planktonic mode could not be targeted by 27#1 or 27v1, but in biofilm mode expression seemed to have been increased to a hotspot phenotype on the surface. The same appeared to count for type III.

Protein 28 could be detected for all phylotypes under iron limited conditions, while being more pronounced in planktonic than in biofilm mode (Fig. S6). The phenotype of IA1, IA2, IB and II revealed strong surface clusters on most cells, alternated by some cells with less signal intensity. Type IC signals were less clustered but mostly covered. For type III, blue stained cells dominated with mostly hotspots and some full coverage occasionally.

Summarizing the results from the perspective of immunocytochemistry under the given conditions, protein 28 showed greatest accessibility and abundance on phylotypes IA1, IA2, IB, IC and II. Only partial opsonization was visible on type III cells. As type III is rarely involved in acne pathogenicity, lower opsonization for these isolates might be of no relevance for an acne vaccine. With IA1, IA2 and IC being the most prominent phylotypes isolated from acne patients, efficacy against these might be of greatest importance. And indeed, H4, 22, 27 and 28 showed full coverage for these phylotypes.

5. Microscopic Evaluation of Opsonophagocytosis

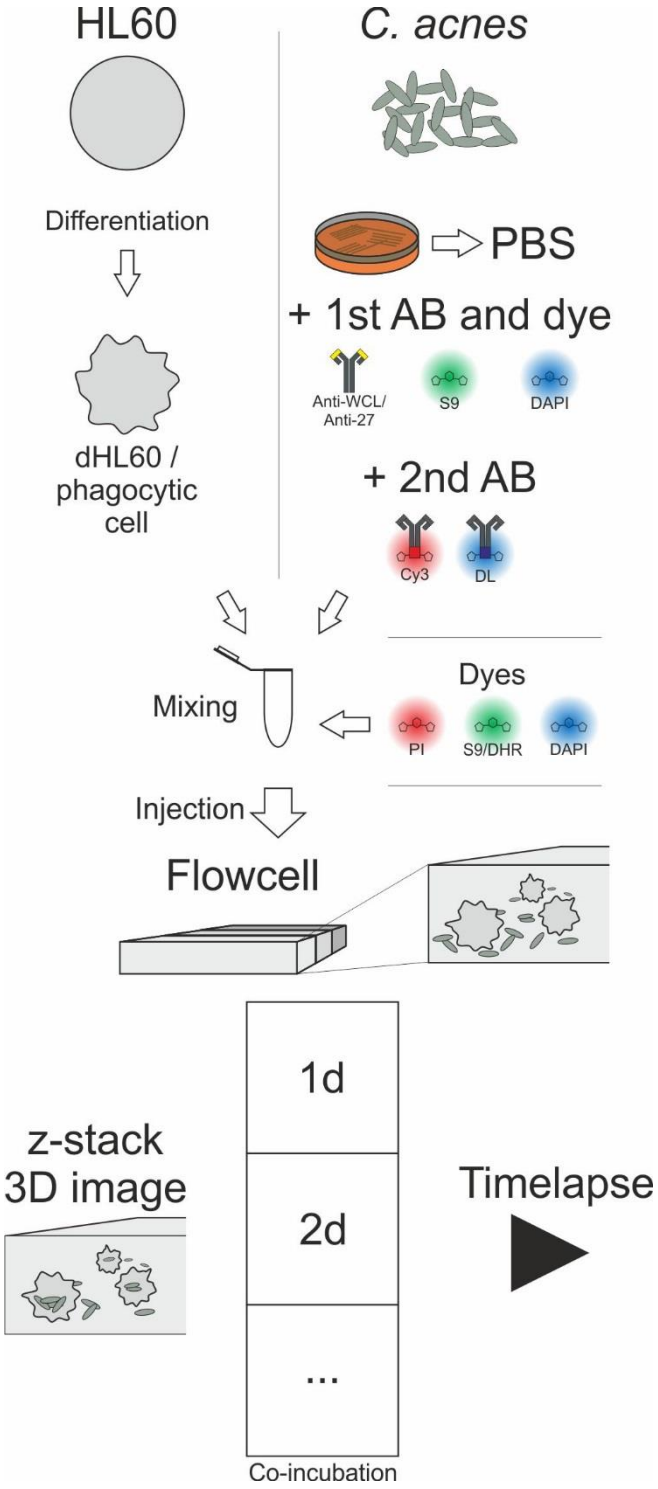

Figure 34: Protocol of the opsonophagocytosis assay. HL60 cells were differentiated to follow a phagocytic character, while *C. acnes* was treated with different combinations of fluorescence dyes and antibodies. After mixing and co-incubating bacteria and immune cells, the suspension was injected into the microscopic chamber and incubated for 1 to 6 days at 37°C aerobically in 5% CO_2 atmosphere and 90% humidity. Microscopic images of all involved fluorescence dyes were made investigating phagocytosis. AB: antibody, PI: propidium iodide, S9: SYTO9 fluorescence dye, DHR: dihyro-rhodamine 123, DAPI: 4',6'-diamino-2-phenylindole, DL: DyLight® 350 conjugated secondary antibody, anti-WCL: antiserum from *C.*

acnes whole cell lysate immunization, anti-27: antiserum against protein 27#1, Cy3: Cy3-conjugated secondary antibody.

One of the most important lines of defense for the human host is the adaptive immune system, represented among others by phagocytic neutrophils and macrophages. Antibodies play a crucial role in mediating phagocytosis. To further decipher the mechanisms of *C. acnes* uptake and lysis, the immunocytochemistry based opsonophagocytosis assay was established in this work. The establishment included developing a handling protocol for a human leukemia cell line (HL60), testing various fluorescence dye combinations, maintaining viability of cell culture in the flowcell system, bacteria-cell culture co-incubation strategies, live-imaging sustainability and optimization of microscopy techniques. Differentiation to phagocytic cells (dHL60) based on a recent publication (Manda-Handzlik et al., 2018). dHL60 were tested on their capacity to phagocyte antibody opsonized *C. acnes* cells and in particular whether (and if yes, when) lysis could be detected within the immune cell. Furthermore, preliminary studies investigated whether lead candidates (herein anti-27#1 serum) could facilitate phagocytosis.

5.1. Endocytosed *C. acnes* possibly resisted full degraded for several days

At first, knowledge from previous ICC experiments (see section 4) was incorporated into the opsonophagocytosis project, visualizing serum plus Cy3 tagged *C. acnes* and DNA by DAPI. *C. acnes* was first opsonized with antiserum from *C. acnes* whole cell lysate immunization (anti-WCL), followed by secondary antibody (Cy3-conjugated) binding for fluorescence visualization of the surface. Co-incubation and uptake of *C. acnes* by dHL60 could be monitored over 6 days (Fig. 35A). Morphology of the bacterial cells maintained the typical rod shape for the first three days, turning into smaller spotty appearances after 4 days and fading into a cloudy phenotype after 6 days, possibly showing bacterial degradation. Untreated *C. acnes* kept its rod shaped form for all measured time points without any loss in signal or contrast.

Three day co-incubated dHL60 cells were imaged in layers of 2 to 14 µm, showing its three dimensional structure (Fig. 35B). When overlaying different fluorescence channels at 8 µm height, *C. acnes* position inside the phagocyte became apparent. Up to 80% of all phagocytes (dHL60) showed this sort of phagocytosis.

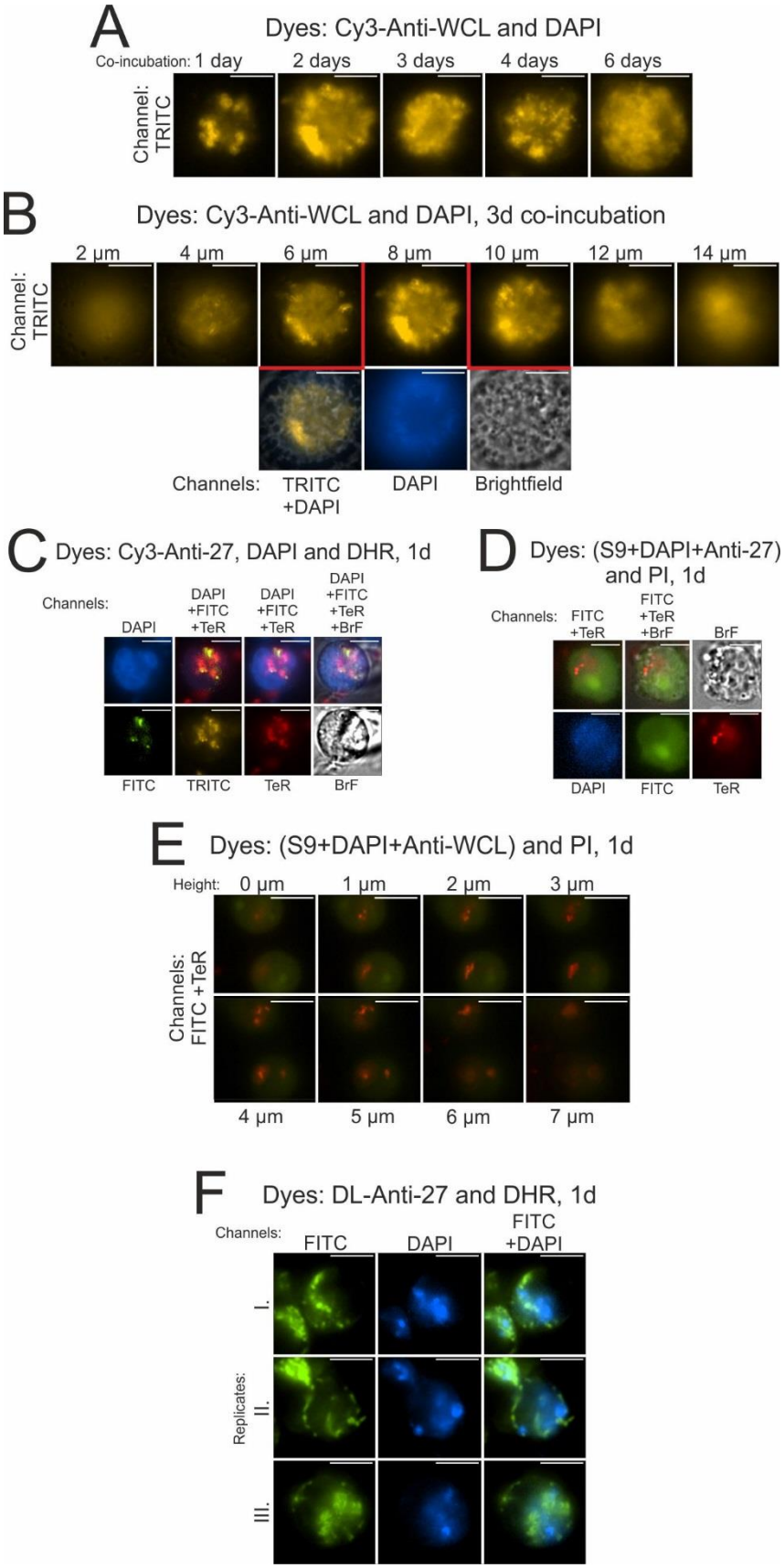

Figure 35: *C. acnes* (IA1-s1) phagocytosis visualization in dHL60. A) Anti-WCL-Cy3 surface tagged *C. acnes* endocytosed by dHL60s over the course of 6 days of co-incubation in TRITC channel. B) Anti-WCL-Cy3 surface tagged *C. acnes* endocytosed by dHL60 after 3 days of co-incubation, showing the 3D-distribution across the phagocyte among 12 µm. At 8

µm, DAPI (showing DAPI DNA stain), brightfield and TRTIC+DAPI channels were shown additionally. C) Various fluorescence dye combinations of a dHL60 cell and Cy3-tagged *C. acnes* (blue = DNA in nucleus, red/orange = *C. acnes* protein 27 on the surface, green = oxidized dihydro-rhodamine [DHR], possibly lysosomes or mitochondria, white = brightfield image) after 1 day of co-incubation. D) Propidium iodide staining of dead anti-S27 serum opsonized *C. acnes* cells (red) within dHL60 (green = SYTO9, blue = DAPI). E) Same as D), but *C. acnes* was opsonized by anti-WCL serum, visualizing 3D-locations of *C. acnes* within dHL60. F) Anti-S27 serum and DyLight 350 tagged *C. acnes* (blue) within dHL60. Oxidized DHR, possibly lysosomes or mitochondria, was shown in green. D+E) *C. acnes* was stained by dyes (shown in brackets) and washed again prior to co-incubation. All) White bars in the top-right of each image refer to 5 µm. In all images strain IA1-s1 was used. Be aware that DAPI generally describes the fluorescence dye, but can also refer to the DAPI filters (when specifically combined with the word channel). PI: propidium iodide, S9: SYTO9 fluorescence dye, DHR: dihyro-rhodamine 123, DAPI: 4',6'-diamino-2-phenylindole, DL: DyLight® 350 conjugated secondary antibody, Anti-WCL: antiserum from whole cell lysate immunization, Anti27: antiserum immunized with protein 27#1, Cy3: Cy3-conjugated secondary antibody.

5.2. Elucidating endocytosed *C. acnes* viability

To be less dependent on *C. acnes* visualization by antibodies (i.e. when comparing it to control without any primary antibody), a different approach was investigated. The bacteria were stained by DAPI and SYTO9 (both targeting DNA) prior to co-incubation, as well as opsonized by anti-WCL, S27 or no serum, then washed (to remove any residual dye) and finally co-incubated (Fig. 36A). Propidium iodide (PI), counter-staining dead cells when used together with SYTO9 (living ones), was added afterwards (Fig. 36B). Cells would be endocytosed (Fig. 36C), but stay viable within the phagosome (Fig. 36D). Only once the phagosome fuse with the lysosome (containing reactive oxygen species, Fig. 36E), *C. acnes* cells should be degraded. Subsequently, PI could enter the cytosol and fluoresce red (Fig. 36F, Fig. 35D and E).

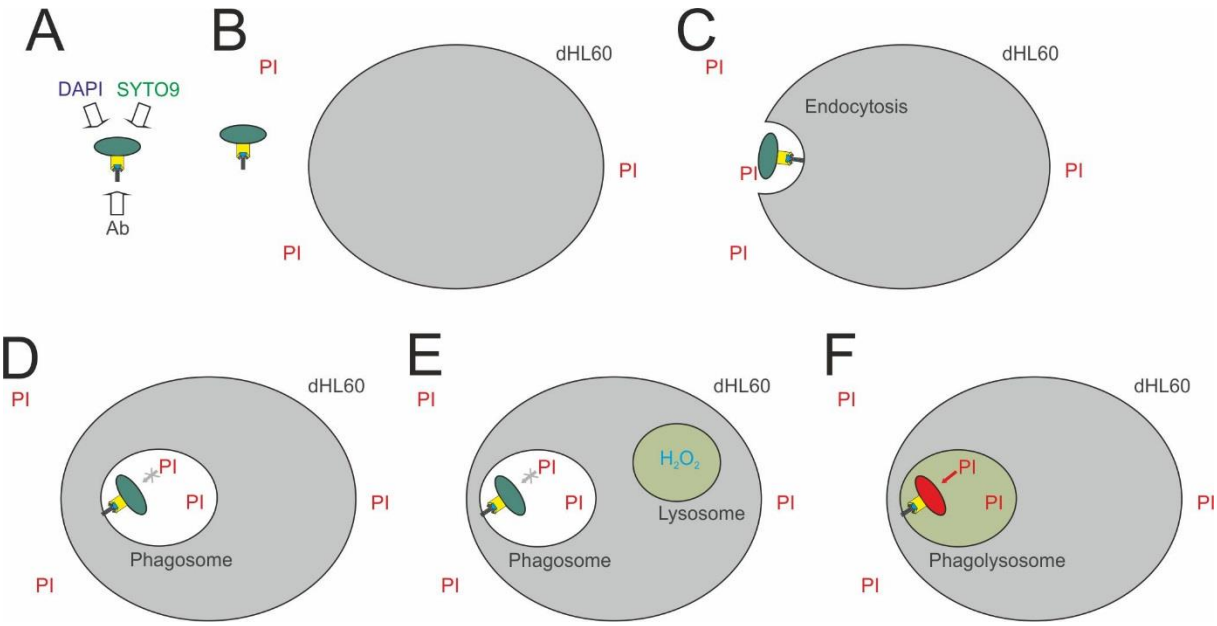

Figure 36: Scheme of the PI based protocol and possible phagocytosis pathway. (A) *C. acnes* is stained by DAPI, SYTO9 and opsonized by primary antibodies, followed by washing steps. (B) Afterwards, *C. acnes* is co-incubated with dHL60 cells, (C) with *C. acnes* being ingested by endocytosis. (D) As *C. acnes* is still supposed to be viable at this point, PI (propidium iodide) cannot permeate the membrane and cells stay SYTO9 stained only, fluorescing green. (E) Lysosomes, containing H_2O_2 and other antimicrobial substances, form. (F) Lysosomes fuse with *C. acnes* containing phagosomes, becoming a phagolysosome and degrading the bacteria. In the process the membrane becomes permeable and PI starts to stain the DNA. The cells fluoresce red. DAPI is added as secondary DNA control. SYTO9 is added as counter-stain to PI as part of the LIVE/DEAD BacLight Viability Kit, as its signal is usually quenched by PI.

Anti-S27 or anti-WCL opsonized *C. acnes* could be shown within dHL60 by a red fluorescence signal (PI), indicating a non-viable status (Fig. 35D and E). In particular, the signal in the DAPI channel showed a slight hotspot close to the presence of the *C. acnes* DNA containing cytosol. However, washing processes, diffusion or a too low initial concentration led to the loss and release of DAPI molecules over time. The FITC channel would reveal SYTO9 signals initially bound to *C. acnes* cytosolic DNA. SYTO9 diffused out of the bacteria into the dHL60 and staining its DNA. PI on the other hand was limited to the extracellular volume, as long as eukaryotic or prokaryotic cell membrane stayed intact. If the dHL60 cell was permeable, PI would diffuse into it, stain it red and at the same time quench the SYTO9 signal. But it stayed green, suggesting its viability. Unfortunately, the high diffusion rate of DAPI and S9 didn't allow to counter-stain viable *C. acnes* cells. Other dyes like Nile red or octadecyl rhodamine were previously tried, but turned out with even less pronounced signals. As DAPI follows similar diffusion patters as PI by permeating through eukaryotic membranes very slowly, DAPI could be added in higher concentrations.

Images of the 3D structure of 1 day co-incubated dHL60 were taken (by 1 µm steps), verifying the localization of PI stained *C. acnes* within two neighboring phagocytes (Fig. 35E).

5.3. No fusion rate of lysosomes and phagosomes according to the DL-based protocol

To further decipher viability status of endocytosed *C. acnes* within dHL60, dihydrorhodamine 123 (DHR) was added to the Cy3 based protocol. DHR migrates freely through membranes and once oxidized (for example by H_2O_2) it turns into the fluorescent rhodamine 123. This can be used to visualize reactive compartments like lysosomes and to some degree also mitochondria.

Co-localization of DHR signal (green, FITC channel) and bacteria (Cy3 or PI signal) would indicate fusion of phagosome and lysosome to phagolysosome, which usually leads to degradation of trapped bacteria. The FITC channel showed oxidized DHR, the channels TRITC and TexasRed (TeR) revealed signal from Cy3-tagged *C. acnes* and the DAPI channel visualized the dHL60 nucleuses DNA by DAPI dye (Fig. 35C). Overlaying channels suggested overlapping or close proximity of bacteria and DHR stained compartments and with it a possible fusion (Fig. 35C, DAPI+FITC+TeR). The bright green spots in FITC channel (visualizing reactive oxygen species [ROS]) appeared to overlap with red areas (TeR channel, Cy3-tagged *C. acnes*).

Unfortunately, rhodamine had a wide fluorescence range weakly overlapping with Cy3 emission (leaking into TRITC and TeR channels). Therefore, *C. acnes* was tagged by a different secondary antibody with excitation around 350 nm (violet) and emission in the DAPI channel. Three different dHL60 cells (I – III) were visualized in DAPI channel (now *C. acnes* surfaces and not DNA), FITC channel (oxidizing environment, lysosomes or mitochondria) and an overlay of both channels after 1 day of co-incubation (Fig. 35F). Interestingly, the signals seemed to exclude themselves. Wherever there was an oxidized DHR signal, *C. acnes* signal was diminished, and vice versa. A previous study of HL60 cells phagocyting *Streptococcus pyogenes* showed complete surrounding of the bacteria by the granule content in case of a successful phagocytosis (Nordenfelt et al., 2009). Comparing the phenotypes suggests that in our case such complete surrounding did not happen, implying no fusion. Another study investigated phagocytosis of *C. acnes* with a different cell line (THP-1) over a time

course of 24 hours and showed lack of co-localization of their lysosomal markers and *C. acnes* (Fischer et al., 2013). Our data verified these from a second perspective (HL60 cells) and on top of that monitored *C. acnes* fate over 6 days. Surprisingly, after 2 to 4 days we could see a shift in phenotype, a phenotype which was solely dHL60 induced (control *C. acnes* without dHL60 maintained strong, rod shaped Cy3 signals at all time points). After 6 days Cy3 signal lost all resembles of bacterial surfaces (Fig. 35A).

Thus, *C. acnes* was hypothesized to possess skills to prevent degradation for several days. This seems remarkable as phagocyted bacteria like *E. coli* usually die within 10 minutes (Hampton et al., 1994). On the other hand, *C. acnes* didn't seem to inherit escape mechanisms, nor was it able to proliferate within a phagocyte. So its only chance to survive seemed to be the phagocyte dying before it. Taken together, the main virulence factors of *C. acnes* seemed to be its extreme persistence and resilience.

6. Immunoblot Assays

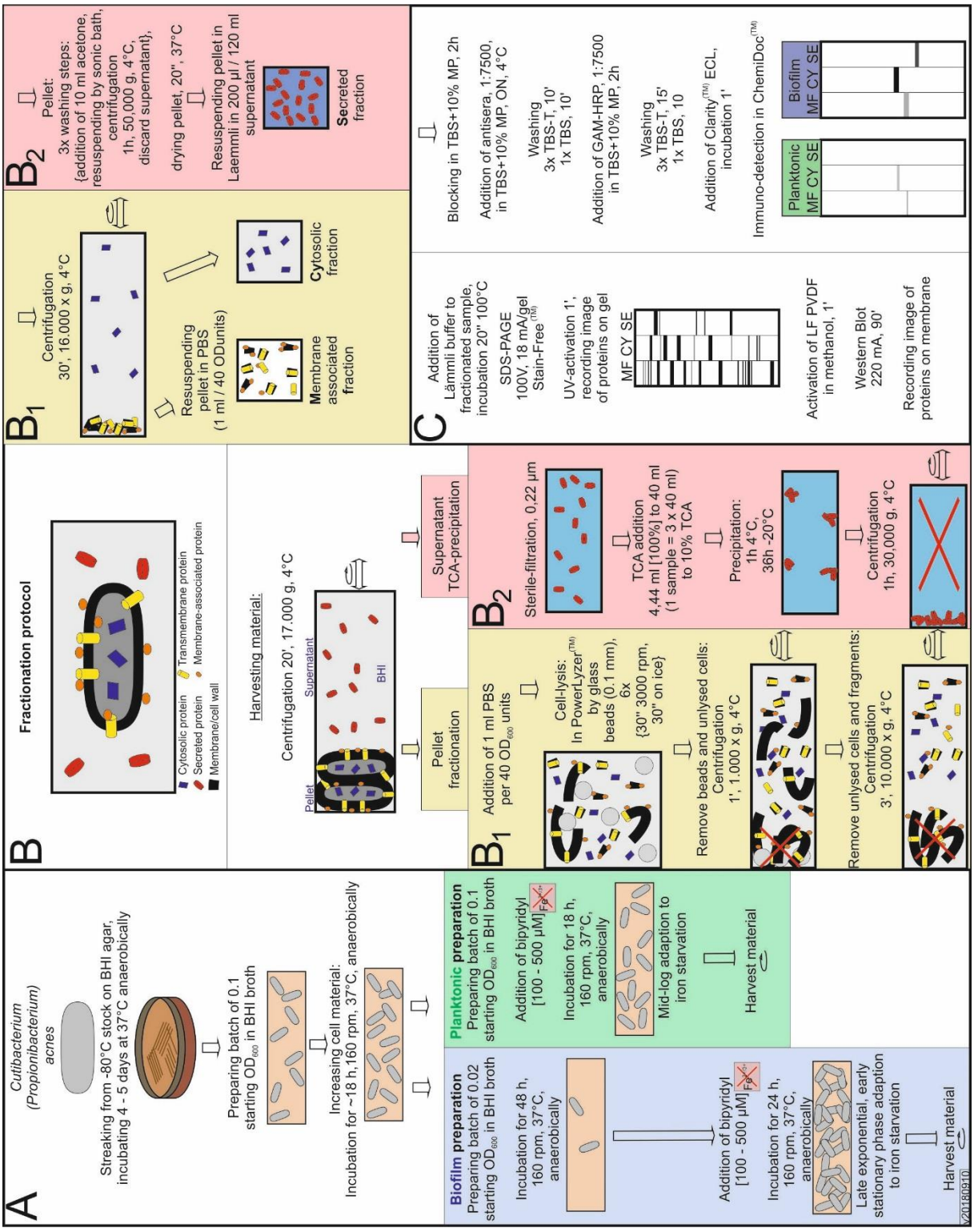

Figure 37: Overview of the immunoblot protocol. (A) *C. acnes* was brought to planktonic or biofilm mode. (B) Fractionation protocol separated cells from supernatant, whereas the cells were processed by isolating a membrane-associated fraction and a cytosolic fraction (B1) and a TCA based protocol precipitated secreted proteins (B2). (C) These fractions were applied to Stain-Free™ gels, separated by SDS-PAGE, blotted onto a membrane, bound by the antisera and detected using a general Western blot protocol.

Goal of the section 6 was to quantify and characterize *C. acnes* proteins targeted by the provided antisera. *C. acnes* cells were brought to planktonic or biofilm stage, fractionated into cytosolic, membrane-associated and secreted fraction and analyzed by immunoblot (Fig. 37).

6.1. Planktonic and biofilm mode as important life-cycles

C. acnes transitions between planktonic and biofilm mode depending on environmental circumstances. The planktonic mode of *C. acnes* is more related to proliferation, whereas the biofilm mode is associated to higher amounts of virulence factors, adhesion, aggregation, stress and stationary phase. The *in vivo* situation is hypothesized to contain a mixture of both physiological states. If the targeted protein candidates are expressed only in planktonic mode, then biofilm cells would be unaffected by antibody treatment. Thus it is essential that the lead protein candidates are highly abundant on the surfaces in both states. To verify this, planktonic and biofilm derived cells were both analyzed for antibody binding quantity and quality. See section 3 for planktonic and biofilm mode establishment and Fig. 37A for the protocol.

6.2. Cell compartment fractionation protocol and verification of quantitative analysis

Efficacy of antibodies, mediated by host immune defense strategies like phagocytosis, among others depends on accessibility of the epitope of the target protein to the environment. Thus, the target protein should be found in great abundance on the *C. acnes* surface. For this, we established a protocol lysing *C. acnes* and enriching membrane-associated proteins based on differential centrifugation steps. Mass spectrometry (section 3) and in silico analysis of the investigated proteins predicted at least 62% of those to be transmembrane or membrane-associated. The soluble remains of these centrifugation steps represented the cytosolic fraction (Fig. 37B1).

To work with greatest efficiency and efficacy, a phagocytic cell theoretically enters the inflammatory site and antibodies lead it to the source of inflammation – the pathogen. If the target protein is strongly expressed on the cell’s surface, it could serve as competitive inhibitor of phagocytosis. Thus target proteins could be more efficient if they are not secreted or secreted less than other candidates. To characterize lead protein candidates on this topic, a protocol was established precipitating and purifying secreted proteins (Fig. 37B2).

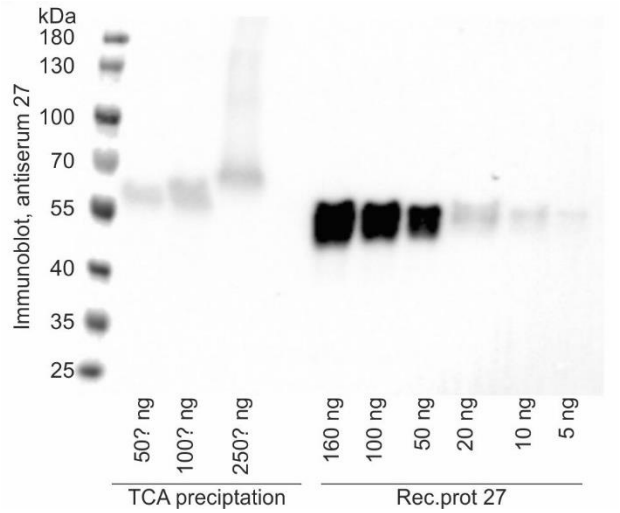

Figure 38: TCA precipitation protocol verification and calibration curve. Immunoblot with rabbit anti-S27 serum (see Fig. 37 for protocol) showed TCA precipitated yield with expected amount being indicated by question marks (left part). Additionally, a serial dilution of defined but untreated recombinant protein 27 was visualized and subsequently quantified. Comparison of untreated recombinant protein 27 to the TCA precipitated version showed TCA precipitation yield of approximately 20% (100? ng signal correlated to 20 ng recombinant protein signal).

The protocol used trichloroacetic acid to precipitate a large portion of proteins of the medium (120 ml BHI) and acetone centrifugation steps for purification and de-acidification. The resulting pellets were only partially soluble in PBS. To avoid loss of proteins, it was resolved in Lämmli buffer instead. To verify that the target proteins of the antisera survived the TCA precipitation protocol, defined amounts of the original recombinant proteins (used to immunize the rabbits with) were added to fresh BHI and processed in parallel to other samples. Afterwards, the TCA precipitated samples and the initial recombinant proteins were applied to the SDS-PAGE/immunoblot protocol and quantified on its signal from antiserum 27 (Fig. 38). Additionally, a serial dilution of untreated recombinant protein 27 was added. Signal intensities of supposedly 100 ng TCA precipitated protein correlated with approximately 20 ng of untreated protein. This conferred to 20% protein preservation. The experiment was repeated with protein 28 showing similar results.

The immunoblot was supposed to quantify signal intensity of the antibodies (within the antisera) bound to its target *C. acnes* proteins. To verify that quantification was generally possible, a calibration curve and linear regression was performed. Therein, a serial dilution of recombinant protein 27 was processed according to the immunoblot protocol (Fig. 37C) and detected using the anti-27 serum as primary antibody (Fig. 38, right side). Applying protein amount on the x-axis and signal intensities calculated by

ImageLab™ on the y-axis revealed a linear correlation from 5 ng to 160 ng under the given protocol.

6.3. Protein 28 expression depended on bipyridyl concentration

As discussed in section 4.3, the environment on the skin features low iron accessibility. To simulate this condition, the iron chelator bipyridyl was added to planktonic IA1-s1 cells in various concentrations. As protein 28 is affected by iron levels, the change in expression and its quantity should be visible in an immunoblot using anti-28 serum as primary antibody.

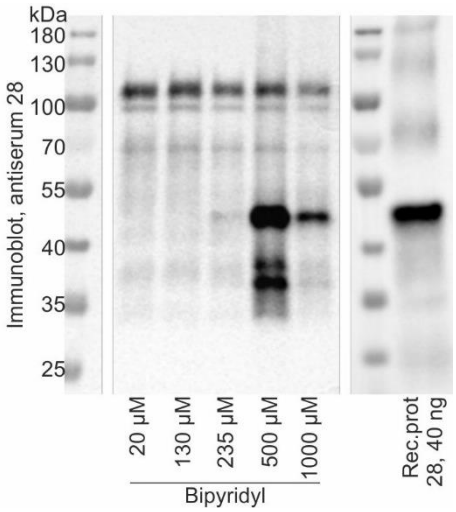

Figure 39: Effects of different bipyridyl concentrations on protein 28 expression in IA1-s1. Planktonic *C. acnes* IA1-s1 was treated with bipyridyl concentrations of 20 µM to 1000 µM according to the immunoblot protocol (see Fig. 37 or Material and Methods). As comparison, 40 ng recombinant protein 28 was applied to a second blot. Both blots were incubated with rabbit anti-S28#1 serum. Whole cell lysate was applied to the gels. The lane with the 500 µM bipyridyl treated sample showed a strong band corresponding to the size of the recombinant protein, suggesting its increased expression under these conditions. Weaker band signal intensity could also be detected for 235 µM and 1000 µM.

Protein expression of recombinant protein 28 depended on bipyridyl concentration (Fig. 39). Whereas band intensities between 55 and 40 kDa stayed the same for 20 and 130 µM bipyridyl, a slight signal increase could be detected for 235 µM peaking at 500 µM with maximum expression. Beyond this point, signal intensity went down again (also due to growth inhibition, reaching MIC). This data was consistent with the immunocytochemistry results (Fig. 31) and served as additional information for determining the bipyridyl concentrations for the final immunoblots and immunocytochemistry analysis for anti-S28 serum.

6.4. Lead protein candidates were present in membrane-associated and secreted fractions of most phylotypes

Although in the progress of immunoblot establishment and optimization many candidates were screened, this work focused on the results of the most recent, most promising ones: H4, 22, 27, 28 and 71 (Figs. S7 – S9). The antisera were mouse derived. To indicate that mouse serum inherited no initial antibody response against the protein candidates, an equal amount of mice was immunized with PBS only in parallel. The resulting serum showed no signal even after long exposition times.

Intensities from the different sample signals were compared to 40 ng of the recombinant protein and quantified by ImageLab™ software (Figs. S10 - S14). Resulting values in each combination's first lane show the detected µg protein (compared to the recombinant protein). As quantification took place at an early exposition time point, a second (subjective) characterization for long exposition times was added to each combination to indicate weaker signals. A weak, but well pronounced band was marked as "+", a maximum signal was marked as "++++". Faint, barely visible bands were described as "~" and no signal as "X". In case of strong neighboring bands overlaid a particular lane and no signal detection was possible, "?" was used.

As example, the blot of MIS 22v2 (Fig. S7C) contained membrane-associated fractions in planktonic mode of 11 strains (lane 3 – 8 and 10 – 14). In lane 1 40 ng of recombinant protein 22 was applied, leading to a band close to the 40 kDa marker band (lane 2 and 9). Lane 5 with IA2 strain IA2-s2 (P.acn31) (see lower box for all lane content) revealed the strongest signal to be around 70 kDa. With the kDa sizes increasing by ~ 100%, deviations from the initial recombinant size could be due to dimer formation. Another weaker band at ~ 130 kDa could be interpreted as tetramer. Such interpretations, however, must be aligned to the proteins functional prediction, which unfortunately couldn't be done in this work as the origin was undisclosed.

In general, results from the immunoblot correlated with the results from immunocytochemistry. Signals from 22, 27 and H4 were strong for IA1, IA2 and IC in all fractions. Signals from type II strains varied

Serum 22 showed a strong signal (14 – 75 ng per sample) for representative strains of IA1, IA2, IC and one type II strain (Fig. S11) in membrane and secreted fraction. The

biofilm signal was more pronounced than the planktonic signal. Type IB, III and three type II isolates showed very low to no protein signals. Serum 27 detected the target protein in biofilm mode for IA1, IA2, IC and two type II strains (Fig. S11). Planktonic signals were weaker. Protein 28 under iron starvation conditions was detected for all fractions except type III and a few type II isolates (Fig. S12). The signal was stronger in planktonic mode (8 – 28 ng) than in biofilm mode (1 – 8 ng). Interestingly, protein 28 could be detected massively in the secreted fraction for all mentioned isolates, in planktonic and biofilm mode (30 – 177 ng). H4 could target IA2, IC and IA1 isolates, as well as two type II isolates (Fig. S14). Planktonic signals were weaker than biofilm signals. To describe possible variations of the assay, two independent PL MF detection runs were shown. The tendencies of the signal were similar with a ng variation from 15 to 26 ng. A similar double run was performed for serum 71 (Fig. S13), showing similar results and reproducibility. Protein 71 generally showed a weaker signal than the other candidates, describing it possibly as a worse candidate for acne vaccination (in comparison to the other candidates).

IV. Conclusion

The thesis contained two general scientific approaches comprising basic academic research and applied research. The basic research was performed to gain experience on *C. acnes* in general, on its ability to form biofilm structures and on the quantity and physiology. The applied research was grounded on this foundation and tried to utilize it for therapeutic investigations, in particular characterizing possible antibody mediated therapeutic functionality.

Firstly, two independent assays were established, showing biofilm quantification by a high-throughput, MTP based assay, as well as a fluorescence microscopy based assay, quantifying microscopic cells (overall biomass) and describing possible biofilm structures. In the MTP assay, *C. acnes* exposed a high, isolate specific biofilm forming heterogeneity. When summed up into phylotype groups, IA1 turned out to produce 2 to 8-fold higher biofilm than the other phylotypes. Further deciphered, biofilm formation could be pinpointed to the SLST subtypes A1, A2 and A37, translating to the clonal complex 18 (Aarhus scheme). CC18 was recently found to be dominant for acneic follicles, disclosing a possible correlation which should be further investigated. Using the flowcell-based fluorescence microscopy assay, the structures of *C. acnes* in situ biofilms were characterized and quantified. IA1, IA2 and IC isolates showed typical biofilm structures and increased attachment to abiotic surfaces. Combining the results of both assays and public knowledge of IA1, IA2 and IC phylotypes being significantly associated to acne, a possible correlation between biofilm formation and acne pathogenesis could be hypothesized. At the same time, sorting isolates according to their point of isolation (skin vs implant) did not yield in significantly increased biofilm formation differences. From this perspective it could be argued that there is no long-term selection pressure within the human body for biofilm specific properties. This seems to be consistent with the findings that deep tissue and implant infections are not necessarily correlated to the phylotypes IA1, IA2 and IC.

The MTP and fluorescence microscopy based biofilm assays, once established and optimized for *C. acnes*, were adapted to *S. epidermidis* and used to define their biofilm formation capacity. The results from the two independent assays came to surprisingly similar biofilm formation results (Fig. 40), verifying that the applied methods correctly

depicted the biological truth determining biofilm. At the same time it could be shown that these assays could be readily converted for other biofilm forming isolates.

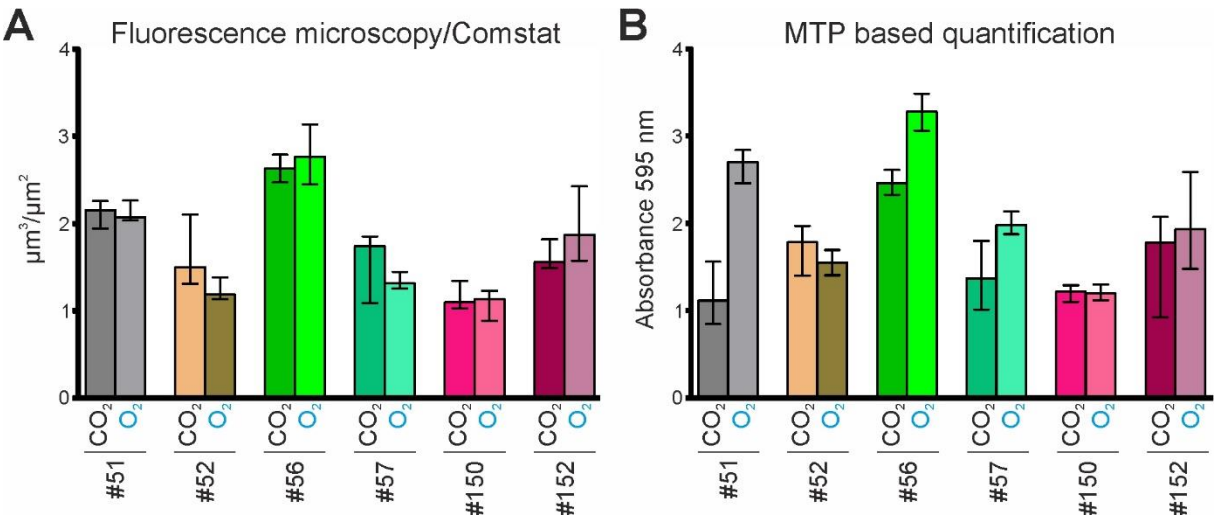

Figure 40: MTP based biofilm formation compared to fluorescence microscopy quantification. Biofilm formations of six *S. epidermidis* reference strains were measured by two independent methods. In both cases, cells were grown at ~ 20 h at 37°C aerobically or anaerobically in either a microscopic chamber (A) or 96-well MTP (B) system. Shown are medians with interquartile range. (A) After washing of non-sessile cells out of the flowcell, bacteria were stained with SYTO9 and image stacks were created (with steps of 0.5 µm). These were analyzed for the biomass using the COMSTAT 2 software (Heydorn et al., 2000; Vorregaard, 2008). Two image stacks from at least three independent experiments were analyzed for each strain. Values correspond to Fig. 23A. (B) Each column included 6 wells in 5 separate plates (= 30 values) showing 595 nm absorbance of crystal violet. Values correspond to Fig.9, B plus E (anaerobic) and D (aerobic).

To investigate therapeutic effects of antibodies against *C. acnes*, antibodies against *C. acnes* whole cell lysate were tested in the MTP assay for its capacity to reduce or effect biofilm formation but no significant effects could be detected. To rule out that this was due to MTPs general lack of ability to detect the phenotype change, the assay was optimized for reduced variation and tested for its functionality. In particular, it was treated with proteinase K and DNase I, revealing a gradual reduction in biofilm formation depending on proteinase K or DNase I quantity for IA1 strains, verifying the MTP assay's functionality. At the same time, it was shown that *C. acnes* biofilms and attachment did rely on proteins and extracellular DNA. Removing either would reduce or completely destabilize biofilm quantity, as well as significantly impair attachment abilities. With proteins being shown to be essential for biofilm formation and attachment, antibody binding against proteins should theoretically be able to influence biofilm and attachment, providing support for its possible therapeutic significance.

When treating a strong biofilm producer of *S. epidermidis* with antibodies directed against WCL in the MTP assay, the biofilm formation increased 4-fold. Although the effect went into the opposite direction of what is supposedly desired for a treatment, the results showed that antibodies affected biofilm and that the established MTP assay was able to detect it.

From a different perspective, increased biofilm formation of *S. epidermidis* by a whole cell lysate derived immune response opened new questions. Are immune responses against *S. epidermidis* always leading to a biofilm formation increase? If yes, is it actually the human host immune system further fortifying *S. epidermidis* biofilm? If not, do we see random immune responses from each individual rabbit with some of them having no effects and some also reducing the biofilm formation? Following on that one and spinning it back to acne, does this also count for *C. acnes*? Is it possible that it is randomly determined at the beginning of an immune response whether the antibodies increase or reduce biofilm compactness? In any case, these questions confirm the need to further investigate the antibody – bacterial cell interactions in biofilm and emphasize its therapeutic relevance.

The therapeutic strategy of our industrial collaboration partner targeted acne vulgaris (*C. acnes*) and implant-associated infections (*C. acnes* and *S. epidermidis*) by developing vaccines against specific epitopes on the surface of *C. acnes*. The possibilities of these protein epitopes to mediate increased, protective and functional immune responses were characterized by investigating the efficacy of antiserum derived antibodies in several assays. As preparation for this and to mirror two important life cycles of *C. acnes*, a planktonic and proliferation based physiological state, as well as a biofilm and stationary phase based state were defined, investigated and verified from perspective of aggregation, attachment and protein composition. Whereas planktonic cells were exclusively comprised of small units of a few cells only for all phylotypes, biofilm derived cells formed aggregates of hundreds and thousands of cells with up to 200 µm in diameter. Furthermore, the protein composition of the membrane-associated fraction of a strong biofilm producer (IA1) and a weak biofilm producer (IB) were analyzed by mass spectrometry, showing a dominance of metabolic enzymes in the planktonic mode and a dominance of virulence factors and possible biofilm modulating enzymes in the biofilm mode. One protein candidate, the membrane-associated NlpC/P60 family protein (A0A0E1YGP6 or aka A0A3D8Z303) showed

increased expression levels in biofilm mode. To this date, it was predicted to be a hydrolase. Cell wall-associated hydrolases, in particular NlpC/P60 proteins are known to be involved biofilm formation and regulation in other species like *Mycobacterium tuberculosis* and might exhibit similar properties in *C. acnes*.

An immunoblot protocol was established, using the antisera as primary antibodies to detect the size of its protein binding partner and the binding quantity. Herein, 11 representative strains from all phylotypes were brought into planktonic and biofilm mode. The cells were lysed and fractionated into the cytosolic, membrane-associated and secreted fraction. The immunoblot resolved several questions, i.e. the kDa size of the targeted protein (does this fit to in silico prediction or the recombinant protein?), its general quantity compared to a recombinant standard (the more signal, the higher its possible abundance on the surface), its relative quantity between PL and BF modes (is it expressed in both stages of *C. acnes*?), quantity of different phylotypes (does the antibody target all phylotypes of *C. acnes*?) and the target protein's distribution among the different fractions (is it located in the membrane and thus possibly accessible to the antibodies or is it cytosolic only where antibodies cannot target it?).

Combining knowledge from the fluorescence microscopy, the planktonic vs biofilm investigation and the immunoblot allowed for the development of a protocol of living *C. acnes* cells opsonized by the antiserum and visualized under the microscope (immunocytochemistry). Planktonic and biofilm derived cells from all phylotypes were analyzed, revealing antibody accessibility and distribution on the surface on viable cells in situ. The lead protein candidates 22, 27, 28 and H4 were analyzed by immunoblot and immunocytochemistry, verifying that all of these proteins were generally associated to the outer surface of *C. acnes* and highly abundant. Analyses on the secondary structures revealed kDa sizes close to the heterologously expressed proteins (and possible formation of polymers). Immunocytochemistry could show accessibility also in an in situ situation. Strongest signals came from the phylotypes IA1, IA2 and IC. Recalling the indications from above, an immune response targeting these phylotypes could be most effective in the reduction of acne vulgaris.

To work on an in situ method to visualize *C. acnes* and host immune system interaction, the knowledge from the immunocytochemistry section, general *C. acnes* handling and the newly established HL60 cell line was used to develop the opsonophagocytosis assays. HL60s were differentiated into phagocytic cells and co-

incubated with *C. acnes*. Utilizing several fluorescence dye combinations, endocytosis could be generally shown under the microscope. The results indicated a high phagocytosis persistence of *C. acnes* by possibly inhibiting fusion with lysosomes. In total, *C. acnes* seemed to prolong phagocytosis speed from a few minutes to several days, possibly revealing one of the key factors of acne related host immune resistance. In the future, this assay could be optimized to decipher efficacy of antibodies on phagocytosis by live-imaging and in combination with enhanced in vivo similarity like adding sebum, keratinocyte extracellular matrices, larger biofilm structures, different *C. acnes* phylotypes or inclusion other cutaneous bacteria such as *S. epidermidis*.

V. List of Figures

VI. List of Tables

VII. Abbreviations

AB	antibody
aka	also known as
BF	biofilm
CAMP	Christie-Atkins-Munch-Peterson
CC	clonal complex
CFU	colony forming units
CY	cytosolic fraction
dHL60	differentiated HL60 cells with phagocytic character
eDNA	extracellular DNA
eMLST	expanded MLST
GAM	goat anti mouse
GAR	goat anti rabbit
HL60	human leukemia cell line 60
HRP	horseradish peroxidase
kDa	kilo-daltons or 1000 unified atomic mass units
LF PVDF	low fluorescence polyvinylidene difluoride
MF	membrane-associated fraction
MLST	multilocus sequence typing
MPX	multichannel pipette "X"
MTP	mikrotiterplate
ON	overnight
PL	planktonic
RAU	relative absorbance units
RIU	relative intensity units
ROS	reactive oxygen species
rpm	revolutions per minute
RT	room temperature
RT4/RT5	ribotype
SCFA	short-chain fatty acid
SDS-PAGE	sodium dodecyl sulfate polyacrylamide gel electrophoresis
SE	secreted fraction
SLST	single locus sequence typing
ST	sequence type
TeR	TexasRed fluorescence channel
WCL	whole cell lysate

VIII. References

Abee, T., Kovács, A.T., Kuipers, O.P., van der Veen, S., 2011. Biofilm formation and dispersal in Gram-positive bacteria. Current opinion in biotechnology 22 (2), 172–179.

Achermann, Y., Goldstein, E.J.C., Coenye, T., Shirtliff, M.E., 2014. *Propionibacterium acnes*: From commensal to opportunistic biofilm-associated implant pathogen. Clinical microbiology reviews 27 (3), 419–440.

Alexeyev, O.A., Jahns, A.C., 2012. Sampling and detection of skin *Propionibacterium acnes*: Current status. Anaerobe 18 (5), 479–483.

Anantharaman, V., Aravind, L., 2003. Evolutionary history, structural features and biochemical diversity of the NlpC/P60 superfamily of enzymes. Genome Biol 4 (2), R11.

Aubin, G.G., Portillo, M.E., Trampuz, A., Corvec, S., 2014. *Propionibacterium acnes*, an emerging pathogen: From acne to implant-infections, from phylotype to resistance. Medecine et maladies infectieuses 44 (6), 241–250.

Barnard, E., Liu, J., Yankova, E., Cavalcanti, S.M., Magalhães, M., Li, H., Patrick, S., McDowell, A., 2016. Strains of the *Propionibacterium acnes* type III lineage are associated with the skin condition progressive macular hypomelanosis. Scientific reports 6, 31968.

Barnard, E., Nagy, I., Hunyadkurti, J., Patrick, S., McDowell, A., 2015. Multiplex touchdown PCR for rapid typing of the opportunistic pathogen *Propionibacterium acnes*. Journal of clinical microbiology 53 (4), 1149–1155.

Bayston, R., Ashraf, W., Barker-Davies, R., Tucker, E., Clement, R., Clayton, J., Freeman, B.J.C., Nuradeen, B., 2007. Biofilm formation by *Propionibacterium acnes* on biomaterials in vitro and in vivo: Impact on diagnosis and treatment. Journal of biomedical materials research. Part A 81 (3), 705–709.

Bek-Thomsen, M., Lomholt, H.B., Scavenius, C., Enghild, J.J., Brüggemann, H., 2014. Proteome analysis of human sebaceous follicle infundibula extracted from healthy and acne-affected skin. PloS one 9 (9), e107908.

Beylot, C., Auffret, N., Poli, F., Claudel, J.-P., Leccia, M.-T., Del Giudice, P., Dreno, B., 2014. *Propionibacterium acnes*: An update on its role in the pathogenesis of acne. Journal of the European Academy of Dermatology and Venereology : JEADV 28 (3), 271–278.

Brüggemann, H., Henne, A., Hoster, F., Liesegang, H., Wiezer, A., Strittmatter, A., Hujer, S., Durre, P., Gottschalk, G., 2004. The complete genome sequence of *Propionibacterium acnes*, a commensal of human skin. Science (New York, N.Y.) 305 (5684), 671–673.

Brzuszkiewicz, E., Weiner, J., Wollherr, A., Thurmer, A., Hupeden, J., Lomholt, H.B., Kilian, M., Gottschalk, G., Daniel, R., Mollenkopf, H.-J., Meyer, T.F., Bruggemann, H., 2011. Comparative genomics and transcriptomics of *Propionibacterium acnes*. PloS one 6 (6), e21581.

Byrd, A.L., Belkaid, Y., Segre, J.A., 2018. The human skin microbiome. Nature reviews. Microbiology 16 (3), 143–155.

Christensen, G.J.M., Brüggemann, H., 2014. Bacterial skin commensals and their role as host guardians. Beneficial microbes 5 (2), 201–215.

Coenye, T., Peeters, E., Nelis, H.J., 2007. Biofilm formation by *Propionibacterium acnes* is associated with increased resistance to antimicrobial agents and increased production of putative virulence factors. Research in microbiology 158 (4), 386–392.

Davidsson, S., Mölling, P., Rider, J.R., Unemo, M., Karlsson, M.G., Carlsson, J., Andersson, S.-O., Elgh, F., Söderquis, B., Andrén, O., 2016. Frequency and typing of *Propionibacterium acnes* in prostate tissue obtained from men with and without prostate cancer. Infectious agents and cancer 11, 26.

Domenech, M., García, E., Prieto, A., Moscoso, M., 2013. Insight into the composition of the intercellular matrix of *Streptococcus pneumoniae* biofilms. Environmental microbiology 15 (2), 502–516.

Douglas, H.C., Gunter, S.E., 1946. The taxonomic position of *Corynebacterium acnes*. Journal of Bacteriology (52(1)), 15–23.

Dréno, B., 2017. What is new in the pathophysiology of acne, an overview. Journal of the European Academy of Dermatology and Venereology : JEADV 31 Suppl 5, 8–12.

Falcocchio, S., Ruiz, C., Pastor, F.J., Saso, L., Diaz, P., 2006. *Propionibacterium acnes* GehA lipase, an enzyme involved in acne development, can be successfully inhibited by defined natural substances. Journal of Molecular Catalysis B: Enzymatic 40 (3-4), 132–137.

Fischer, N., Mak, T.N., Shinohara, D.B., Sfanos, K.S., Meyer, T.F., Brüggemann, H., 2013. Deciphering the intracellular fate of *Propionibacterium acnes* in macrophages. BioMed research international 2013, 603046.

Fitz-Gibbon, S., Tomida, S., Chiu, B.-H., Nguyen, L., Du, C., Liu, M., Elashoff, D., Erfe, M.C., Loncaric, A., Kim, J., Modlin, R.L., Miller, J.F., Sodergren, E., Craft, N., Weinstock, G.M., Li, H., 2013. *Propionibacterium acnes* strain populations in the human skin microbiome associated with acne. The Journal of investigative dermatology 133 (9), 2152–2160.

Foulston, L., Elsholz, A.K.W., DeFrancesco, A.S., Losick, R., 2014. The extracellular matrix of *Staphylococcus aureus* biofilms comprises cytoplasmic proteins that associate with the cell surface in response to decreasing pH. mBio 5 (5), e01667-14.

Furustrand Tafin, U., Corvec, S., Betrisey, B., Zimmerli, W., Trampuz, A., 2012. Role of rifampin against *Propionibacterium acnes* biofilm in vitro and in an experimental foreign-body infection model. Antimicrobial agents and chemotherapy 56 (4), 1885–1891.

Gribbon, E.M., Cunliffe, W.J., Holland, K.T., 1993. Interaction of *Propionibacterium acnes* with skin lipids in vitro. Journal of general microbiology 139 (8), 1745–1751.

Grice, E.A., Kong, H.H., Conlan, S., Deming, C.B., Davis, J., Young, A.C., Bouffard, G.G., Blakesley, R.W., Murray, P.R., Green, E.D., Turner, M.L., Segre, J.A., 2009. Topographical and temporal diversity of the human skin microbiome. Science (New York, N.Y.) 324 (5931), 1190–1192.

Hampton, M.B., Vissers, M.C., Winterbourn, C.C., 1994. A single assay for measuring the rates of phagocytosis and bacterial killing by neutrophils. Journal of leukocyte biology 55 (2), 147–152.

Heydorn, A., Nielsen, A.T., Hentzer, M., Sternberg, C., Givskov, M., Ersbøll, B.K., Molin, S., 2000. Quantification of biofilm structures by the novel computer program COMSTAT. Microbiology (Reading, England) 146 (Pt 10), 2395–2407.

Holland, C., Mak, T.N., Zimny-Arndt, U., Schmid, M., Meyer, T.F., Jungblut, P.R., Bruggemann, H., 2010. Proteomic identification of secreted proteins of *Propionibacterium acnes*. BMC microbiology 10, 230.

Holmberg, A., Lood, R., Morgelin, M., Soderquist, B., Holst, E., Collin, M., Christensson, B., Rasmussen, M., 2009. Biofilm formation by *Propionibacterium acnes* is a characteristic of invasive isolates. Clinical microbiology and infection :

the official publication of the European Society of Clinical Microbiology and Infectious Diseases 15 (8), 787–795.

Horváth, B., Hunyadkürti, J., Vörös, A., Fekete, C., Urbán, E., Kemény, L., Nagy, I., 2012. Genome sequence of *Propionibacterium acnes* type II strain ATCC 11828. Journal of Bacteriology 194 (1), 202–203.

Jahns, A.C., Eilers, H., Alexeyev, O.A., 2016. Transcriptomic analysis of *Propionibacterium acnes* biofilms in vitro. Anaerobe 42, 111–118.

Jahns, A.C., Lundskog, B., Ganceviciene, R., Palmer, R.H., Golovleva, I., Zouboulis, C.C., McDowell, A., Patrick, S., Alexeyev, O.A., 2012. An increased incidence of *Propionibacterium acnes* biofilms in acne vulgaris: a case-control study. The British journal of dermatology 167 (1), 50–58.

Jeremy, A.H.T., Holland, D.B., Roberts, S.G., Thomson, K.F., Cunliffe, W.J., 2003. Inflammatory events are involved in acne lesion initiation. The Journal of investigative dermatology 121 (1), 20–27.

Kamisango, K., Saiki, I., Tanio, Y., Okumura, H., Araki, Y., Sekikawa, I., Azuma, I., Yamamura, Y., 1982. Structures and biological activities of peptidoglycans of *Listeria monocytogenes* and *Propionibacterium acnes*. Journal of biochemistry 92 (1), 23–33.

Kang, D., Gho, Y.S., Suh, M., Kang, C., 2002. Highly Sensitive and Fast Protein Detection with Coomassie Brilliant Blue in Sodium Dodecyl Sulfate-Polyacrylamide Gel Electrophoresis. Bulletin of the Korean Chemical Society 23 (11), 1511–1512.

Kilian, M., Scholz, C.F.P., Lomholt, H.B., 2012. Multilocus sequence typing and phylogenetic analysis of *Propionibacterium acnes*. Journal of clinical microbiology 50 (4), 1158–1165.

Kuehnast, T., Cakar, F., Weinhäupl, T., Pilz, A., Selak, S., Schmidt, M.A., Rüter, C., Schild, S., 2018. Comparative analyses of biofilm formation among different *Cutibacterium acnes* isolates. International journal of medical microbiology : IJMM 308 (8), 1027–1035.

Lam, H., Kesselly, A., Stegalkina, S., Kleanthous, H., Yethon, J.A., 2014. dAntibodies to PhnD inhibit staphylococcal biofilms. Infection and immunity 82 (9), 3764–3774.

Lheure, C., Grange, P.A., Ollagnier, G., Morand, P., Désiré, N., Sayon, S., Corvec, S., Raingeaud, J., Marcelin, A.-G., Calvez, V., Khammari, A., Batteux, F., Dréno, B., Dupin, N., 2016. TLR-2 Recognizes *Propionibacterium acnes* CAMP Factor 1 from Highly Inflammatory Strains. PloS one 11 (11), e0167237.

Lomholt, H.B., Kilian, M., 2010. Population genetic analysis of *Propionibacterium acnes* identifies a subpopulation and epidemic clones associated with acne. PloS one 5 (8), e12277.

Lomholt, H.B., Scholz, C.F.P., Brüggemann, H., Tettelin, H., Kilian, M., 2017. A comparative study of *Cutibacterium* (*Propionibacterium*) *acnes* clones from acne patients and healthy controls. Anaerobe 47, 57–63.

Makrantonaki, E., Ganceviciene, R., Zouboulis, C., 2011. An update on the role of the sebaceous gland in the pathogenesis of acne. Dermato-endocrinology 3 (1), 41–49.

Manda-Handzlik, A., Bystrzycka, W., Wachowska, M., Sieczkowska, S., Stelmaszczyk-Emmel, A., Demkow, U., Ciepiela, O., 2018. The influence of agents differentiating HL-60 cells toward granulocyte-like cells on their ability to release neutrophil extracellular traps. Immunology and cell biology 96 (4), 413–425.

McDowell, A., 2017. Over a Decade of recA and tly Gene Sequence Typing of the Skin Bacterium *Propionibacterium acnes*: What Have We Learnt? Microorganisms 6 (1).

McDowell, A., Barnard, E., Nagy, I., Gao, A., Tomida, S., Li, H., Eady, A., Cove, J., Nord, C.E., Patrick, S., 2012. An expanded multilocus sequence typing scheme for *Propionibacterium acnes*: investigation of 'pathogenic', 'commensal' and antibiotic resistant strains. PloS one 7 (7), e41480.

McDowell, A., Gao, A., Barnard, E., Fink, C., Murray, P.I., Dowson, C.G., Nagy, I., Lambert, P.A., Patrick, S., 2011. A novel multilocus sequence typing scheme for the opportunistic pathogen *Propionibacterium acnes* and characterization of type I cell surface-associated antigens. Microbiology (Reading, England) 157 (Pt 7), 1990–2003.

McDowell, A., Nagy, I., Magyari, M., Barnard, E., Patrick, S., 2013. The opportunistic pathogen *Propionibacterium acnes*: insights into typing, human disease, clonal diversification and CAMP factor evolution. PloS one 8 (9), e70897.

McDowell, A., Perry, A.L., Lambert, P.A., Patrick, S., 2008. A new phylogenetic group of *Propionibacterium acnes*. Journal of medical microbiology 57 (Pt 2), 218–224.

McDowell, A., Valanne, S., Ramage, G., Tunney, M.M., Glenn, J.V., McLorinan, G.C., Bhatia, A., Maisonneuve, J.-F., Lodes, M., Persing, D.H., Patrick, S., 2005. *Propionibacterium acnes* types I and II represent phylogenetically distinct groups. Journal of clinical microbiology 43 (1), 326–334.

McGinley, K.J., Webster, G.F., Ruggieri, M.R., Leyden, J.J., 1980. Regional variations in density of cutaneous propionibacteria: Correlation of *Propionibacterium acnes* populations with sebaceous secretion. Journal of clinical microbiology 12 (5), 672–675.

Metiko, B., Brooks, K., Burkhart, C.G., Burkhart, C.N., Morrell, D., 2015. Is the current model for acne pathogenesis backwards? Journal of the American Academy of Dermatology 72 (6), e167.

Mollerup, S., Friis-Nielsen, J., Vinner, L., Hansen, T.A., Richter, S.R., Fridholm, H., Herrera, J.A.R., Lund, O., Brunak, S., Izarzugaza, J.M.G., Mourier, T., Nielsen, L.P., Hansen, A.J., 2016. *Propionibacterium acnes*: Disease-Causing Agent or Common Contaminant? Detection in Diverse Patient Samples by Next-Generation Sequencing. Journal of clinical microbiology 54 (4), 980–987.

Nakatsuji, T., Tang, D.-c.C., Zhang, L., Gallo, R.L., Huang, C.-M., 2011. *Propionibacterium acnes* CAMP factor and host acid sphingomyelinase contribute to bacterial virulence: Potential targets for inflammatory acne treatment. PloS one 6 (4), e14797.

Nordenfelt, P., Bauer, S., Lönnbro, P., Tapper, H., 2009. Phagocytosis of *Streptococcus pyogenes* by all-trans retinoic acid-differentiated HL-60 cells: Roles of azurophilic granules and NADPH oxidase. PloS one 4 (10), e7363.

Omer, H., McDowell, A., Alexeyev, O.A., 2017. Understanding the role of *Propionibacterium acnes* in acne vulgaris: The critical importance of skin sampling methodologies. Clinics in dermatology 35 (2), 118–129.

Padhi, A., Naik, S.K., Sengupta, S., Ganguli, G., Sonawane, A., 2016. Expression of *Mycobacterium tuberculosis* NLPC/p60 family protein Rv0024 induce biofilm formation and resistance against cell wall acting anti-tuberculosis drugs in *Mycobacterium smegmatis*. Microbes and infection 18 (4), 224–236.

Ramage, G., Tunney, M.M., Patrick, S., Gorman, S.P., Nixon, J.R., 2003. Formation of *Propionibacterium acnes* biofilms on orthopaedic biomaterials and their susceptibility to antimicrobials. Biomaterials 24 (19), 3221–3227.

Sadhasivam, S., Sinha, M., Saini, S., Kaur, S.P., Gupta, T., Sengupta, S., Ghosh, S., Sardana, K., 2016. Heterogeneity and antibiotic resistance in *Propionibacterium acnes* isolates and its therapeutic implications: Blurring the lines between commensal and pathogenic phylotypes. Dermatologic therapy 29 (6), 451–454.

Sampedro, M.F., Piper, K.E., McDowell, A., Patrick, S., Mandrekar, J.N., Rouse, M.S., Steckelberg, J.M., Patel, R., 2009. Species of *Propionibacterium* and *Propionibacterium acnes* phylotypes associated with orthopedic implants. Diagnostic microbiology and infectious disease 64 (2), 138–145.

Scholz, C.F.P., Jensen, A., Lomholt, H.B., Brüggemann, H., Kilian, M., 2014. A novel high-resolution single locus sequence typing scheme for mixed populations of *Propionibacterium acnes* in vivo. PloS one 9 (8), e104199.

Scholz, C.F.P., Kilian, M., 2016. The natural history of cutaneous propionibacteria, and reclassification of selected species within the genus *Propionibacterium* to the proposed novel genera *Acidipropionibacterium* gen. nov., *Cutibacterium* gen. nov. and *Pseudopropionibacterium* gen. nov. International journal of systematic and evolutionary microbiology 66 (11), 4422–4432.

Schupp, J.C., Tchaptchet, S., Lützen, N., Engelhard, P., Müller-Quernheim, J., Freudenberg, M.A., Prasse, A., 2015. Immune response to *Propionibacterium acnes* in patients with sarcoidosis--in vivo and in vitro. BMC pulmonary medicine 15, 75.

Seper, A., Pressler, K., Kariisa, A., Haid, A.G., Roier, S., Leitner, D.R., Reidl, J., Tamayo, R., Schild, S., 2014. Identification of genes induced in *Vibrio cholerae* in a dynamic biofilm system. International journal of medical microbiology : IJMM 304 (5-6), 749–763.

Shu, M., Wang, Y., Yu, J., Kuo, S., Coda, A., Jiang, Y., Gallo, R.L., Huang, C.-M., 2013. Fermentation of *Propionibacterium acnes*, a commensal bacterium in the human skin microbiome, as skin probiotics against methicillin-resistant *Staphylococcus aureus*. PloS one 8 (2), e55380.

Sörensen, M., Mak, T.N., Hurwitz, R., Ogilvie, L.A., Mollenkopf, H.J., Meyer, T.F., Brüggemann, H., 2010. Mutagenesis of *Propionibacterium acnes* and analysis of two CAMP factor knock-out mutants. Journal of microbiological methods 83 (2), 211–216.

Thompson, C.C., Carabeo, R.A., 2011. An optimal method of iron starvation of the obligate intracellular pathogen, *Chlamydia trachomatis*. Frontiers in microbiology 2, 20.

Tunney, M.M., Dunne, N., Einarsson, G., McDowell, A., Kerr, A., Patrick, S., 2007. Biofilm formation by bacteria isolated from retrieved failed prosthetic hip implants in

an in vitro model of hip arthroplasty antibiotic prophylaxis. Journal of orthopaedic research : official publication of the Orthopaedic Research Society 25 (1), 2–10.

Valanne, S., McDowell, A., Ramage, G., Tunney, M.M., Einarsson, G.G., O'Hagan, S., Wisdom, G.B., Fairley, D., Bhatia, A., Maisonneuve, J.-F., Lodes, M., Persing, D.H., Patrick, S., 2005. CAMP factor homologues in *Propionibacterium acnes*: A new protein family differentially expressed by types I and II. Microbiology (Reading, England) 151 (Pt 5), 1369–1379.

Vorregaard, M., 2008. Comstat2 - a modern 3D image analysis environment for biofilms, in Informatics and Mathematical Modelling. Technical University of Denmark: Kongens Lyngby, Denmark.

Wyckoff, T.J., Taylor, J.A., Salama, N.R., 2012. Beyond growth: Novel functions for bacterial cell wall hydrolases. Trends in microbiology 20 (11), 540–547.

Yu, Y., Champer, J., Garbán, H., Kim, J., 2015. Typing of *Propionibacterium acnes*: a review of methods and comparative analysis. The British journal of dermatology 172 (5), 1204–1209.

IX. Supplemental

DVD Content:

Dissertation File> PhD thesis Kuehnast 2019.docx
Dissertation File> PhD thesis Kuehnast 2019.pdf
Supplemental File> PhD suppl Kuehnast 2019.docx
Supplemental File> PhD suppl Kuehnast 2019.pdf
Figures and Supplemental Figures> Figure X> Figure X.jpg
Figures and Supplemental Figures> Figure X> Figure X.cdr
Figures and Supplemental Figures> Figure X> Raw> Raw data files for Fig. X.

[Figure X = Figure 1 – Figure 40 and Figure S1 – Figure S20.]

List of Supplemental Figures

Figure S19: Biofilm morphology of *S. epidermidis* strain 150.

Figure S20: Biofilm morphology of *S. epidermidis* strain 152.

- Place Supplemental DVD -